Comparison of hot cores using millimetre spectroscopy

Tisanić, Krešimir

SVEUČILIŠTE U ZAGREBU
PRIRODOSLOVNO-MATEMATIČKI FAKULTET
FIZIČKI ODSJEK

Krešimir Tisanić

USPOREDBA VRUĆIH JEZGRI POMOĆU MILIMETARSKE SPEKTROSKOPIJE

Diplomski rad

Zagreb, 2016.

SVEUČILIŠTE U ZAGREBU
PRIRODOSLOVNO-MATEMATIČKI FAKULTET
FIZIČKI ODSJEK

SMJER: ISTRAŽIVAČKI

Krešimir Tisanić

Diplomski rad

Usporedba vrućih jezgri pomoću milimetarske spektroskopije

Voditelj diplomskog rada: izv. prof. dr. sc. Vernesa Smolčić

Ocjena diplomskog rada: _____

Povjerenstvo: 1. _____

2. _____

3. _____

Datum polaganja: _____

Zagreb, 2016.

Oskari Miettinen, I'm grateful for your guidance and suggestions. You immensely improved my scientific writing skills and introduced me to the interesting field of Astrochemistry.
I wish to thank Professor Vernesa Smočić for her comments. Prof. Kumerički, your comments on group theory were helpful in justifying the assumptions I made. I would like to thank Prof. Pavlovski for his comments on translating nomenclature in Croatian.
Thank you mum and dad for putting up with my all-nighters and strange sleeping habits. Marko, thank you for your love and understanding the haste I was in.
Finally, thanks goes to Gegi, Goldeen, Lemon and Shiro Ni for you nibbling on and uprooting aquarium plants, you made debugging and waiting for outputs seem to pass faster.

Sažetak

Analizirali smo spektre vrućih jezgri G327.3-0.6 i NGC 6334 I u milimetarskom području koje su bile opažane pomoću SHeFI instrumenta na APEX teleskopu u Čileu. Rotacijski i populacijski dijagrami su korišteni pri određivanju kinetičkih temperatura plina i stupčanih gustoća detektiranih molekula u izvorima. Identificirali smo sljedeće molekularne vrste u promatranim vrućim jezgrama: aceton, karbonil sulfid, dimetil eter, etanol, etil cijanid, mravlju kiselinu, keten, metanol, metil acetilen, metilamin, metil cijanid, metil format, sumporov dioskid, vinil cijanid kao i neke od njihovih izotopologa.

Ključne riječi: Molekularna spektroskopija, Nastanak zvijezda velike mase, Masivni mladni zvjezdani objekti (MYSO), Vruće jezgre, izvori: G327.3-0.6, NGC 6334 I, Metoda rotacijskih dijagrama, Metoda populacijskih dijagrama.

COMPARISON OF HOT CORES USING MILLIMETRE SPECTROSCOPY

Abstract

We have analyzed milimeter-wave spectra of the hot cores G327.3-0.6 and NGC 6334 I, which were taken by the SHeFI instrument at the APEX telescope in Chile. Rotational and population diagrams were used to derive the gas kinetic temperatures and column densities of the detected molecules in the sources. We have identified the following molecular species in the observed hot cores: acetone, carbonyl sulfide, dimethyl ether, ethanol, ethyl cyanide, formic acid, ketene, methanol, methyl acetylene, methylamine, methyl cyanide, methyl formate, sulfur dioxide, and vinyl cyanide along with some of their isotopologues.

Key words: Molecular spectroscopy, High-mass star formation, Massive Young Stellar Objects (MYSOs), Hot cores, individual: G327.3-0.6, NGC 6334 I, Rotational diagram method, Population diagram.

Contents

List of Figures

List of Tables

Abbreviations

ALMA The Atacama Large Millimeter/submillimeter Array. iii, 4

APEX Atacama Pathfinder EXperiment. vi, ix, xvii, 15

CDMS Cologne Database for Molecular Spectroscopy. xii, 16

CLASS Continuum and Line Analysis Single-dish Software. x, 15

IRAM Institut de Radioastronomie Millimétrique. x, 15

JPL Jet Propulsion Laboratory. xii, 16

LTE Local Thermodynamic Equilibrium. xvii, 18

MYSO Massive Young Stellar Objects. i, iii, 1, 5

OMC Orion Molecular Cloud. ii, 3, 24

P-ArTéMiS an ESO PI project of a large bolometer camera in the submillimeter range; Architectures de bolometres pour des Telescopes a grand champ de vue dans le domaine sub-Millimetrique au Sol. ii, 4

RMS Root Mean Square. xi, xii, 15, 17

Sgr Sagittarius. 24, 27

SHeFI Swedish Heterodyne Facility Instrument. ix, 15

TMC Taurus Molecular Cloud. 24, 27

Prošireni sažetak (Extended Abstract)

Masivni mladi zvjezdani objekti (MYSO-i) su zvijezde koje imaju mase veće od 8 Sunčevih masa. Iako je stvaranje zvijezda male mase dobro poznat proces (npr. Dunham et al. 2014), za zvijezde velike mase isti evolucijski niz nije moguće primijeniti. Njihove vremenske skale su puno kraće te one počinju ranije utjecati na svoju okolinu nego zvijezde manje mase. Također je zanimljivo da zvijezde velike mase dolaze na glavni niz dok prirast tvari na njih još traje. U ranoj fazi njihova života, MYSO-i stvaraju puno ultraljubičaste svjetlosti, a vjerojatno i jak zvjezdani vjetar, što utječe na strukturu i kemijski sastav njihovog okruženja (Garay & Lizano 1999).

S.1 Vruće jezgre

Vruće molekularne jezgre (nadalje vruće jezgre) su nakupine molekularnog plina i prašine povezane sa ranim stadijima stvaranja zvijezda velike mase (Garay & Lizano 1999; Kurtz et al. 2000). Vruće jezgre i kompaktna HII područja su uronjena u veće nakupine molekularnog plina raznolike gustoće. Kinetičke temperature plina u vrućim jezgrama kreću se od 100 do $300\,\mathrm{K}$ (Gibb et al. 2000), dok su im mase i promjeri od 200 do $300\,M_\odot$[1] (Garay & Lizano 1999), odnosno $\leq 0.1\,\mathrm{pc}$[2] (Kurtz et al. 2000). Vjeruje se da vruće jezgre evoluiraju u hiper/ultrakompaktna HII područja te konačno u HII područja koja okružuju novonastalu zvijezdu velike mase (Beuther et al. 2007). Vruće jezgre su poznate po svojoj bogatoj kemiji i spektrima na (pod)milimetarskim valnim duljinama.

Osim molekularnog plina, vruće jezgre sadrže prašinu. Struktura zrnca prašine može se podijeliti na silikatno-karbonatnu jezgru i ledenu koru koja ju okružuje. Ledena kora se sastoji od molekula poput CO_2, H_2O i CH_3OH, a njezino isparavanje omogućava stvaranje kompliciranijih molekula u plinovitom stanju (Ehrenfreund et al. 1998).

Brown et al. (1988) opisuju vruće jezgre jednostavnim modelom. U tom su modelu vruće jezgre rezultat gravitacijskog kolapsa hladnog plina koji traje $> 10^6\,\mathrm{god}$, nakon kojeg se plin naglo zagrijava u razdoblju od $\sim 100\,\mathrm{god}$ pod utjecajem centralnog MYSO-a. Tijekom kolapsa, molekularne vrste se iz plinovitog stanja kondenziraju na zrnca prašine u obliku ledene kore od molekularnog leda ugljika, dušika i kisika. Pri kraju stvaranja ledene kore na zrncima prašine, ona sadrži molekule poput H_2O, CH_4, NH_3, CH_3CN i HCN. Zagrijavanjem, H_2O isparava odnoseći sa sobom materijal zarobljen u ledu. Brown et al. (1988) su pokazali da će ovako oslobođene molekule preživjeti u plinovitom stanju sljedećih $10^4\,\mathrm{god}$. Preživljavanje je pripisano činjenici da su svi preostali slobodni atomi već pretvoreni u hidride, a udio iona poput H_3^+, He^+ i C^+ je malen. Razlog malog udjela iona leži u visokim H_2 gustoćama vrućih jezgri.

[1] Masa Sunca, $1\,M_\odot \sim 2 \times 10^{30}\,\mathrm{kg}$

[2] Parsek, $1\,\mathrm{pc} \sim 3 \times 10^{16}\,\mathrm{m}$.

Udio H_3^+ i He^+ (nastalih ionizacijom pomoću kozmičkih zraka) je obrnuto proporcionalan gustoći (Millar & Nejad 1985). Posljedično, razaranje molekula ion-molekula interakcijama je otežano.

Precizniji modeli uključuju niz reakcija kojima se stvaraju brojni spojevi poput dimetil etera (CH_3OCH_3), metanola (CH_3OH), ketena (H_2CCO), acetaldehida (CH_3CHO), mravlje kiseline (HCOOH), etanola (CH_3CH_2OH), karbonil sulfida (OCS), izocijanične kiseline (HNCO), formamida (NH_2CHO), vinil cijanida (CH_2CHCN) te etil cijanida (CH_3CH_2CN) (Charnley et al. 2004). Ove molekule također imaju izotopologe koji također mogu biti prisutni pri stvaranju ledene kore na česticama prašine te time i u reakcijama pri isparavanju. Charnley et al. (2004) daje pregled teorijskih relacija za koncentracije između izotopomera kojima je jedan C atom zamijenjen sa ^{13}C (normirano na koncentraciju ^{12}C). Primjerice za metanol i etil cijanid vrijedi

$$\left[\frac{CH_3OH}{^{13}CH_3OH}\right] = \left[\frac{CO_2}{^{13}CO_2}\right]_{led} \tag{S.1}$$

$$\left[\frac{CH_3CH_2CN}{^{13}CH_3CH_2CN}\right] > \left[\frac{CO_2}{^{13}CO_2}\right]_{led}, \tag{S.2}$$

gdje led označava omjer koncentracija u ledu.

Ovi izrazi sugeriraju da je omjer $^{12}C/^{13}C$ u etil cijanidu veći nego u metanolu. Blake et al. (1984) su pronašli da je omjer $CH_3OH/^{13}CH_3OH \sim 15$ za OMC-1, ali predviđaju puno veći omjer, ~ 40, zbog saturacije linija metanola. U poglavlju *Ciljani izvori* detaljnije su opisane vruće jezgre kojima su u ovome radu određene koncentracije pojedinih molekula i njihovih izotopologa.

S.2 Ciljani izvori

U ovom radu su analizirani spektri vrućih jezgara G327.3-0.6 i NGC 6334 I koje su detaljnije opisane u ovom poglavlju.

S.2.1 G327.3-0.6

G327.3-0.6 je vruća jezgra u Mliječnoj stazi koja se nalazi na južnoj nebeskoj polutci, na koordinatama $(\alpha_{J2000}, \delta_{J2000}) = (15\,\mathrm{h}\,53\,\mathrm{m}\,08.78\,\mathrm{s},\ -54°37'01.20'')$ (zviježđe *Pravilo*) na udaljenosti od $2.9\,\mathrm{kpc}$ (Simpson & Rubin 1990). Njezina ukupna masa je $\sim 420\,M_\odot$, promjer ~ 0.1 pc, a ukupni joj je bolometrijski luminozitet $0.5-1.5\times10^5\,L_\odot$[3] (Wyrowski et al. 2006). Sjeverozapadno od vruće jezgre nalazi se HII područje G327.3-0.5, zajendno sa G327.3-0.6 prikazano na slici S.1. Blizu ovog izvora nalaze se još 2 HII područja. Sjeverozapadno se nalazi infracrveni tamni oblak RCW97 (pozicije B i D na desnoj slici slike S.1). Prema jugozapadu se nalazi HII područje BBW29401. Brzina lokalnog standarda mirovanja sustava (nadalje LSR brzina) vruće jezgre G327.3-0.6 je $v_{\mathrm{LSR}} = -45\,\mathrm{km/s}$.

[3]Luminozitet Sunca, $L_\odot \sim 3.8\times10^{26}\,\mathrm{W}$.

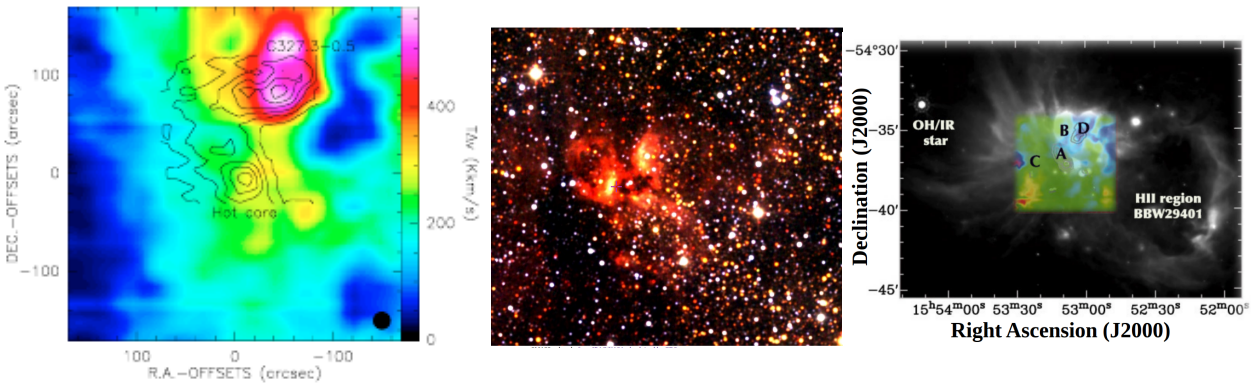

Slika S.1: *Lijevo:* ^{12}CO(3-2) emisija prikazana bojom, konture prikazuju C^{18}O(3-2) emisiju prema G327.3-0.5/G327.3-0.6 sistemu (Wyrowski et al. 2006). *Sredina:* 2MASS infracrvena fotografija $12.29' \times 12.29'$ područja oko G327.3-0.6 (Bonnarel et al. 2000; Boch & Fernique 2014). *Desno:* Mapa prvog momenta CO(3-2) linijske emisije (slika u boji) koja prekriva MIPS 24 μm emisiju (prikazana u crno-bijeloj gradaciji). Boje od plave do crvene odgovaraju brzinama s pomakom u plavo, odnosno crveno. Sive konture prikazaju P-ArTéMiS 450 μm emisiju. Preuzeto iz Minier et al. 2009.

G327.3-0.6 je poznata po spektru bogatom linijama, koje su pretežito gausijanskog oblika. Ovaj izvor je značajan za buduća istraživanja visoke razlučivosti temeljena na interferometriji, posebice s ALMA interferometrom (Wyrowski et al. 2006). Bitan parametar za daljnju analizu je stupčana gustoća vodika H_2. Nova procjena stupčane gustoće je $N_L(H_2) \sim 3 \times 10^{22}\,\mathrm{cm}^{-2}$ (Leurini et al. 2013). Starija procjena dalje nešto veću vrijednost, $N_G(H_2) \sim 3.2 \times 10^{23}\,\mathrm{cm}^{-2}$ (Gibb et al. 2000). Radi usporedbe, obje smo vrijednosti uvrstili u tablice, označene početnim slovima prezimena njihovih prvih autora, L i G.

S.2.2 NGC 6334 I

Izvor NGC 6334 I (prikazan u optičkom dijelu spektra u lijevom okviru slike S.2) je relativno blisko područje stvaranja zvijezda visoke mase čija je udaljenost $\sim 1.3\,\mathrm{kpc}$ (Reid et al. 2014; Chibueze et al. 2014). Nalazi se u zviježđu *Škorpion* na koordinatama $(\alpha_{J2000}, \delta_{J2000}) = (17\,\mathrm{h}\,20\,\mathrm{m}\,53.35\,\mathrm{s}, -35°47'01.5'')$ (Sandell 2000). Sistemska brzina izvora je $v_{\mathrm{LSR}} = -7.0\,\mathrm{km/s}$. NGC 6334 I već ima barem jedan MYSO u svom središtu. Ukupna masa ove vruće jezgre je $106\,M_\odot$, promjer joj je ~ 0.1 pc, a bolometrijskog je luminoziteta od $1.38 \times 10^5\,L_\odot$ (Sandell 2000; Chibueze et al. 2014).

Vruća je jezgra praćena ultrakompaktnim HII područjem NGC 6334 F (srednji okvir slike S.2). Izvor NGC 6334 I također izbacuje plin velikom brzinom od 70 km/s (Bachiller & Cernicharo 1990). Također, Morales Ortiz et al. (2014) su pronašli omotače oko ovog izvora, a zaključuju da je ekspanzija ovih omotača posljedica većeg termalnog tlaka ionizirajućih fotona iz ultrakompaktnog HII područja unutar NGC 6334 I od okolnog tlaka u omotaču. Između omotača postoji gradijent brzina od $1.5\,\mathrm{km/s}$ ali Morales Ortiz et al. (2014) naglašavaju da se zapravo radi o laganoj

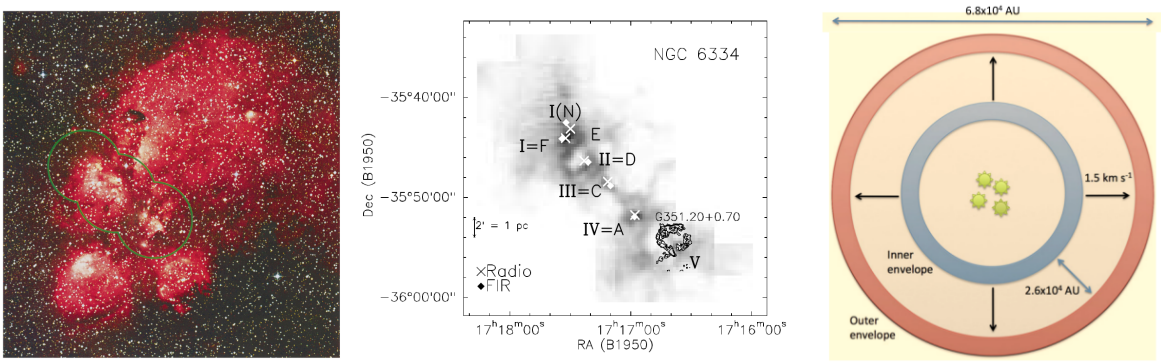

Slika S.2: *Lijevo:* Trobojna (RGB filteri) optička slika NGC 6334 sa područjem prikazanim u desnom okviru označenim zelenom bojom (Burton et al. 2000). *Sredina:* CO(2-1) emisijska mapa NGC 6334 filamenta (tamnija boja znači intenzivniju emisiju). Radio izvori su označeni križićima i slovnim oznakama dok su daleko-infracrveni izvori označeni rombovima i rimskim brojkama. Preuzeto iz Kraemer & Jackson 1999. *Desno:* Prikaz širećeg omotaća oko NGC 6334 I. Prilagođeno iz Morales Ortiz et al. (2014).

gradaciji brzine unutar omotača, a ne o naglom prelasku. Schilke et al. (2006) su proveli usporednu analizu naših ciljanih izvora, a njihovi su rezultati dani u tablici S.1. Primjerice, pronašli su da hladnije komponente matanola (CH_3OH) i metil cijanida (CH_3CN) imaju za red veličine veću stupčanu gustoću u vrućoj jezgri G327.3-0.6 nego u NGC 6334 I. Sumporov dioksid (SO_2) je za red veličine veće stupčane gustoće i 100 K topliji u G327.3-0.6. S druge strane, metil format (CH_3OCHO) i dimetil eter (tj. toplije komponente CH_3OCH_3 u NGC 6334 I) ne prate ovaj uzorak jer imaju iste stupčane gustoće i sličnu temperaturu u oba izvora.

Sljedeće poglavlje opisuje teorijsku pozadinu potrebnu za obradu i interpretaciju spektara analiziranih u ovom radu.

S.3 Teorija

U ovom je poglavlju dan pregled teorijske pozadine potrebne za analizu i interpretaciju spektara vrućih jezgri. U prvom se potpoglavlju izvodi temperatura antene kao jedinica snage zaprimljene teleskopom u određenom frekvencijskom rasponu. Nakon toga izvedene su relacije primijenjene u obradi spektara metodama rotacijskih i populacijskih dijagrama. Budući da su za metodu populacijskih dijagrama bitni kvantni brojevi, u potpoglavlju *Kvantni brojevi* opisani su kvantni brojevi opaženih molekula kao i degeneracije njihovih energetskih nivoa. Poglavlje završava diskusijom mehanizama širenja spektralnih linija koji su prisutni u uvjetima vrućih jezgara.

Tablica S.1: Usporedna analiza vrućih jezgri G327.3-0.6 i NGC 6334 I (preuzeto iz Schilke et al. (2006)). Originalan opis objašnjava komentare u tablici: (1) Temeljeno na samo nekoliko linija; (2) temeljeno samo na slabim ili preklopljenim linijama; (3) uključuje linije vibracijski pobuđenog stanja; (4) uključuje optički deble linije; (5) temeljeno na $C^{34}S$ uz pretpostavku $^{32}S/^{34}S=23$.

Line	Size	T_{ex}	N(mol)	Δv	Comment
	$''$	K	cm^{-2}	km s^{-1}	
NGC 6334(I)					
c-C_2H_4O	ext	150	4.0 (14)	3.0	1
C_2H_5CN	ext	150	2.0 (15)	5.0	2
CH_3CN	1.5	200	1.5 (17)	4.0	3, 4
	ext	50	1.0 (15)	4.0	
CH_3OCH_3	1.2	200	2.0 (18)	3.0	4
	ext	50	1.5 (16)	5.0	
CH_3OCHO	1.5	200	1.0 (18)	3.0	4
CH_3OH	1.5	150	5.0 (18)	3.0	4
	ext	50	3.0 (16)	5.0	
CS	ext	150	2.5 (15)	3.0	1, 5
HNCO	1.5	200	5.0 (16)	5.0	1
N_2H^+	ext	50	5.0 (13)	5.0	1
NH_2CHO	ext	150	1.0 (14)	3.0	
SO	ext	150	1.0 (15)	5.0	1
SO_2	1.5	150	2.0 (17)	3.0	4
G327.3-0.6					
c-C_2H_4O	ext	150	8.0 (14)	5.0	1
C_2H_5CN	1.5	200	3.0 (17)	3.0	
	ext	50	8.0 (15)	3.0	
CH_3CN	1.1	300	5.0 (17)	4.0	3, 4
	ext	50	5 (14)	4.0	
CH_3OCH_3	ext	200	1.0 (16)	3.0	2
CH_3OCHO	1.5	150	2.0 (18)	3.0	2
CH_3OH	ext	50	2.0 (17)	5.0	1
HNCO	ext	150	1.0 (15)	5.0	1
N_2H^+	ext	50	3.0 (14)	5.0	1
NH_2CHO	ext	150	3.0 (14)	5.0	2
SO_2	1.0	250	2.0 (18)	8.0	4

S.3.1 Temperatura antene

Usmjereno emitirana snaga, $P(\theta, \phi)$, je snaga primljena kroz prostorni kut antene. Možemo je normirati njezinom maksimalnom vrijednosti na prostornom kutu, $P_{\max}$

$$P_n(\theta, \phi) = \frac{P(\theta, \phi)}{P_{\max}}. \tag{S.3}$$

U realističnoj anteni postoji glavni režanj antene, interval u θ i ϕ gdje je normalizirana usmjereno emitirana snaga znatno veća nego u ostalim kutevima. Za glavnu zraku, možemo definirati prostorni kut glavne zrake kao

$$\Omega_{MB} = \int_{\text{glavna zraka}} P_n(\theta, \phi)\, \mathrm{d}\Omega, \tag{S.4}$$

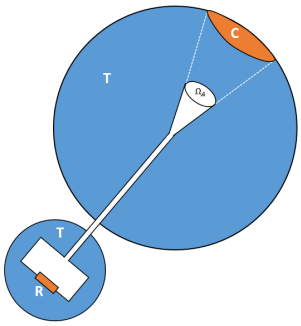

Slika S.3: Skica antene bazirana na slici iz Wilson et al. (2009).

gdje je Ω prostorni kut. Efektivni otvor antene, A_e, je snaga zahvaćena antenom, tj. zahvaćena snaga, P_e, normirana usrednjenim Poyntingovim vektorom, $|\langle \mathbf{S} \rangle|$, $A_e = P_e/|\langle \mathbf{S} \rangle|$.

Prikaz antene dan je na slici S.3, prijamnik R i ploha C kroz koju prolazi zračenje (koja zauzima prostorni kut Ω_A) su zatvoreni u crno tijelo na temperaturi T. Ako promatramo distribuciju sjaja $B_\nu(\theta, \phi)$, ukupna snaga po pojasu će biti

$$P_\nu = \frac{A_e}{2} \int B_\nu(\theta, \phi) P_n(\theta, \phi) \, \mathrm{d}\Omega. \tag{S.5}$$

Pomoću Nyquistovog teorema, ukupnu snagu po pojasu, P_ν, možemo povezati s temperaturom antene, T_A,

$$kT_A = P_\nu, \tag{S.6}$$

gdje je k Boltzmannova konstanta. Ovu temperaturu moramo korigirati za primljenu snagu koja ne dolazi iz dijela neba koji želimo promatrati nego nastaje na površini Zemlje (preljev). Prateći Kutner & Ulich (1981), prostorni kut možemo podijeliti na prostorni kut s normalnim difrakcijskim uzorkom (označen Ω_D) i ostatak na kojemu preljev igra značajnu ulogu. Možemo definirati učinkovitost

$$\eta_{MB} = \frac{\int\limits_{\Omega_D} P_n(\theta, \phi) \, \mathrm{d}\Omega}{\int\limits_{2\pi \, \mathrm{sr}} P_n(\theta, \phi) \, \mathrm{d}\Omega}. \tag{S.7}$$

Na frekvencijama na kojima je promatrano APEX-ovim teleskopom, $\eta_{MB} \sim 0.75$[4]. Odgovarajuća temperatura glavne zrake je

$$T_{MB} = \frac{T_A}{\eta_{MB}}. \tag{S.8}$$

U ovom radu ćemo pretpostaviti da je ukupna efikasnost η jednaka η_{MB}.

[4] http://www.apex-telescope.org/telescope/efficiency/

S.3.2 Rotacijski i populacijski dijagrami

Ako izvor ima optičku dubinu τ, njegova temperatura sjaja će biti (Goldsmith & Langer 1999)

$$T_B = \frac{h\nu/k}{e^{\frac{h\nu}{kT}} - 1} \frac{1 - e^{-\tau}}{\tau} \tau, \tag{S.9}$$

gdje je h Planckova konstanta, a ν frekvencija. Optička dubina prijelaza s donjeg stanja l na gornje u je

$$\tau = \frac{h}{\Delta v} N_u B_{ul} (e^{\frac{h\nu}{kT}} - 1). \tag{S.10}$$

U ovoj jednadžbi, Δv je puna širina na pola maksimuma linije mjerena u jedinicama brzine, B_{ul} Einsteinov koeficijent za prijelaz ul, a N_u stupčana gustoća molekula u stanju u. Izražavanjem Einsteinovog B_{ul} koeficijenta preko Einsteinovog A_{ul} koeficijenta i integrirajući preko cijele linije dobivamo stupčanu gustoću gornjeg stanja

$$N_u = \frac{8\pi k \nu^2}{hc^3 A_{ul} \eta} \int T_A \, \mathrm{d}v \frac{\tau}{1 - e^{-\tau}}, \tag{S.11}$$

gdje je C_τ korekcija zbog optičke dubine. Množenjem s degeneracijom gornjeg stanja, stupčanu gustoću N možemo dobiti pomoću Boltzmannove distribucije

$$\frac{N_u}{N} = \frac{g_u}{Z} e^{-\frac{E_u}{kT}}, \tag{S.12}$$

gdje je Z particijska funkcija, dok su g_u i E_u degeneracija i energija stanja u. Mijenjajući jedinicu brzine u frekvenciju i logaritmiranjem jednadžbe (S.12) dobivamo lineariziranu jednadžbu za metodu rotacijskih dijagrama

$$\ln(N/Z) - \frac{E_u}{kT} = \ln \frac{\gamma \nu [\mathrm{MHz}] \int T_A [\mathrm{K}] \mathrm{d}\nu [\mathrm{MHz}]}{g_u \eta A_{\mathrm{ul}} [\mathrm{s}^{-1}] \nu^2 [\mathrm{MHz}^2]}. \tag{S.13}$$

Konstanta $\gamma \sim 6.37\,[\mathrm{cm}^{-2}]$ služi za pretvaranje mjernih jedinica. Desnu stranu ove jednadžbe skratit ćemo pokratom

$$\ln \frac{N_u}{g_u}. \tag{S.14}$$

Za većinu molekula, particijska funkcija je preuzeta sa *Splatalogue* baze podataka[5] (Remijan et al. 2007). Ona nudi particijske funkcije samo na određenim temperaturama te je stoga ukupna particijska funkcija bila aproksimirana izrazom

$$Z(T) = AT^{3/2} Z_{\mathrm{vib}}(T). \tag{S.15}$$

gdje $T^{3/2}$ potiče od rotacijske particijske funkcije. Vibracijska particijska funkcija je aproksimirana jednostavnom eksponencijalnom prilagodbom dajući izraz

$$Z(T) = AT^{3/2} e^{\alpha T}. \tag{S.16}$$

[5] www.splatalogue.net

U slučajevima kada particijske funkcije nisu bile dane u bazi podataka *Splatalogue*, aproksimirali smo ih rotacijskim particijskim funkcijama. Ova je aproksimacija bila nužna za, primjerice, metanol (simetrijskog broja $\sigma = 1$)

$$Z \sim \sqrt{\pi}\left(\frac{k}{h}\right)^{3/2} \frac{10^{-9}T^{3/2}}{\sqrt{A[\mathrm{MHz}]B[\mathrm{MHz}]C[\mathrm{MHz}]}}, \tag{S.17}$$

gdje su A, B i C rotacijske konstante.

Gustoće H_2 potrebne za termalizaciju populacije različitih stanja su u rasponu od $10^8\,\mathrm{cm}^{-3}$ za $K = \pm 3$ stanja do $10^6\,\mathrm{cm}^{-3}$ za $\Delta K = \pm 1$ prijelaze (Goldsmith & Langer 1999). Različiti prijelazi imaju različite apsorpcijske koeficijente te stoga imaju različitu optičku dubinu za isti molekulski udio. Kako bi se ova razlika uzela u obzir, molekule su odvojene po kvantnim brojevima i simetrijskim vrstama. Ova proširena verzija rotacijskog dijagrama zove se populacijski dijagram.

S.3.3 Kvantni brojevi

Glavni kvantni broj N, ukupni angularni moment J, projekcija angularnog momenta na glavnu os K i vibracijski kvantni broj ν su najjednostavniji kvantni brojevi koje nalazimo u molekularnim spektrima. Općenita definicija degeneracije gornjeg stanja je (npr. Mangum & Shirley 2015)

$$g_u = (2J_u + 1)g_K g_I, \tag{S.18}$$

gdje je J_u ukupni angularni moment gornjeg stanja, a g_K i g_I su degeneracija K nivoa i degeneracija nuklearnog spina. U slučaju kada nismo mogli naći g_u u literaturi, izračunali smo ga na dolje opisani način.

Za molekule s dvije metilne grupe (poput dimetil etera) postoji mogućnost torzije, te se pribjegava opisu molekule pomoću $C_{3v}^- \otimes C_{3v}^+$ grupe (Myers & Bright Wilson 1960). Grupa C_{3v} ima tri ireducibilne reprezentacije: A_1, A_2 i E, što daje simetrijske vrste EE, EA_1, EA_2, A_1E itd. Zbog usporedbe sa Splatalogue-om, ispustili smo indekse 1 i 2 (Clark et al. 1979). Grupe C_{3v}^- i C_{3v}^+ daju svoje kvantne brojeve K_- i K_+. (K_a i K_c na Splatalogue-u). Oni odgovaraju projekcijama angularnog momenta na a i c glavne osi molekule koje ulaze u hamiltonijan molekule (Xu & Lovas 1997). Također, u opis prijelaza ulazi i paritet gornjeg i donjeg stanja. Primjerice, prijelaz $25_{1\,25} - 24_{2\,22}$ AA smo klasificirali na dva različita načina, kao AA vrstu i kao $oo - ee$ prijelaz.

U tablici S.2 je dan pregled Splatalogue-ovih kodova za kvantne brojeve detektiranih molekula s primjerima. Ukratko, kvantni broj F je zbroj ukupnog angularnog momenta i nuklearnog spina I. Degeneracije g_u i g_K dana su u tablici S.3 (Turner 1991). Za molekule sa C_{3v} simetrijom, g_I je oblika (Gordy & Cook 1984)

$$g_I = \begin{cases} \frac{\sigma}{3}\left(1 + \frac{2}{(2I+1)^2}\right) & K \in 3\mathbb{N} \\ \frac{\sigma}{3}\left(1 - \frac{1}{(2I+1)^2}\right) & K \notin 3\mathbb{N} \end{cases}. \tag{S.19}$$

Jedina molekula ove simetrije za koju je trebalo izračunavati degeneracije je metil cijanid ($\sigma = 3$, $I = 1$). Možemo aproksimirati $\frac{1}{(2I+1)^2} \approx 0$, što daje $g_I \approx 1$.

Tablica S.2: Opis Splatalogue kvantnih brojeva s primjerima.

QN kod	kvantni brojevi	primjeri
101	N	Thioformylium
102	N J	Thioxoethenylidene
202	N K	Methyl acetylene, methyl cyanide
303	N K_a K_c	Ethyl cyanide, ketene,
1202	J	Silicon Monoxide
1404	N K_a K_c v	Dimethyl ether, methyl formate

Tablica S.3: Degeneracije K nivoa, g_K, i nuklearna spinska degeneracija, g_I, za odabrane tipove molekula.

Tip		g_K	g_I
2 metilne grupe	ee ili oo; AA	6	1
2 metilne grupe	ee ili oo; AE	2	1
2 metilne grupe	ee ili oo; EA	4	1
2 metilne grupe	ee ili oo; EE	16	1
2 metilne grupe	oe ili eo; AA	10	1
2 metilne grupe	oe ili eo; AE	6	1
2 metilne grupe	oe ili eo; EA	4	1
2 metilne grupe	oe ili eo; EE	16	1
1 metilna grupa	A	1	2
1 metilna grupa	E	2	1
C_{3v} simetrija	$K = 0$	1	1[a]
C_{3v} simetrija	$K \neq 0$	2	1[a]

[a] Aproksimacija za metil cijanid

S.3.4 Brzine i širenje linija

Kod opisa brzina, ne možemo uzeti baricentar Sunčevog sustava kao sustav mirovanja (baricentrički standard mirovanja) jer Sunce ima vlastitu brzinu naspram objekata na istoj udaljenosti od galaktičkog centra kao Sunce. Za podatke kojima je eliminirano gibanje Sunca kažemo da su dani u lokalnom standardu mirovanja (LSR) (Wilson et al. 2009). Spektralna linija može biti pomaknuta od ove vrijednosti. Ovdje primjenjujemo konvenciju brzina iz radio astronomije[6]. Uobičajena formula koja povezuje radijalne brzine i frekvencije je (npr. Carroll & Ostlie 2007).

$$\frac{\nu}{\nu_{ul}} = \sqrt{\frac{1 - v/c}{1 + v/c}}, \tag{S.20}$$

gdje je ν opažena frekvencija, a ν_{ul} laboratorijski izmjerena frekvencija linije. Razvijajući korijen dobivamo

$$\frac{\nu}{\nu_{ul}} = 1 - \frac{v}{c} + O\left(\frac{v^2}{c^2}\right). \tag{S.21}$$

Izražavanjem brzine dobivamo izraz

$$v_{\text{radio}} = c\frac{\nu_{ul} - \nu}{\nu_{ul}}. \tag{S.22}$$

Širina linije (definirana kao širina na pola visine) transformirana u m/s je

$$\Delta v = c\frac{\Delta\nu}{\nu_{ul}}. \tag{S.23}$$

Kao što se vidi iz jednadžbe (S.23), isti razmaci u frekvenciji odgovaraju istim razmacima u brzini što omogućava odabir skale brzina za spektre.

Prirodno širenje linija je zanemarivo u usporedbi s opaženim širinama linija u radio području kod vrućih jezgri (npr. tablica S.1). Uz masu molekule m možemo se ograničiti samo na termalno širenje linija

$$R = \sqrt{\frac{2kT\ln 2}{m}}\frac{2}{\Delta v}, \tag{S.24}$$

za određivanje omjera termalne i ukupne širine linija. Ako je ovaj omjer malen, tj. $R \ll 1$, u izvoru postoji širenje turbulencijom (Larson 1981).

U sljedećem su poglavlju opisana opažanja i metode obrade spektara izvora G327.3-0.6 i NGC 6334 I.

S.4 Opažanja i obrada podataka

Opažanja vrućih jezgri G327.3-0.6 i NGC 6334 I izvršena su na *Atacama Pathfinder EXperiment*, odnosno APEX teleskopu u Llano de Chajnantor u Sjevernom Čileu. Nadmorska visina mjesta je $5105\,\mathrm{m}$, a promjer tanjura teleskopa je $12\,\mathrm{m}$. Korišten je

[6] Pogledati https://www.iram.fr/IRAMFR/ARN/may95/node4.html za detaljnu raspravu.

Tablica S.4: Rezultati računa degeneracije gornjeg stanja za prijelaze za koje Splatalogue nije imao podatke.

Ime	Kemijska formula	ν_{ul} (MHz)	Prijelaz	g_u
G327.3-0.6				
Acetone	$(CH_3)_2CO$ $\nu = 0$	229127.3761	$12_{10\,2} - 11_{9\,2}$ EE	200
Methyl cyanide	CH_3CN $\nu = 0$	220594.4231	$12_6 - 11_6$	50
NGC 6334 I				
Acetone	$(CH_3)_2CO$ $\nu = 0$	220551.1144	$12_{8\,5} - 11_{7\,5}$ EE	200
Acetone	$(CH_3)_2CO$ $\nu = 0$	223732.8258	$12_{9\,4} - 11_{8\,4}$ EE	200
Acetone	$(CH_3)_2CO$ $\nu = 0$	224724.3324	$12_{10\,3} - 11_{9\,2}$ EA	50
Methyl cyanide	CH_3CN $\nu = 0$	220594.4231	$12_6 - 11_6$	50

Swedish Heterodyne Facility Instrument - SHeFI. Podaci su javno dostupni sa APEX-ovog arhiva podataka[7]. Opažanja G327.3-0.6 su napravljena kao dio projekta 081.F-9602(A) i nalaze se u rasponu od $213\,\mathrm{GHz}$ do $268\,\mathrm{GHz}$, $337-338\,\mathrm{GHz}$ te $350-351\,\mathrm{GHz}$ (Vassilev et al. 2008). Izvor NGC 6334 I je promatran unutar projekta O-091.F-9314A-2013 (neobjavljeno) u rasponu frekvencija od 219 do $227\,\mathrm{GHz}$. Za vruću jezgru G327.3-0.6, teleskop je opažao prema lokaciji $(\alpha_{J2000}, \delta_{J2000}) = (15\,\mathrm{h}\,53\,\mathrm{m}\,08.19\,\mathrm{s}, -54°37'06.6'')$, a za NGC 6334 I ciljana lokacija je bila $(\alpha_{J2000}, \delta_{J2000}) = (17\,\mathrm{h}\,20\,\mathrm{m}\,53.44\,\mathrm{s}, -35°46'57.9'')$.

[7] http://www.apex-telescope.org/observing/archiving/

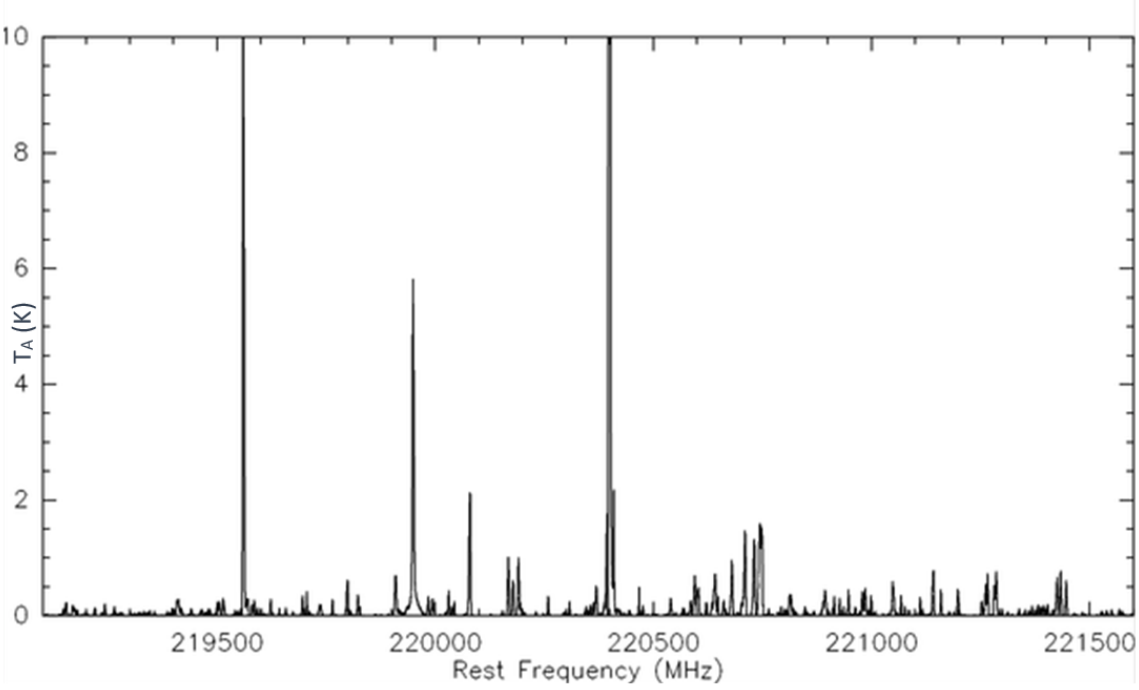

Slika S.4: Spektri NGC 6334 I u rasponu frekvencija [219,220] GHz nakon oduzimanja bazne linije

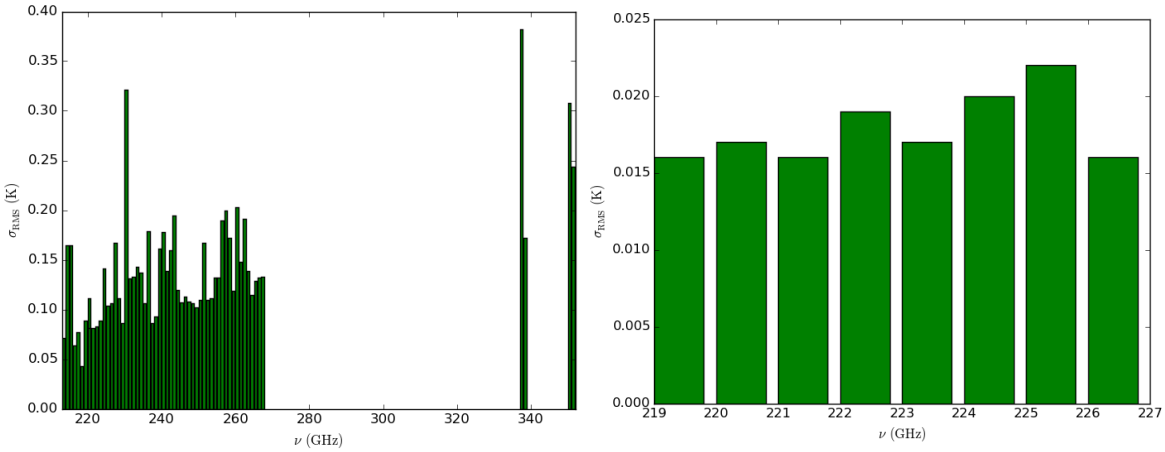

Slika S.5: RMS šum u ovisnosti o frekvenciji za G327.3-0.6 (lijevi okvir) i NGC 6334 I (desni okvir).

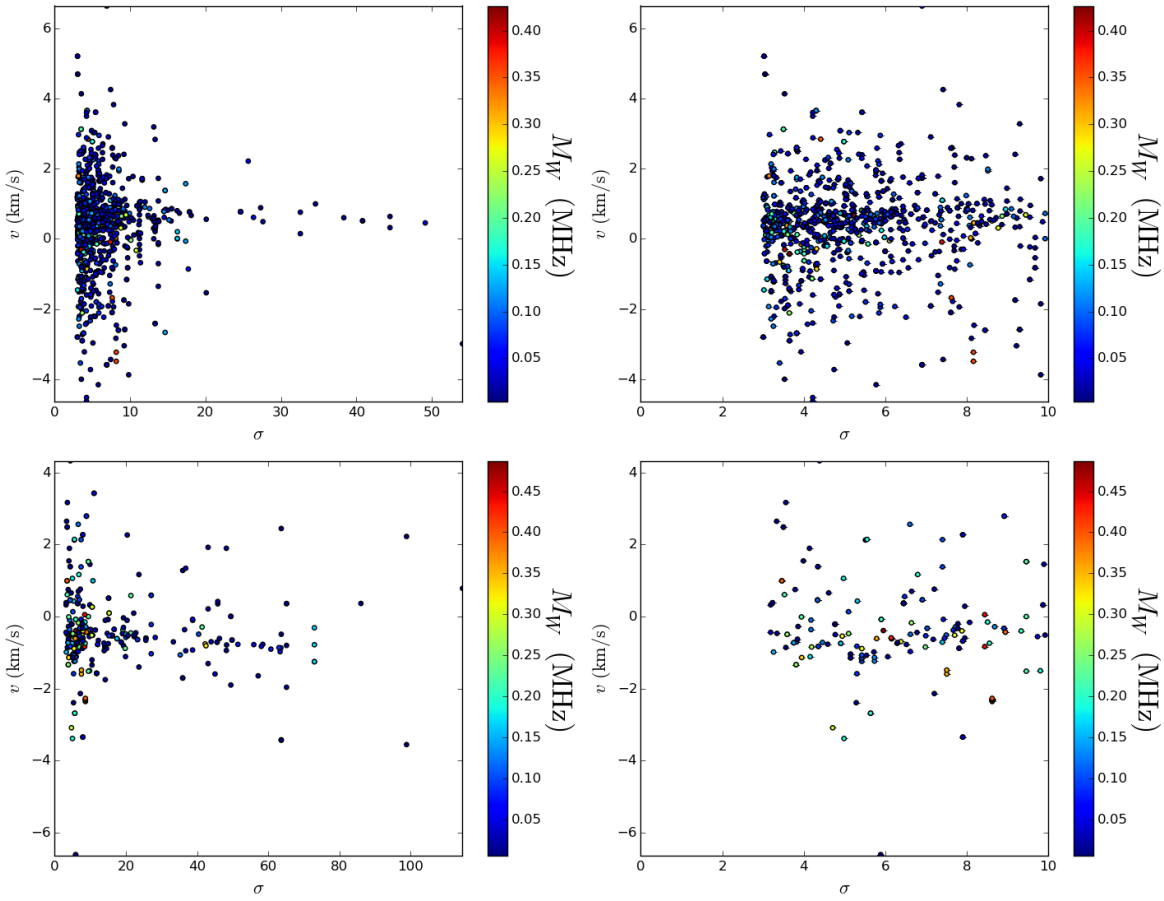

Slika S.6: Brzine linija u ovisnosti o parametru σ sa standardnim greškama širine linija M_W danih bojim. Okvir na desno daje isječak u parametru σ, $\sigma \in [3, 10]$. Gornji red se odnosi na G327.3-0.6, ta donji na NGC 6334 I.

Tablica S.5: Točke izuzete prilikom analize

Ime	Kemijska formula	T (K)	$\ln \frac{N_u}{g_u g_K g_I}$	Prijelaz
G327.3-0.6				
Dimethyl ether	CH_3OCH_3	393.15	21.33	28(4,25)-27(5,22)AA eo-oe
Dimethyl ether	CH_3OCH_3	393.15	20.4	28(4,25)-27(5,22)EE eo-oe
Dimethyl ether	CH_3OCH_3	393.15	23.16	28(4,25)-27(5,22)EA eo-oe
Dimethyl ether	CH_3OCH_3	393.15	22.35	28(4,25)-27(5,22)AE eo-oe
Dimethyl ether	CH_3OCH_3	265.92	25.163	22(5,17)-23(2,22)EE oo-ee
Dimethyl ether	CH_3OCH_3	159.03	26.35	16(5,12)-17(2,15)AA oe-eo
Methanol	$^{13}CH_3OH\ \nu_t = 0$	103.93	32.72	8(2,6)-8(-1,8) ee-oe
Ethyl cyanide	$CH_3CH_2CN\ \nu = 0$	321.32	27.7	29(11,19)-30(10,20)oo-ee
Ethyl cyanide	$CH_3CH_2CN\ \nu = 0$	321.32	27.7	29(11,19)-30(10,20)oo-ee
Ethyl cyanide	$CH_3CH_2CN\ \nu = 0$	321.32	27.7	29(11,18)-30(10,21)oe-eo
NGC 6334 I				
Gauche-ethanol	$g - CH_3CH_2OH$	187.15	29.22	15(5,10)-15(4,11),$\nu_t = 0 - 0$ oe-eo
Gauche-ethanol	$g - CH_3CH_2OH$	279.71	29.52	21(5,17)-21(4,18),$\nu_t = 0 - 0$ oo-ee
Gauche-ethanol	$g - CH_3CH_2OH$	358.92	28.72	26(3,24)-26(2,25),$\nu_t = 0 - 0$ oe-eo
Gauche-ethanol	$g - CH_3CH_2OH$	262.18	29.38	20(5,16)-20(4,17),$\nu_t = 0 - 0$ oe-eo
Gauche-ethanol	$g - CH_3CH_2OH$	229.66	28.97	18(5,13)-18(4,14),$\nu_t = 0 - 0$ oo-ee
Gauche-ethanol	$g - CH_3CH_2OH$	358.92	28.72	26(3,24)-26(2,25),$\nu_t = 0 - 0$ oe-eo

Podaci o spektralnim linijama su obrađeni u IRAM programskom paketu CLASS. Linearna bazna linija je oduzeta od područja bez linija pomoću naredbe BASE 1 (vidljive linije su pritom izuzete naredbom SET WINDOW). Spektri su potom usrednjeni u jedno mjerenje za dan raspon frekvencija s integracijskim vremenom kao težinskim faktorom. Primjer takve procedure dan je na slici S.4, a gotovi spektri dani su u prilozima A i B. RMS šum je označen kao σ_{RMS}, a prikazan je na slici S.5. Na spektralne linije su prilagođeni Gausijani, a parametri prilagodbi su tabelirani u ASCII tabelu. Sveukupno je 2848 linija prilagođeno za G327.3-0.6 i 636 linija za NGC 6334 I. Napisan je program u *Python*-u za preuzimanje podataka o spektralnim linijama sa Splatalogue-a (baziran na skripti Magnusa Perssona *Splatsearch.py*[8]). Program je dao 11640 kandidata za G327.3-0.6 i 2097 kandidata za NGC 6334 I. U ovom je programskom jeziku napisan i program za daljnju obradu i prikaz rezultata. Korištene su spektroskopske baze podataka Cologne Database for Molecular Spectroscopy (CDMS; Müller et al. 2005) i Jet Propulsion Laboratory (JPL; Pickett et al. 1998) molecular spectroscopy database. U podacima su napravljeni rezovi na temelju različitih parametara opisanih u ovom odlomku. Za izbjegavanje zabune u pridjeljivanju molekularnih vrsta linijama, linije koje su imale više različitih molekula kadnidata su izuzete iz daljnje analize, kao i linije kojima je omjer $\sigma = T_A/\sigma_{\mathrm{RMS}}$ manji od 3 ili im je relativna pogreška u širini ili površini veća od 0.5.

Ovisnost brzina naspram σ je dana na slici S.6. Kao što je prikazano na slici,

[8] http://vilhelmp.blogspot.com/2011/10/querying-splataloguenet-with-python.html

najslabije linije imaju najveći rasap u brzinama, što opravdava rez $\sigma \geq 3$. U tablici S.4 dajemo popis prijelaza za koji Splatalogue nije imao podatke o degeneraciji gornjeg stanja s pripadnim izračunatim degeneracijama.

U sljedećem su poglavlju prikazani rezultati rotacijskih i populacijskih dijagrama za vruće jezgre G327.3-0.6 i NGC 6334 I.

S.5 Rezultati

U analizi je bilo potrebno izuzeti prijelaze navedene u tablici S.5 jer u protivnom rotacijski dijagrami nisu producirali dobro slaganje prilagodbe s podacima. Energija gornjeg stanja izabrana je u rasponu od 0 do 450 K za molekule osim acetona i metilamina u G327.3-0.6 te acetona i vinil cijanida $CH_2CH^{13}CN$ u NGC6334 I. Za njih je odabran raspon od 0 do 200 K. Kinetičke temperature plina dobivene rotacijskim dijagramima dane su u tablici S.6. U tablicama se nalazi i Pearsonov koeficijent (ρ), a kriterij za upis u tablicu je $\rho > 0.5$. Temperature plina su u rasponu od 50 do 150 K, uz iznimku trans-etanola (~ 350 K) za G327.3-0.6. Stupčane gustoće su u razumnom rasponu za oba izvora, $10^{12} - 10^{17}\,\mathrm{cm}^{-2}$. Distribucije particijskih funkcija dane su na slici S.7. Slike u dodacima B, C, E i F prikazuju rotacijske i populacijske dijagrame za izvore G327.3-0.6 i NGC 6334 I. Kao što je prikazano na slici S.8, temperature i stupčane gustoće ne variraju puno između izvora, osim temperatura sumporovog dioksida, vinil cijanida i metil formata. Širine linija i R omjeri su slični u oba izvora jer je R omjer povezan s temperaturom.

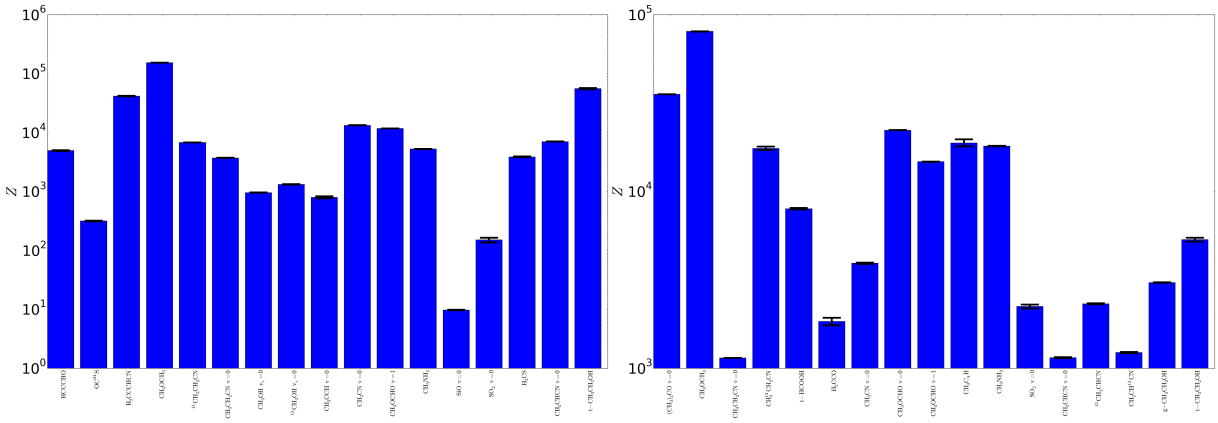

Slika S.7: Distribucija particijskih funkcija za G327.3-0.6 (lijevi okvir) i NGC6334 I (desni okvir).

Tablica S.6: Rezultati metode rotacijskih dijagrama za oba izvora.

G327.3-0.6 - rotacijski dijagrami									
Ime	Kemijska formula	Temperatura (K)	Pearson	$N\,(\mathrm{cm}^{-2})$	x_G[a]	x_L[a]	$v_{\mathrm{LSR}}\,(\mathrm{km/s})$[b]	$\Delta v\,(\mathrm{km/s})$[c]	$R\,(\%)$[d]
Carbonyl sulfide	$OC^{34}S$	96.2 ± 2.4	-1.0	$(5.2 \pm 0.2) \times 10^{14}$	$(1.61 \pm 0.05) \times 10^{-9}$	$(1.72 \pm 0.05) \times 10^{-8}$	-44.52 ± 0.03	5.05 ± 0.07	5.3 ± 0.1
Cyanoallene	$H_2CCCHCN$	105.3 ± 1.9	-1.0	$(2.7 \pm 0.2) \times 10^{15}$	$(8.3 \pm 0.6) \times 10^{-9}$	$(8.9 \pm 0.6) \times 10^{-8}$	-45.1 ± 0.6	6.0 ± 0.7	4.5 ± 0.5
Dimethyl ether	CH_3OCH_3	123.0 ± 0.1	-0.7	$(5.850 \pm 0.007) \times 10^{16}$	$(1.828 \pm 0.002) \times 10^{-7}$	$(1.950 \pm 0.002) \times 10^{-6}$	-45.1 ± 0.1	6.4 ± 0.1	5.5 ± 0.1
Trans-ethanol	$t - CH_3CH_2OH$	340 ± 20	-1.0	$(2.5 \pm 0.1) \times 10^{16}$	$(8.0 \pm 0.3) \times 10^{-8}$	$(8.5 \pm 0.4) \times 10^{-7}$	-44.0 ± 0.5	5.6 ± 0.6	10.3 ± 1.1
Ethyl cyanide	$CH_3CH_2CN\,\nu = 0$	64.75 ± 0.06	-0.9	$(1.059 \pm 0.002) \times 10^{15}$	$(3.309 \pm 0.008) \times 10^{-9}$	$(3.530 \pm 0.008) \times 10^{-8}$	-44.24 ± 0.05	6.07 ± 0.08	3.83 ± 0.05
Ethyl cyanide	$^{13}CH_3CH_2CN$	47.00 ± 0.07	-0.9	$(1.77 \pm 0.01) \times 10^{16}$	$(5.53 \pm 0.03) \times 10^{-8}$	$(5.90 \pm 0.04) \times 10^{-7}$	-44.5 ± 0.4	6.5 ± 0.6	3.0 ± 0.3
Methanol	$CH_3OH\,\nu_t = 0$	134.7 ± 0.2	-0.7	$(1.143 \pm 0.003) \times 10^{16}$	$(3.570 \pm 0.008) \times 10^{-8}$	$(3.808 \pm 0.009) \times 10^{-7}$	-44.45 ± 0.08	6.5 ± 0.1	6.8 ± 0.1
Methanol	$^{13}CH_3OH\,\nu_t = 0$	164.1 ± 1.0	-0.9	$(2.80 \pm 0.03) \times 10^{15}$	$(8.76 \pm 0.09) \times 10^{-9}$	$(9.3 \pm 0.1) \times 10^{-8}$	-44.6 ± 0.2	5.6 ± 0.2	8.5 ± 0.3
Methyl Acetylene	$CH_3CCH\,\nu = 0$	83.6 ± 6.8	-1.0	$(2.0 \pm 0.2) \times 10^{15}$	$(6.2 \pm 0.7) \times 10^{-9}$	$(6.6 \pm 0.8) \times 10^{-8}$	-44.61 ± 0.08	4.6 ± 0.1	6.7 ± 0.3
Methyl cyanide	$CH_3CN\,\nu = 0$	164.0 ± 2.8	-0.9	$(1.12 \pm 0.02) \times 10^{15}$	$(3.51 \pm 0.07) \times 10^{-9}$	$(3.74 \pm 0.08) \times 10^{-8}$	-44.3 ± 0.3	7.7 ± 0.6	5.6 ± 0.4
Methyl formate	$CH_3OCHO\,\nu = 1$	54.8 ± 0.1	-1.0	$(5.20 \pm 0.06) \times 10^{17}$	$(1.62 \pm 0.02) \times 10^{-6}$	$(1.73 \pm 0.02) \times 10^{-5}$	-44.8 ± 0.2	5.2 ± 0.2	3.9 ± 0.2
Methylamine	CH_3NH_2	36.6 ± 0.4	-1.0	$(1.30 \pm 0.05) \times 10^{16}$	$(4.1 \pm 0.2) \times 10^{-8}$	$(4.3 \pm 0.2) \times 10^{-7}$	-46.1 ± 0.8	5.0 ± 0.5	4.6 ± 0.4
2-Propynal	HCCCHO	107.4 ± 3.2	-0.9	$(5.1 \pm 0.4) \times 10^{16}$	$(1.6 \pm 0.1) \times 10^{-7}$	$(1.7 \pm 0.1) \times 10^{-6}$	-45.6 ± 0.8	6.1 ± 0.7	4.9 ± 0.6
Silicon Monoxide	$SiO\,\nu = 0$	19.5 ± 0.2	-1.0	$(1.45 \pm 0.04) \times 10^{13}$	$(4.5 \pm 0.1) \times 10^{-11}$	$(4.8 \pm 0.1) \times 10^{-10}$	-44.225 ± 0.002	9.2 ± 0.2	1.55 ± 0.03
Sulfur dioxide	$SO_2\,\nu = 0$	26.1 ± 4.7	-1.0	$(9.1 \pm 6.0) \times 10^{14}$	$(2.8 \pm 1.9) \times 10^{-9}$	$(3.0 \pm 2.0) \times 10^{-8}$	-43.8 ± 0.1	8.0 ± 0.3	1.7 ± 0.2
Thioformaldehyde	H_2CS	227.5 ± 6.1	-0.9	$(1.55 \pm 0.03) \times 10^{15}$	$(4.84 \pm 0.08) \times 10^{-9}$	$(5.16 \pm 0.08) \times 10^{-8}$	-44.8	5.8 ± 0.1	8.2 ± 0.2
Vinyl cyanide	$CH_2CHCN\,\nu = 0$	60.9 ± 0.1	-1.0	$(1.030 \pm 0.006) \times 10^{15}$	$(3.22 \pm 0.02) \times 10^{-9}$	$(3.43 \pm 0.02) \times 10^{-8}$	-44.3 ± 0.2	7.8 ± 0.3	2.9 ± 0.1
NGC 6334 I - rotacijski dijagrami									
Ime	Kemijska formula	Temperatura (K)	Pearson	$N\,(\mathrm{cm}^{-2})$	x_o[a]	x_i[a]	$v_{\mathrm{LSR}}\,(\mathrm{km/s})$[b]	$\Delta v\,(\mathrm{km/s})$[c]	$R\,(\%)$[d]
Acetone	$(CH_3)_2CO\,\nu = 0$	25.89 ± 0.04	-0.9	$(2.31 \pm 0.02) \times 10^{16}$	$(2.3 \pm 1.8) \times 10^{-7}$	$(1.154 \pm 0.008) \times 10^{-7}$	-7.7 ± 0.2	5.3 ± 0.3	2.7 ± 0.2
Dimethyl ether	CH_3OCH_3	86.5 ± 0.1	-0.7	$(3.583 \pm 0.006) \times 10^{16}$	$(3.6 \pm 2.9) \times 10^{-7}$	$(1.792 \pm 0.003) \times 10^{-7}$	-7.4 ± 0.2	5.5 ± 0.2	5.4 ± 0.2
Gauche-ethanol	$g - CH_3CH_2OH$	56.4 ± 0.3	-1.0	$(2.00 \pm 0.04) \times 10^{16}$	$(2.0 \pm 1.6) \times 10^{-7}$	$(1.00 \pm 0.02) \times 10^{-7}$	-7.8 ± 0.4	8.2 ± 0.7	2.9 ± 0.2
Trans-ethanol	$t - CH_3CH_2OH$	80.9 ± 4.1	-1.0	$(2.28 \pm 0.09) \times 10^{16}$	$(2.3 \pm 1.8) \times 10^{-7}$	$(1.14 \pm 0.05) \times 10^{-7}$	-6.7	7.1 ± 1.2	4.0 ± 0.7
Ethyl cyanide	$CH_3CH_2CN\,\nu = 0$	29.44 ± 0.04	-1.0	$(3.31 \pm 0.02) \times 10^{15}$	$(3.3 \pm 2.6) \times 10^{-8}$	$(1.65 \pm 0.01) \times 10^{-8}$	-6.8 ± 0.1	4.7 ± 0.2	3.3 ± 0.1
Ethyl cyanide	$CH_3^{13}CH_2CN$	88.7 ± 3.9	-1.0	$(1.0 \pm 0.2) \times 10^{17}$	$(1.0 \pm 0.8) \times 10^{-6}$	$(4.8 \pm 0.9) \times 10^{-7}$	-6.9	3.3 ± 0.1	8.1 ± 0.3
Formic Acid	$t - HCOOH$	280.0 ± 5.8	-0.9	$(5.29 \pm 0.07) \times 10^{14}$	$(5.3 \pm 4.2) \times 10^{-9}$	$(2.65 \pm 0.04) \times 10^{-9}$	-8.09 ± 0.09	4.8 ± 0.3	11.1 ± 0.6
Ketene	H_2CCO	98.3 ± 9.5	-1.0	$(2.3 \pm 0.3) \times 10^{14}$	$(2.3 \pm 1.9) \times 10^{-9}$	$(1.2 \pm 0.1) \times 10^{-9}$	-7.3 ± 0.2	5.17 ± 0.08	6.4 ± 0.3
Methylamine	CH_3NH_2	82.9 ± 0.6	-0.8	$(3.62 \pm 0.03) \times 10^{15}$	$(3.6 \pm 2.9) \times 10^{-8}$	$(1.81 \pm 0.01) \times 10^{-8}$	-6.1 ± 0.9	6.3 ± 0.8	5.6 ± 0.7
Methyl diacetylene	CH_3C_4H	170 ± 20	-1.0	$(4.2 \pm 0.8) \times 10^{14}$	$(4.2 \pm 3.5) \times 10^{-9}$	$(2.1 \pm 0.4) \times 10^{-9}$	-7.2 ± 1.0	4.2 ± 0.2	8.2 ± 0.6
Methyl cyanide	$CH_3CN\,\nu = 0$	79.2 ± 1.4	-1.0	$(7.7 \pm 0.1) \times 10^{14}$	$(7.7 \pm 6.2) \times 10^{-9}$	$(3.87 \pm 0.07) \times 10^{-9}$	-7.5 ± 0.7	7.5 ± 1.2	4.0 ± 0.6
Methyl formate	$CH_3OCHO\,\nu = 0$	81.9 ± 0.2	-0.9	$(1.784 \pm 0.008) \times 10^{16}$	$(1.8 \pm 1.4) \times 10^{-7}$	$(8.92 \pm 0.04) \times 10^{-8}$	-7.55 ± 0.07	4.3 ± 0.1	5.9 ± 0.2
Methyl formate	$CH_3OCHO\,\nu = 1$	63.1 ± 0.2	-1.0	$(8.9 \pm 0.1) \times 10^{16}$	$(8.9 \pm 7.2) \times 10^{-7}$	$(4.47 \pm 0.06) \times 10^{-7}$	-7.3 ± 0.1	4.5 ± 0.2	4.9 ± 0.2
Sulfur dioxide	$SO_2\,\nu = 0$	157.1 ± 8.0	-0.9	$(8.5 \pm 0.4) \times 10^{14}$	$(8.5 \pm 6.8) \times 10^{-9}$	$(4.3 \pm 0.2) \times 10^{-9}$	-7.9 ± 0.1	5.4 ± 0.5	6.2 ± 0.6
Vinyl cyanide	$CH_2CHCN\,\nu = 0$	19.0 ± 0.3	-0.9	$(2.9 \pm 0.2) \times 10^{15}$	$(2.9 \pm 2.4) \times 10^{-8}$	$(1.5 \pm 0.1) \times 10^{-8}$	-3.9 ± 0.2	7.5 ± 0.3	1.72 ± 0.06
Vinyl cyanide	$^{13}CH_2CHCN$	28.0 ± 0.4	-0.8	$(4.5 \pm 0.2) \times 10^{14}$	$(4.5 \pm 3.6) \times 10^{-9}$	$(2.27 \pm 0.08) \times 10^{-9}$	-7.0	6.3 ± 1.2	2.5 ± 0.5
Vinyl cyanide	$CH_2CH^{13}CN$	18.7 ± 0.3	-1.0	$(2.3 \pm 0.2) \times 10^{15}$	$(2.3 \pm 1.8) \times 10^{-8}$	$(1.1 \pm 0.1) \times 10^{-8}$	-6.1 ± 0.6	6.1 ± 1.0	2.1 ± 0.3

[a] Udjeli bazirani na stupčanoj gustoći vodika Leurini et al. (2013) (L) i Gibb et al. (2000) (G) za G327.3-0.3 te i i o za unutarnji i vanjski omotač NGC 6334 I. [b] Brzine naspram LSR.
[c] Srednje širine linija. [d] R omjeri usrednjeni preko detektiranih prijelaza za danu molekulu.

Tablica S.7: Rezultati metode populacijskih dijagrama za oba izvora.

G327.3-0.6 - populacijski dijagrami									
Ime	Kemijska formula	Temperatura (K)	Pearson	$N\,(\mathrm{cm}^{-2})$	x_G[a]	x_L[a]	$v_{\mathrm{LSR}}\,(\mathrm{km/s})$[b]	$\Delta v\,(\mathrm{km/s})$[c]	$R\,(\%)$[d]
Acetone	$(CH_3)_2CO\,\nu=0$ oo − oe	350 ± 160	-1.0	$(3.7 \pm 1.0) \times 10^{16}$	$(1.2 \pm 0.3) \times 10^{-7}$	$(1.2 \pm 0.3) \times 10^{-6}$	-44.8 ± 0.1	4.7 ± 0.4	11.3 ± 2.7
Acetone	$(CH_3)_2CO\,\nu=0$ AE	280 ± 20	-1.0	$(1.70 \pm 0.07) \times 10^{17}$	$(5.3 \pm 0.2) \times 10^{-7}$	$(5.7 \pm 0.2) \times 10^{-6}$	-45.1 ± 0.3	5.0 ± 0.3	9.5 ± 0.6
Dimethyl ether	CH_3OCH_3 ee − oo	118.4 ± 0.4	-0.7	$(6.77 \pm 0.02) \times 10^{16}$	$(2.116 \pm 0.007) \times 10^{-7}$	$(2.258 \pm 0.007) \times 10^{-6}$	-45.1 ± 0.4	6.3 ± 0.3	5.5 ± 0.3
Dimethyl ether	CH_3OCH_3 oo − ee	145.9 ± 0.3	-0.6	$(7.60 \pm 0.01) \times 10^{16}$	$(2.375 \pm 0.004) \times 10^{-7}$	$(2.533 \pm 0.004) \times 10^{-6}$	-45.2 ± 0.2	6.7 ± 0.2	5.7 ± 0.2
Dimethyl ether	CH_3OCH_3 eo − oe	111.5 ± 0.7	-0.7	$(4.31 \pm 0.03) \times 10^{16}$	$(1.347 \pm 0.009) \times 10^{-7}$	$(1.44 \pm 0.01) \times 10^{-6}$	-45.0 ± 0.5	7.1 ± 0.2	4.7 ± 0.2
Dimethyl ether	CH_3OCH_3 oe − eo	105.1 ± 0.2	-0.7	$(4.01 \pm 0.01) \times 10^{16}$	$(1.252 \pm 0.003) \times 10^{-7}$	$(1.335 \pm 0.003) \times 10^{-6}$	-45.1 ± 0.2	6.0 ± 0.2	5.4 ± 0.2
Dimethyl ether	CH_3OCH_3 AA	140.8 ± 0.3	-0.6	$(5.40 \pm 0.01) \times 10^{16}$	$(1.688 \pm 0.004) \times 10^{-7}$	$(1.800 \pm 0.005) \times 10^{-6}$	-43.9 ± 0.3	6.2 ± 0.2	6.1 ± 0.2
Dimethyl ether	CH_3OCH_3 EA	143.0 ± 0.4	-0.7	$(1.340 \pm 0.004) \times 10^{17}$	$(4.19 \pm 0.01) \times 10^{-7}$	$(4.47 \pm 0.01) \times 10^{-6}$	-45.8 ± 0.3	6.5 ± 0.2	5.9 ± 0.2
Dimethyl ether	CH_3OCH_3 AE	128.1 ± 0.4	-0.7	$(1.367 \pm 0.004) \times 10^{17}$	$(4.27 \pm 0.01) \times 10^{-7}$	$(4.56 \pm 0.01) \times 10^{-6}$	-46.0 ± 0.3	6.6 ± 0.3	5.4 ± 0.2
Dimethyl ether	CH_3OCH_3 EE	121.4 ± 0.2	-0.7	$(2.479 \pm 0.006) \times 10^{16}$	$(7.75 \pm 0.02) \times 10^{-8}$	$(8.26 \pm 0.02) \times 10^{-7}$	-44.8 ± 0.1	6.3 ± 0.2	5.5 ± 0.2
Ethyl cyanide	$CH_3CH_2CN\,\nu=0$ ee − oo	195.3 ± 2.9	-0.9	$(1.37 \pm 0.02) \times 10^{16}$	$(4.27 \pm 0.07) \times 10^{-8}$	$(4.56 \pm 0.07) \times 10^{-7}$	-44.3 ± 0.1	5.2 ± 0.1	7.7 ± 0.2
Ethyl cyanide	$CH_3CH_2CN\,\nu=0$ oo − ee	261.7 ± 8.4	-0.8	$(3.57 \pm 0.06) \times 10^{16}$	$(1.11 \pm 0.02) \times 10^{-7}$	$(1.19 \pm 0.02) \times 10^{-6}$	-45.1 ± 0.3	5.4 ± 0.2	8.6 ± 0.4
Ethyl cyanide	$CH_3CH_2CN\,\nu=0$ eo − oe	145.8 ± 0.9	-0.9	$(7.42 \pm 0.05) \times 10^{15}$	$(2.32 \pm 0.02) \times 10^{-8}$	$(2.47 \pm 0.02) \times 10^{-7}$	-44.1 ± 0.1	5.7 ± 0.2	6.1 ± 0.2
Ethyl cyanide	$^{13}CH_3CH_2CN$ ee − eo	18.0 ± 0.2	-1.0	$(6.0 \pm 0.7) \times 10^{18}$	$(1.9 \pm 0.2) \times 10^{-5}$	0.00020 ± 0.00002	-46.3 ± 1.1	6.6 ± 1.1	1.8 ± 0.3
Methanol	$^{13}CH_3OH\,\nu_t=0$ −−	190 ± 10	-0.9	$(3.1 \pm 0.2) \times 10^{15}$	$(9.8 \pm 0.8) \times 10^{-9}$	$(1.05 \pm 0.08) \times 10^{-7}$	-44.2 ± 0.5	6.5 ± 0.8	8.0 ± 1.0
Methanol	$^{13}CH_3OH\,\nu_t=0$ +−	96.0 ± 0.7	-0.9	$(2.14 \pm 0.03) \times 10^{15}$	$(6.7 \pm 0.1) \times 10^{-9}$	$(7.1 \pm 0.1) \times 10^{-8}$	-44.4 ± 0.1	5.2 ± 0.2	7.1 ± 0.3
Methanol	$^{13}CH_3OH\,\nu_t=0$ −+	222.1 ± 6.4	-0.9	$(2.9 \pm 0.2) \times 10^{15}$	$(9.0 \pm 0.6) \times 10^{-9}$	$(9.6 \pm 0.6) \times 10^{-8}$	-44.5 ± 0.3	5.9 ± 0.6	9.5 ± 0.9
Methanol	$CH_3OH\,\nu_t=0$	98.4 ± 0.2	-0.7	$(1.064 \pm 0.004) \times 10^{16}$	$(3.32 \pm 0.01) \times 10^{-8}$	$(3.55 \pm 0.01) \times 10^{-7}$	-44.5 ± 0.1	6.3 ± 0.2	5.9 ± 0.2
Methanol	$CH_3OH\,\nu_t=0$ ++	218.0 ± 0.8	-0.8	$(1.81 \pm 0.01) \times 10^{16}$	$(5.67 \pm 0.04) \times 10^{-8}$	$(6.04 \pm 0.04) \times 10^{-7}$	-44.4 ± 0.3	6.5 ± 0.3	8.7 ± 0.4
Methanol	$CH_3OH\,\nu_t=0$ −−	118.0 ± 1.0	-0.8	$(9.2 \pm 0.1) \times 10^{15}$	$(2.87 \pm 0.04) \times 10^{-8}$	$(3.06 \pm 0.04) \times 10^{-7}$	-44.5 ± 0.1	6.5 ± 0.2	6.4 ± 0.2
Methanol	$CH_3OH\,\nu_t=0$ +−	148.4 ± 0.7	-0.9	$(5.43 \pm 0.05) \times 10^{15}$	$(1.70 \pm 0.02) \times 10^{-8}$	$(1.81 \pm 0.02) \times 10^{-7}$	-44.33 ± 0.08	6.5 ± 0.2	7.1 ± 0.2
Methanol	$CH_3OH\,\nu_t=0$ −+	129.4 ± 0.8	-0.9	$(5.55 \pm 0.06) \times 10^{15}$	$(1.73 \pm 0.02) \times 10^{-8}$	$(1.85 \pm 0.02) \times 10^{-7}$	-44.5 ± 0.1	7.1 ± 0.2	6.1 ± 0.2
Methanol	$^{13}CH_3OH\,\nu_t=0$ ++	85.3 ± 3.0	-1.0	$(2.9 \pm 0.2) \times 10^{15}$	$(9.0 \pm 0.8) \times 10^{-9}$	$(9.7 \pm 0.8) \times 10^{-8}$	-44.4 ± 0.5	5.5 ± 0.6	6.3 ± 0.7
Methyl formate	$CH_3OCHO\,\nu=0$ oe − eo	201.9 ± 4.8	-1.0	$(9.0 \pm 0.2) \times 10^{16}$	$(2.81 \pm 0.06) \times 10^{-7}$	$(3.00 \pm 0.06) \times 10^{-6}$	-45.4 ± 0.5	6.3 ± 0.2	6.2 ± 0.2
Methyl formate	$CH_3OCHO\,\nu=0$ ee − oo	163.9 ± 5.4	-1.0	$(7.3 \pm 0.2) \times 10^{16}$	$(2.27 \pm 0.08) \times 10^{-7}$	$(2.42 \pm 0.08) \times 10^{-6}$	-44.9	5.7 ± 0.4	6.2 ± 0.4
Methyl formate	$CH_3OCHO\,\nu=0$ oo − ee	73.6 ± 1.7	-0.9	$(8.6 \pm 0.4) \times 10^{16}$	$(2.7 \pm 0.1) \times 10^{-7}$	$(2.9 \pm 0.1) \times 10^{-6}$	-44.8	6.0 ± 0.5	3.9 ± 0.3
Methyl formate	$CH_3OCHO\,\nu=0$ eo − oe	197.9 ± 3.4	-1.0	$(2.78 \pm 0.05) \times 10^{17}$	$(8.7 \pm 0.2) \times 10^{-7}$	$(9.3 \pm 0.2) \times 10^{-6}$	-45.2 ± 0.5	5.5 ± 0.7	7.0 ± 0.9
Methyl formate	$CH_3OCHO\,\nu=1$ ee − oo	38.9 ± 0.4	-1.0	$(2.6 \pm 0.2) \times 10^{19}$	$(8.0 \pm 0.6) \times 10^{-5}$	0.00085 ± 0.00007	-45.6 ± 0.9	6.5 ± 1.0	2.7 ± 0.4
Methyl formate	$CH_3OCHO\,\nu=1$ eo − oe	49.9 ± 0.3	-1.0	$(1.27 \pm 0.04) \times 10^{18}$	$(4.0 \pm 0.1) \times 10^{-6}$	$(4.2 \pm 0.1) \times 10^{-5}$	-45.5 ± 0.6	5.2 ± 0.3	3.7 ± 0.2
Methyl formate	$CH_3OCHO\,\nu=1$ A	67.6 ± 0.2	-1.0	$(1.64 \pm 0.02) \times 10^{17}$	$(5.13 \pm 0.07) \times 10^{-7}$	$(5.47 \pm 0.07) \times 10^{-6}$	-44.9	4.9 ± 0.2	4.6 ± 0.2
Methyl formate	$CH_3OCHO\,\nu=1$ E	156.2 ± 5.7	-1.0	$(2.4 \pm 0.2) \times 10^{17}$	$(7.5 \pm 0.6) \times 10^{-7}$	$(8.0 \pm 0.6) \times 10^{-6}$	-44.6 ± 0.3	5.6 ± 0.4	6.2 ± 0.5
2-Propynal	HCCCHO eo − ee	17.5 ± 0.5	-0.7	$(5.6 \pm 0.7) \times 10^{17}$	$(1.8 \pm 0.2) \times 10^{-6}$	$(1.9 \pm 0.2) \times 10^{-5}$	-44.9	5.3 ± 0.9	2.3 ± 0.4
Thioformaldehyde	H_2CS oo − oe	178.6 ± 6.7	-0.9	$(1.45 \pm 0.04) \times 10^{15}$	$(4.5 \pm 0.1) \times 10^{-9}$	$(4.8 \pm 0.1) \times 10^{-8}$	-44.9	6.1 ± 0.2	7.0 ± 0.3
Vinyl cyanide	$CH_2CHCN\,\nu=0$ oe − oo	24.60 ± 0.07	-1.0	$(9.7 \pm 0.3) \times 10^{16}$	$(3.02 \pm 0.08) \times 10^{-7}$	$(3.22 \pm 0.09) \times 10^{-6}$	-44.3 ± 0.5	8.4 ± 0.7	1.7 ± 0.2
Vinyl cyanide	$CH_2CHCN\,\nu=0$ ee − eo	66.2 ± 0.2	-1.0	$(8.24 \pm 0.09) \times 10^{14}$	$(2.58 \pm 0.03) \times 10^{-9}$	$(2.75 \pm 0.03) \times 10^{-8}$	-43.9 ± 0.3	7.4 ± 0.7	3.2 ± 0.3
Vinyl cyanide	$CH_2CHCN\,\nu=0$ eo − ee	45.2 ± 0.3	-1.0	$(4.5 \pm 0.2) \times 10^{15}$	$(1.42 \pm 0.06) \times 10^{-8}$	$(1.51 \pm 0.06) \times 10^{-7}$	-44.6 ± 0.4	7.6 ± 0.7	2.6 ± 0.3
Vinyl cyanide	$CH_2CHCN\,\nu=0$ oo − oe	84.2 ± 0.7	-1.0	$(5.5 \pm 0.1) \times 10^{14}$	$(1.72 \pm 0.03) \times 10^{-9}$	$(1.84 \pm 0.04) \times 10^{-8}$	-44.4 ± 0.3	8.2 ± 0.7	3.3 ± 0.3
NGC 6334 I - populacijski dijagrami									
Ime	Kemijska formula	Temperatura (K)	Pearson	$N\,(\mathrm{cm}^{-2})$	x_o[a]	x_i[a]	$v_{\mathrm{LSR}}\,(\mathrm{km/s})$[b]	$\Delta v\,(\mathrm{km/s})$[c]	$R\,(\%)$[d]
Acetone	$(CH_3)_2CO\,\nu=0$ EE	11.90 ± 0.01	-0.9	$(1.24 \pm 0.01) \times 10^{17}$	$(1.2 \pm 1.0) \times 10^{-6}$	$(6.19 \pm 0.05) \times 10^{-7}$	-7.4 ± 0.2	4.9 ± 0.6	2.0 ± 0.2
Acetone	$(CH_3)_2CO\,\nu=0$ AA	12.59 ± 0.05	-0.9	$(3.31 \pm 0.09) \times 10^{16}$	$(3.3 \pm 2.6) \times 10^{-7}$	$(1.65 \pm 0.05) \times 10^{-7}$	-6.9	5.4 ± 1.1	1.8 ± 0.4
Acetone	$(CH_3)_2CO\,\nu=0$ ee − oo	50.1 ± 0.7	-0.9	$(1.81 \pm 0.06) \times 10^{17}$	$(1.8 \pm 1.5) \times 10^{-6}$	$(9.1 \pm 0.3) \times 10^{-7}$	-7.5 ± 0.5	5.9 ± 1.5	3.4 ± 0.8
Dimethyl ether	CH_3OCH_3 oe − eo	185.9 ± 8.1	-0.9	$(4.4 \pm 0.4) \times 10^{16}$	$(4.4 \pm 3.5) \times 10^{-7}$	$(2.2 \pm 0.2) \times 10^{-7}$	-7.5 ± 0.2	5.4 ± 0.3	8.0 ± 0.5
Dimethyl ether	CH_3OCH_3 oo − ee	123.6 ± 0.8	-0.9	$(4.99 \pm 0.04) \times 10^{16}$	$(5.0 \pm 4.0) \times 10^{-7}$	$(2.50 \pm 0.02) \times 10^{-7}$	-7.3 ± 0.3	4.6 ± 0.3	7.6 ± 0.5
Dimethyl ether	CH_3OCH_3 EE	88.4 ± 0.2	-0.7	$(1.707 \pm 0.006) \times 10^{16}$	$(1.7 \pm 1.4) \times 10^{-7}$	$(8.54 \pm 0.03) \times 10^{-8}$	-7.6 ± 0.2	5.8 ± 0.4	5.1 ± 0.4
Dimethyl ether	CH_3OCH_3 AA	113.8 ± 0.3	-0.7	$(4.16 \pm 0.01) \times 10^{16}$	$(4.2 \pm 3.3) \times 10^{-7}$	$(2.082 \pm 0.007) \times 10^{-7}$	-7.1 ± 0.5	5.5 ± 0.5	6.2 ± 0.5
Dimethyl ether	CH_3OCH_3 EA	62.5 ± 0.3	-0.9	$(4.63 \pm 0.03) \times 10^{16}$	$(4.6 \pm 3.7) \times 10^{-7}$	$(2.31 \pm 0.01) \times 10^{-7}$	-7.4 ± 0.5	5.3 ± 0.5	4.7 ± 0.5
Ethyl cyanide	$CH_3CH_2CN\,\nu=0$ ee − eo	270.0 ± 9.2	-1.0	$(2.23 \pm 0.06) \times 10^{14}$	$(2.2 \pm 1.8) \times 10^{-9}$	$(1.12 \pm 0.03) \times 10^{-9}$	-6.75 ± 0.06	5.2 ± 0.2	9.2 ± 0.3
Ethyl cyanide	$CH_3CH_2CN\,\nu=0$ eo − ee	51.1 ± 1.7	-1.0	$(2.3 \pm 0.4) \times 10^{15}$	$(2.3 \pm 1.9) \times 10^{-8}$	$(1.1 \pm 0.2) \times 10^{-8}$	-6.5 ± 0.1	4.5 ± 0.2	4.6 ± 0.2
Methyl formate	$CH_3OCHO\,\nu=0$ oe − eo	109.0 ± 3.4	-1.0	$(1.5 \pm 0.1) \times 10^{16}$	$(1.5 \pm 1.2) \times 10^{-7}$	$(7.4 \pm 0.6) \times 10^{-8}$	-7.62 ± 0.04	3.9 ± 0.3	7.5 ± 0.6
Methyl formate	$CH_3OCHO\,\nu=0$ ee − oo	100.3 ± 3.0	-0.8	$(2.09 \pm 0.04) \times 10^{16}$	$(2.1 \pm 1.7) \times 10^{-7}$	$(1.05 \pm 0.02) \times 10^{-7}$	-7.7 ± 0.1	3.6 ± 0.2	7.7 ± 0.5
Methyl formate	$CH_3OCHO\,\nu=0$ oo − oe	46.0 ± 0.1	-0.9	$(3.35 \pm 0.02) \times 10^{16}$	$(3.3 \pm 2.7) \times 10^{-7}$	$(1.67 \pm 0.01) \times 10^{-7}$	-7.6 ± 0.2	5.0 ± 0.3	3.8 ± 0.2
Methyl formate	$CH_3OCHO\,\nu=0$ oo − ee	132.3 ± 3.4	-0.9	$(2.0 \pm 0.1) \times 10^{16}$	$(2.0 \pm 1.6) \times 10^{-7}$	$(9.9 \pm 0.5) \times 10^{-8}$	-7.38 ± 0.09	4.0 ± 0.1	8.0 ± 0.2
Methyl formate	$CH_3OCHO\,\nu=0$ eo − oe	75.6 ± 0.7	-0.9	$(1.39 \pm 0.02) \times 10^{16}$	$(1.4 \pm 1.1) \times 10^{-7}$	$(6.94 \pm 0.09) \times 10^{-8}$	-7.61 ± 0.08	3.8 ± 0.3	6.4 ± 0.5
Methyl formate	$CH_3OCHO\,\nu=0$ A	77.5 ± 0.2	-0.9	$(1.956 \pm 0.009) \times 10^{16}$	$(2.0 \pm 1.6) \times 10^{-7}$	$(9.78 \pm 0.05) \times 10^{-8}$	-7.62 ± 0.09	4.4 ± 0.2	5.6 ± 0.2
Methyl formate	$CH_3OCHO\,\nu=1$ oo − oe	173.2 ± 2.9	-1.0	$(1.23 \pm 0.04) \times 10^{16}$	$(1.2 \pm 1.0) \times 10^{-7}$	$(6.1 \pm 0.2) \times 10^{-8}$	-7.5 ± 0.2	4.5 ± 0.4	8.1 ± 0.7
Methyl formate	$CH_3OCHO\,\nu=1$ oo − ee	75.5 ± 8.6	-1.0	$(2.7 \pm 1.3) \times 10^{17}$	$(2.7 \pm 2.5) \times 10^{-6}$	$(1.3 \pm 0.6) \times 10^{-6}$	-6.2 ± 0.6	4.6 ± 0.6	5.2 ± 0.7
Methyl formate	$CH_3OCHO\,\nu=1$ A	75.0 ± 0.5	-1.0	$(6.0 \pm 0.2) \times 10^{16}$	$(6.0 \pm 4.8) \times 10^{-7}$	$(3.01 \pm 0.09) \times 10^{-7}$	-7.3 ± 0.2	4.6 ± 0.2	5.2 ± 0.2
Methyl formate	$CH_3OCHO\,\nu=1$ E	53.1 ± 0.1	-1.0	$(1.46 \pm 0.02) \times 10^{17}$	$(1.5 \pm 1.2) \times 10^{-6}$	$(7.3 \pm 0.1) \times 10^{-7}$	-7.3 ± 0.2	4.3 ± 0.3	4.7 ± 0.3

[a] Udjeli bazirani na stupčanoj gustoći vodika Leurini et al. (2013) (L) i Gibb et al. (2000) (G) za G327.3-0.3 te i i o za unutarnji i vanjski omotač NGC 6334 I. [b] Brzine naspram LSR.
[c] Srednje širine linija. [d] R omjeri usrednjeni preko detektiranih prijelaza za danu molekulu.

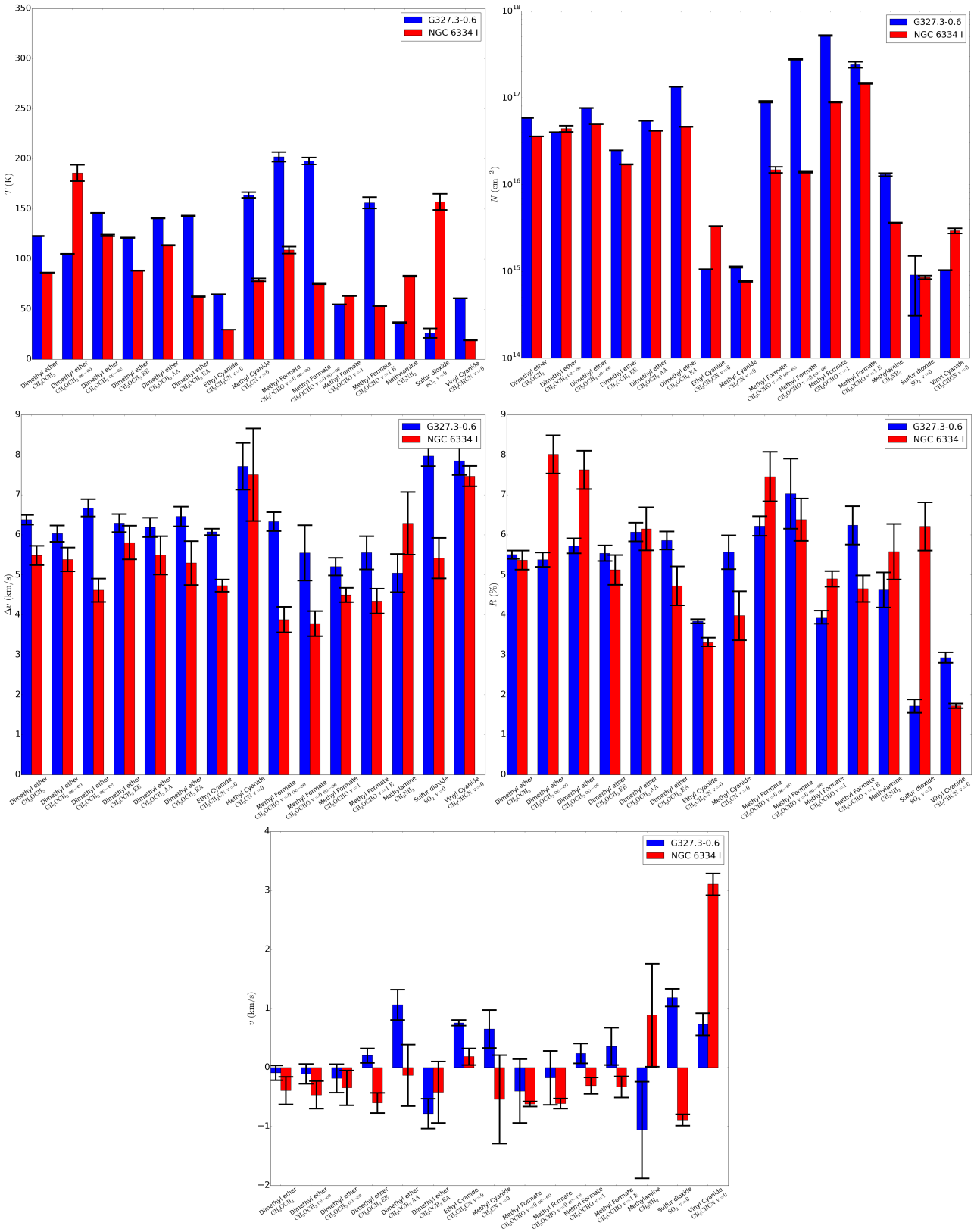

Slika S.8: Usporedba rezultata dobivenih rotacijskim i populacijskim dijagramima za oba izvora.

S.6 Zaključak

Analizirali smo milimetarske APEX spektre dviju vrućih jezgri G327.3-0.6 i NGC 6334 I. Izvedene temperature i stupčane gustoće odgovaraju vrijednostima iz literature za većinu molekula. U nekim je slučajevima određivanje precizne temperature plina i stupčane gustoće otežano velikim rasapom u podacima, što ukazuje na nepostojanje lokalne termodinamičke ravnoteže (LTE) i/ili efekte optičke dubine (Goldsmith & Langer 1999). Metoda koja je olakšala proces određivanja temperatura i stupčanih gustoća je uključivala rađenje odvojenih prilagodbi za različite paritete i simetrijske vrste. Ova je procedura smanjila rasap ali je povećala nepouzdanost podataka zbog malog broja podataka za velik broj molekula. Osim za metanol u G327.3-0.6, jasan utjecaj optičke dubine nije viđen. U izvorima smo pronašli sljedeće molekularne kandidate koji imaju dobro slaganje s vrijednostima iz literature: aceton, karbonil sulfid, dimetil eter, etanol, etil cijanid, mravlju kiselinu, keten, metanol, metil acetilen, metilamin, metil cijanid, metil format, sumporov dioksid, vinil cijanid kao i neke od njihovih najčešćih izotopologa. Pregršt kompleksnih molekularnih vrsta identificiranih u ciljanim izvorima ilustrira kemijsko bogatsvo vrućih jezgri kao stadija u nastanku zvijezda velike mase.

Intermission

This work is structured as follows:

In chapter *Introduction* we first give the motivation for studying hot molecular cores and describe their properties and then give an overview of the target hot molecular cores G327.3-0.6 and NGC 6334 I.

In chapter *Theory* we outline the theory necessary for analyzing and interpreting hot core spectra. In the first section, we establish a relation between the total power per unit bandwidth to the antenna temperature. In *Rotational and population diagrams* we describe the methods used in the molecular line analysis, while in *Quantum numbers* we discuss group theoretical properties of molecular spectra and their impact in determining upper state degeneracies for transitions. Finally, in *Velocities and line broadening* we describe line broadening mechanisms present in hot cores.

Observations towards the hot cores G327.3-0.6 and NGC 6334 I are described in chapter *Observations and data reduction* along with the methods used in the spectral line analysis.

In chapters *Results* and *Discussion* we give and analyze the results of the rotational and population diagram analysis for the hot cores G327.3-0.6 and NGC 6334 I.

In Appendix A, we show spectra of hot cores G327.3-0.6 and NGC 6334 I, while in appendices B and C we give bar plots of results for both sources made using the rotational diagram and population diagram method, respectively. The rotational and population diagrams are shown in Appendices D and E.

In Appendix F we comment on programs written for analysis of rotational and population diagrams.

1 Introduction

Massive young stellar objects (MYSOs) are stars having mass greater than 8 solar masses. While the formation of low-mass stars is a relatively well known process with distinct evolutionary stages (e.g. Dunham et al. 2014), for high-mass stars the same evolutionary sequence does not apply. Their evolutionary timescales are much shorter and they start to influence their surroundings sooner than lower-mass stars. Another interesting feature is that they arrive at the main sequence while still accreting matter.

In an early phase in their life, MYSOs begin to produce a lot of UV light, possibly accompanied by a strong stellar wind. This feedback is likely to change the structure of their environment and its chemistry (Garay & Lizano 1999).

1.1 Hot cores

Hot molecular cores (hereafter hot cores) are objects associated with the early stages of high-mass star formation (Garay & Lizano 1999; Kurtz et al. 2000). Hot cores and compact HII regions are embedded in larger-scale pockets of molecular gas of varying densities. The gas kinetic temperatures in hot cores range from 100 to $300\,\mathrm{K}$ (Gibb et al. 2000), while the masses and diameters are 200 to 300 $M_\odot$[9] (Garay & Lizano 1999) and $\leq 0.1\,\mathrm{pc}$[10] (Kurtz et al. 2000), respectively. Hot cores are believed to evolve into hyper/ultracompact HII regions, and ultimately into HII regions surrounding the newly formed high-mass star (Beuther et al. 2007). Hot cores are known for their rich chemistry and molecular line spectra at (sub)millimeter wavelengths. A summary of selected hot cores is given in Table 1.1.

Besides molecular gas, hot cores contain dust. The dust grain structure can be roughly divided into a nucleus of silicates and carbonaceous materials, and the icy mantle surrounding the nucleus. The icy grain mantle is composed of molecules like CO_2, H_2O and CH_3OH, and the evaporation of the mantle species enables the formation of more complex molecules in the gas phase (Ehrenfreund et al. 1998).

Gas-phase chemistry in a cold collapsing clump of gas differs from high temperature gas-phase chemistry. Brown et al. (1988) give a simple model of a hot core as a result of cold gas collapse lasting $> 10^6\,\mathrm{yr}$, after which the gas heats up abruptly within $\sim 100\,\mathrm{yr}$ under the influence of a central MYSO. During collapse, gas-phase species start to condensate on dust grains in the form of an icy mantle. Chemically, atoms C, N and O create molecular ices. By the end of mantle creation, its composition includes molecules like H_2O, CH_4, NH_3, CH_3CN and HCN.

As a result of the heating by the central source, H_2O starts to evaporate carrying material trapped in the ice with it. Brown et al. (1988) have shown that these freed

[9] Solar mass, $1\,M_\odot \sim 2 \times 10^{30}\,\mathrm{kg}$.
[10] Parsec, $1\,\mathrm{pc} \sim 3 \times 10^{16}\,\mathrm{m}$.

Table 1.1: Selected Galactic hot cores and their physical properties (adopted from Kurtz et al. (2000)).

Source Name	Distance (kpc)	T_{kin} (K)	Diameter (pc)	Mass[a] ($M_\odot$)	L_{IR}[a] ($L_\odot$)	Ref.[b] Code
Orion-KL	0.5	300	0.05	10	1.0 10^5	1
SgrB2N[c]	8.5	200	0.1	2000	6.5 10^6	2 3
SgrB2M[c]	8.5	200	0.1	2000	"	2
G5.89–0.39[c]	4.0	90	0.18	2800	7.1 10^5	4 5
G9.62+0.19	5.7	>100	0.059	55–160	4.4 10^5	6 7
G10.47+0.03[c]	5.8	150	0.078	2200	5.0 10^5	6 8 9 10
G10.62–0.38[c]	6.0	144	0.05	1100[d]	1.1 10^6	11 12
G19.62–0.23	3.5	230	0.032	450	1.6 10^5	13
G29.96–0.02	7.4	100	0.052	460	1.4 10^6	6 8 14
G31.41+0.31	7.9	110	0.080	2500	2.6 10^5	6 8 9
G34.26+0.15	3.8	250	0.066	1400	6.3 10^5	4 15 16 17 18
G45.07+0.13[c]	8.3	140	0.027	<7800	1.1 10^6	19
G45.12+0.13[c]	8.3	120	0.056	<37000	1.3 10^6	19 20
G45.47+0.05[c]	8.3	90	0.056–0.3	250	1.1 10^6	20
IRAS 20126+4104	1.7	200	0.012	10	1.3 10^4	21
DR 21(OH) MM1	3.0	>80	0.05	350	5.0 10^4	22 23
W3(H_2O)	2.2	220	0.014	10	1.0 10^5	24
W51 e2[c]	8.0	140	0.093	200–400	1.5 10^6	25 26
W51 e8[c]	8.0	130	0.096	<200	"	25 26
W51 N-Dust	8.0	200	0.1	400	"	25 26

molecules will survive in the gas phase for the first $10^4\,\mathrm{yr}$. This behavior was ascribed to the fact that all the remaining free atoms were already converted into hydrides with the abundance of ions such as H_3^+, He^+ and C^+ being small. Hence, ion-molecule interaction, whereby molecules are destroyed, is hindered. The reason for this is that at the high H_2 densities of hot cores, the fractional abundance of H_3^+ and He^+ - both being formed as a result of cosmic ray (CR) ionization - is inversely proportional to the density (Millar & Nejad 1985). The low abundance of He^+ leads to a diminished abundance of C^+ ions that are formed through the reaction

$$\mathrm{He^+ + CO \rightarrow C^+ + O + He.} \tag{1.1}$$

In addition to C, N and O, there is also H_2S in the ice that via a series of reactions forms SO. If the gas temperature is $T < 230\,\mathrm{K}$ SO forms SO_2 within 10^5 years (Charnley 1997). More precise models include a series of other reactions leading to many other compounds like dimethyl ether (CH_3OCH_3)(see Fig. 1.1). For many of them it has been shown that they require dust grains to form. These in-

clude species like methanol (CH_3OH), ketene (H_2CCO), acetaldehyde (CH_3CHO), formic acid (HCOOH), ethanol (CH_3CH_2OH), carbonyl sulfide (OCS), isocyanic acid (HNCO), formamide (NH_2CHO), vinyl cyanide (CH_2CHCN) and ethyl cyanide (CH_3CH_2-CN) (Charnley et al. 2004).

The aforementioned molecules have both different isotopologues and their isotopomers as well. Some of the different isotopologues can be present already during the ice mantle formation, and then be released into the gas phase and be incorporated into subsequent chemical reactions. Charnley et al. (2004) give an overview of theoretical relations between isotopomers that had one C atom replaced by ^{13}C expressed in units of concentration ratio of CO_2 vs. $^{13}CO_2$. For example, the following relationships for methanol and ethyl cyanide have been found

$$\left[\frac{CH_3OH}{^{13}CH_3OH}\right] = \left[\frac{CO_2}{^{13}CO_2}\right]_{ice} \tag{1.2}$$

$$\left[\frac{CH_3CH_2CN}{^{13}CH_3CH_2CN}\right] > \left[\frac{CO_2}{^{13}CO_2}\right]_{ice}, \tag{1.3}$$

where *ice* denotes the concentration ratio in the ice.

These relations suggest that ethyl cyanide shows a higher $^{12}C/^{13}C$ ratio than methanol. For comparison, Blake et al. (1984) found a ratio of $CH_3OH/^{13}CH_3OH \sim 15$ for OMC-1 , but predict a much larger ratio of ~ 40 because of methanol line saturation.

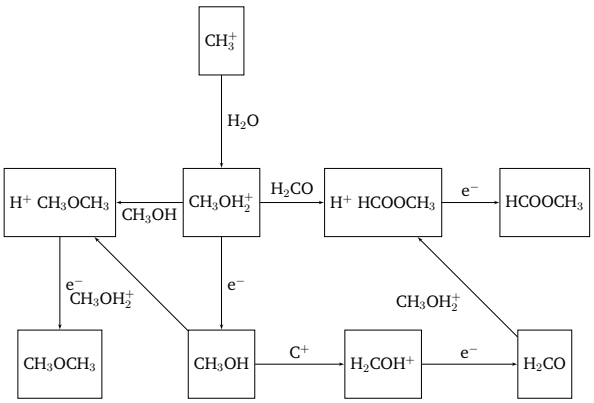

Figure 1.1: Some possible reactions that lead to the formation of dimethyl ether (CH_3OCH_3) and other chemically related species like methanol, for molecular cloud OMC-1. Adapted from Blake et al. (1987).

1.2 Target sources

In this work, we analyzed spectra of hot cores G327.3-0.6 and NGC 6334 I, which are further discussed in this section.

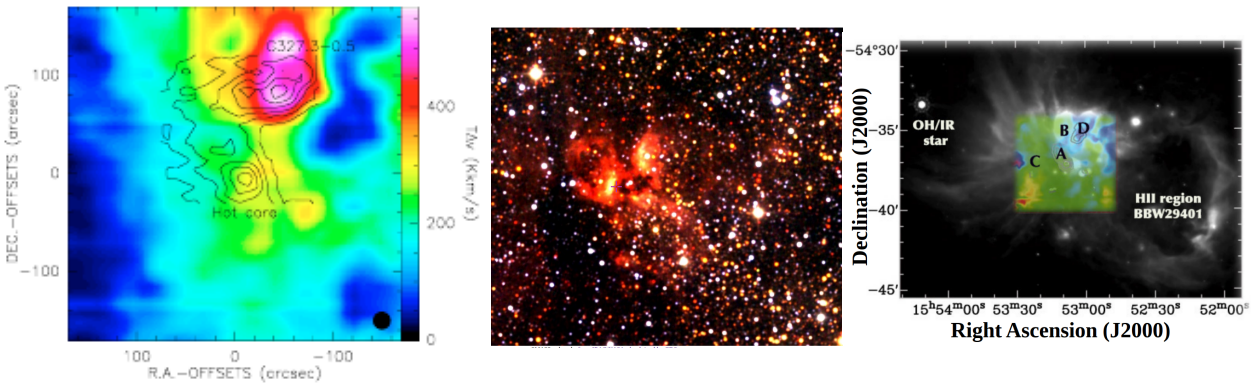

Figure 1.2: *Left panel:* ^{12}CO(3-2) emission shown with color, overlaid with contours showing the C^{18}O(3-2) emission toward the G327.3-0.5/G327.3-0.6 system (Wyrowski et al. 2006). *Middle panel:* 2MASS infrared image of $12.29' \times 12.29'$ region around G327.3-0.6 (Bonnarel et al. 2000; Boch & Fernique 2014). *Right panel:* First moment map of the CO(3-2) line emission (color image) superimposed on the MIPS 24 μm emission image (gray scale). Blue to red colors correspond to blue- and redshifted velocities. The gray contours represent the P-ArTéMiS 450 μm emission. Adopted from Minier et al. (2009).

1.2.1 G327.3-0.6

G327.3-0.6 is one of the most prominent hot cores in the Milky Way. It is found on the southern hemisphere, on coordinates $(\alpha_{J2000}, \delta_{J2000}) = (15\,\mathrm{h}\,53\,\mathrm{m}\,08.78\,\mathrm{s}, -54°37'01.20'')$ (constellation *Norma*), at the distance of $2.9\,\mathrm{kpc}$ (Simpson & Rubin 1990). Its total mass is $\sim 420\,M_\odot$, size ~ 0.1 pc and its bolometric luminosity is $0.5 - 1.5 \times 10^5\,L_\odot$[11] (Wyrowski et al. 2006). To the northwest of the hot core, there is the HII region G327.3-0.5. Images toward the two sources are shown in Fig. 1.2. Two other HII regions are also present near G327.3-0.6. To the northwest of the infrared dark cloud is RCW97 (positions B and D in right panel of Fig. 1.2). To the southwest, lies the HII region known as BBW29401. The velocity field around G327.3-0.6 can be divided, to a first approximation, across an east-west axis in two velocity components: a blueshifted velocity domain (–50 km/s) to the west, mainly located west of RCW97 (position D in right panel of Fig. 1.2); and a redshifted velocity domain (–46 km/s) to the east (position C, right panel in Fig. 1.2) (Minier et al. 2009). The systemic local standard of rest (hereafter LSR) velocity of G327.3-0.6 is $v_{\mathrm{LSR}} = -45\,\mathrm{km/s}$.

G327.3-0.6 is known for its rich line spectrum with Gaussian shaped lines. For that reason, this source is easier to analyze than more dynamic hot cores, like Sgr B2 near the Galactic Center. The significance of this source is that it has the possibility to become a hot core template for future high-resolution studies based on interferometric observations, particularly with the ALMA interferometer (Wyrowski et al. 2006). An important parameter for our further analysis is the H_2 column density of the source. By new estimates, the column density is $N_L(H_2) \sim 3{\times}10^{22}\,\mathrm{cm}^{-2}$ (Leurini et al.

[11] Solar luminosity, $L_\odot \sim 3.8 \times 10^{26}$ W.

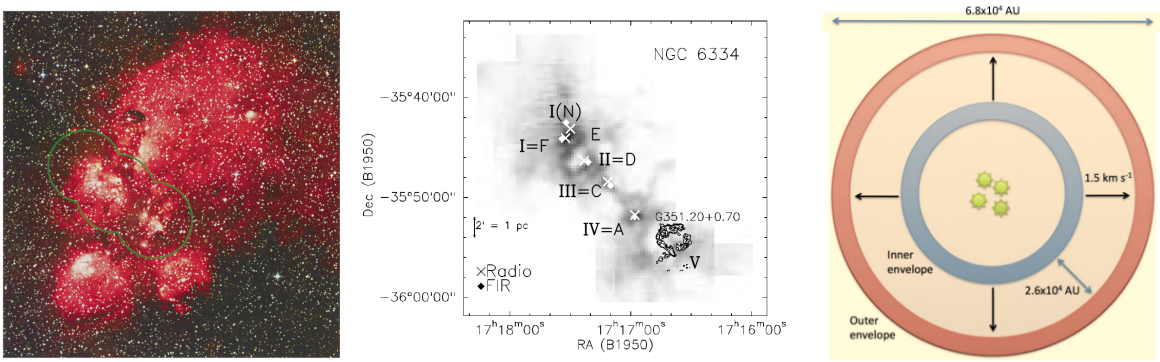

Figure 1.3: *Left panel:* Three-color (RGB filters) optical image of NGC 6334 with the area shown in the right panel outlined in green (Burton et al. 2000). *Middle panel:* CO(2-1) emission map of the NGC 6334 filament (darker is more intense). Compact continuum sources indicated are radio sources (crosses, alphabetical names), far-IR and submillimeter sources (diamonds, Roman numerals). Adopted from Kraemer & Jackson (1999). *Right panel:* Representation of the expanding envelope toward NGC 6334 I. Adapted from Morales Ortiz et al. (2014).

2013). An older estimate gives a somewhat higher value $N_G(H_2) \sim 3.2 \times 10^{23}\,\mathrm{cm}^{-2}$ (Gibb et al. 2000). For the sake of comparison, both numbers will be given, marked L and G - their respective first authors' initials.

1.2.2 NGC 6334 I

The source NGC 6334 I (shown in optical in the left panel in Fig. 1.3) is a relatively nearby high-mass star-forming region. The distance of NGC 6334 I is estimated to be $\sim 1.3\,\mathrm{kpc}$ (Reid et al. 2014; Chibueze et al. 2014). It is located in the constellation *Scorpio* at $(\alpha_{J2000}, \delta_{J2000}) = (17\,\mathrm{h}\,20\,\mathrm{m}\,53.35\,\mathrm{s}, -35°47'01.5'')$ (Sandell 2000). The systemic velocity of the source is $v_{\mathrm{LSR}} = -7.0\,\mathrm{km/s}$. NGC 6334 I is a hot core, already harboring at least one MYSO. Its total mass is $106\,M_\odot$, size ~ 0.1 pc and its bolometric luminosity is $1.38 \times 10^5\,L_\odot$ (Sandell 2000; Chibueze et al. 2014).

It is associated with an ultracompact HII region NGC 6334 F (see middle panel in Fig. 1.3) that has velocities of ionized gas from $v_{\mathrm{LSR}} \sim 2\,\mathrm{km/s}$ to the northeast to $v_{\mathrm{LSR}} \sim -8\,\mathrm{km/s}$ to the southwest (de Pree et al. 1995). The bubbles in the CO emission contain ionized or atomic gas, photodissociated by the UV radiation of the young OB stars in the region (Kraemer & Jackson 1999).

The source NGC 6334 I also has high-velocity outflows up to 70 km/s (Bachiller & Cernicharo 1990). Envelopes were found by Morales Ortiz et al. (2014) who conclude that the thermal pressure of ionizing photons from the ultracompact HII region inside NGC 6334 I is greater to than the ambient pressure of the envelope, resulting in expansion. Its outer envelope has $N(H_2) = (1.0 \pm 0.8) \times 10^{23}\,\mathrm{cm}^{-2}$ while its inner envelope has $N(H_2) = (2 \pm 1) \times 10^{23}\,\mathrm{cm}^{-2}$ (see right panel in Fig. 1.3). A velocity gradient of $1.5\,\mathrm{km/s}$ exists between the envelopes, but they emphasize that

these two velocity components are probably the two extremes of a gradual change in velocity through the envelope. The CR ionization increases outward, suggesting that the main source of ionization lies outside NGC 6334 I. While ionization in the outer envelope is dominated by CRs, the ionization in the inner envelope may have a contribution from X-ray emission originating in the interior of NGC 6334 I (Ezoe et al. 2006). Morales Ortiz et al. (2014) also argue that the abundance of molecular ions is expected to be lower toward the very central region of NGC 6334 I because of the lower cosmic ray ionization.

Schilke et al. (2006) have conducted a comparative analysis of our target sources. Their results are summarized in Table 1.2. For example, they find that the colder components of methanol (CH_3OH) and methyl cyanide (CH_3CN) have an order of magnitude greater column density than in G327.3-0.6. Sulfur dioxide (SO_2) is an order of magnitude more abundant and 100 K warmer in G327.3-0.6 than in NGC 6334 I. On the other hand, methyl formate (CH_3OCHO) and dimethyl ether (i.e. warmer component of CH_3OCH_3 in NGC 6334 I) do not follow this trend, having the same column densities and similar temperatures in both sources.

The next chapter describes the theoretical background needed for analysis and interpretation of hot core spectra.

Table 1.2: A comparative study of G327.3-0.6 and NGC 6334 I (borrowed from Schilke et al. (2006)). The original caption explains numbered comments: (1) Based on one or a few lines only; (2) based on weak or partially blended lines only; (3) includes lines of the vibrationally excited state; (4) includes optically thick lines; (5) based on $C^{34}S$ assuming $^{32}S/^{34}S=23$.

Line	Size	T_{ex}	N(mol)	Δv	Comment
	$''$	K	cm^{-2}	km s^{-1}	
NGC 6334(I)					
c-C_2H_4O	ext	150	4.0 (14)	3.0	1
C_2H_5CN	ext	150	2.0 (15)	5.0	2
CH_3CN	1.5	200	1.5 (17)	4.0	3, 4
	ext	50	1.0 (15)	4.0	
CH_3OCH_3	1.2	200	2.0 (18)	3.0	4
	ext	50	1.5 (16)	5.0	
CH_3OCHO	1.5	200	1.0 (18)	3.0	4
CH_3OH	1.5	150	5.0 (18)	3.0	4
	ext	50	3.0 (16)	5.0	
CS	ext	150	2.5 (15)	3.0	1, 5
HNCO	1.5	200	5.0 (16)	5.0	1
N_2H^+	ext	50	5.0 (13)	5.0	1
NH_2CHO	ext	150	1.0 (14)	3.0	
SO	ext	150	1.0 (15)	5.0	1
SO_2	1.5	150	2.0 (17)	3.0	4
G327.3-0.6					
c-C_2H_4O	ext	150	8.0 (14)	5.0	1
C_2H_5CN	1.5	200	3.0 (17)	3.0	
	ext	50	8.0 (15)	3.0	
CH_3CN	1.1	300	5.0 (17)	4.0	3, 4
	ext	50	5 (14)	4.0	
CH_3OCH_3	ext	200	1.0 (16)	3.0	2
CH_3OCHO	1.5	150	2.0 (18)	3.0	2
CH_3OH	ext	50	2.0 (17)	5.0	1
HNCO	ext	150	1.0 (15)	5.0	1
N_2H^+	ext	50	3.0 (14)	5.0	1
NH_2CHO	ext	150	3.0 (14)	5.0	2
SO_2	1.0	250	2.0 (18)	8.0	4

2 Theory

In this chapter we give an overview of the theory necessary for analyzing and interpreting hot core spectra. In the first section, we establish a relation between the total power per unit bandwidth to the antenna temperature. In *Rotational and population diagrams* we describe the methods used in the molecular line analysis analysis, while in *Quantum numbers* we discuss group theoretical properties of molecular spectra and their impact in determining upper state degeneracies for transitions. Finally, in *Velocities and line broadening* we describe line broadening mechanisms present in hot cores.

2.1 Antenna Temperature

In this section we derive the antenna temperature, which is related to power per unit bandwidth. Power pattern of an antenna is the power received per unit solid angle of an antenna. It is useful to normalize the power pattern $P(\theta, \phi)$ with $P_{\max}$ being the maximum of P_n over all angles

$$P_n(\theta, \phi) = \frac{P(\theta, \phi)}{P_{\max}}. \tag{2.1}$$

Following derivation in Wilson et al. (2009), we define the beam solid angle Ω_A of an antenna as

$$\Omega_A = \oint P_n(\theta, \phi)\, \mathrm{d}\Omega, \tag{2.2}$$

where the integral in solid angle Ω goes over the whole sphere. If an ideal antenna were to exist, the beam solid angle would represent an area of the sky from which the antenna could receive signals: $P_n = 1, \forall(\theta, \phi) \in \Omega_A$ and 0 otherwise. In a realistic antenna there exists a main lobe - an interval in θ and ϕ where the normalized power pattern has considerably larger values than for other parts of the solid angle. For the main beam, we can define the main beam solid angle as

$$\Omega_{MB} = \int_{\text{main lobe}} P_n(\theta, \phi)\, \mathrm{d}\Omega. \tag{2.3}$$

Another useful quantity is the directive gain

$$G(\theta, \phi) = \frac{4\pi P(\theta, \phi)}{\oint P(\theta, \phi)\, \mathrm{d}\Omega}. \tag{2.4}$$

This is the gain relative to a lossless isotropic source. The maximum directive gain $G_{\max}$ can be expressed via Ω_A as

$$G_{\max} = \frac{4\pi}{\Omega_A}. \tag{2.5}$$

If a great portion of power enters not from the main lobe but through side lobes, we are near the shortest observable wavelength. For the antenna to function as a

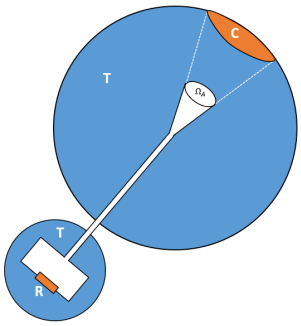

Figure 2.1: A sketch of the antenna, based on a figure from Wilson et al. 2009.

direction measuring device, power must be concentrated in the main lobe. Another useful quantity is the effective aperture of an antenna, A_e. It is the fraction of power that is intercepted by an antenna, that is, the ratio of intercepted power, P_e, and the norm of the averaged Poynting vector, $|\langle \mathbf{S} \rangle|$, i.e. $A_e = P_e/|\langle \mathbf{S} \rangle|$.

The antenna (see Fig. 2.1), the receiver R and the radiating surface C subtending an angle Ω_A are enclosed in a blackbody at temperature T. In thermodynamic equilibrium, C radiates in the frequency interval $\Delta\nu$ the intensity I_ν. Assuming long enough wavelengths (i.e. $h\nu/kT \ll 1$, where h and k are the Planck and Boltzmann constants, respectively), the Rayleigh-Jeans approximation can be used

$$I_\nu = \frac{2kT\Delta\nu}{\lambda^2}. \tag{2.6}$$

As only one polarization is recorded, the antenna collects the total power of

$$W_\nu = A_e \frac{kT}{\lambda^2} \Delta\nu \Omega_A. \tag{2.7}$$

If the antenna is connected to a resistor of resistance R, the Nyquist theorem gives us the transmitted power $L\Delta\nu$

$$L\Delta\nu = kT\Delta\nu. \tag{2.8}$$

Only a fraction thereof is intercepted by the surface C

$$L'\Delta\nu = kT\Delta\nu G_{\max} \frac{\Omega_A}{4\pi}. \tag{2.9}$$

In thermodynamic equilibrium, $W = L'\Delta\nu$. This relation gives us the relation between $G_{\max}$ and A_e

$$G_{\max} = \frac{4\pi A_e}{\lambda^2}. \tag{2.10}$$

Using the definition of directivity from Eq. (2.5), we get the antenna theorem

$$A_e \Omega_A = \lambda^2. \tag{2.11}$$

If we observe a brightness distribution $B_\nu(\theta, \phi)$ in the sky, the total power per unit bandwidth is

$$P_\nu = \frac{A_e}{2} \int B_\nu(\theta, \phi) P_n(\theta, \phi) \, \mathrm{d}\Omega. \tag{2.12}$$

Again invoking the Nyquist theorem, we can relate the total power per unit bandwidth,P_ν, to the antenna temperature, T_A,

$$kT_A = P_\nu. \tag{2.13}$$

This temperature must be corrected for the fact that a part of the power received by the telescope originates from the ground (an effect called spillower). To take this into account, the antenna pattern can be divided into a normal diffraction pattern (denoted Ω_D) and a part where spillower plays a great role (Kutner & Ulich 1981). This way, a main-beam efficiency can be defined as

$$\eta_{MB} = \frac{\int\limits_{\Omega_D} P_n(\theta,\phi)\,\mathrm{d}\Omega}{\int\limits_{2\pi\ \mathrm{sr}} P_n(\theta,\phi)\,\mathrm{d}\Omega}. \tag{2.14}$$

At the frequencies observed with the APEX telescope in the present study, $\eta_{MB} \sim 0.75$[12]. The corresponding main-beam antenna temperature is given by

$$T_{MB} = \frac{T_A}{\eta_{MB}}. \tag{2.15}$$

Another contribution comes from the fact that the solid angle subtended by the source need not be equal to the main beam solid angle. This effect is measured through the so-called beam dilution (filling) factor, f. The combined effect is the beam-source coupling efficiency

$$\eta = \eta_{MB} f. \tag{2.16}$$

In the present study, we make an approximation $\eta \sim \eta_{MB}$.

2.2 Rotational and population diagrams

If the source has an optical depth of τ, its brightness temperature will be given by (Goldsmith & Langer 1999)

$$T_B = \frac{h\nu/k}{e^{\frac{h\nu}{kT}} - 1} \frac{1 - e^{-\tau}}{\tau} \tau. \tag{2.17}$$

The optical depth of the transition from lower l to upper state u is

$$\tau = \frac{h}{\Delta v} N_u B_{ul} (e^{\frac{h\nu}{kT}} - 1). \tag{2.18}$$

In this equation, Δv is the full width at half-maximum of a line measured in velocity units, N_u the upper state column density and B_{ul} is the Einstein coefficient for the transition ul. Expressing the Einstein B_{ul} coefficient by A_{ul} and integrating over the whole line with Δv replaced by $\mathrm{d}v$ we get

$$N_u = \frac{8\pi k \nu^2}{hc^3 A_{ul} \eta} \int T_A\,\mathrm{d}v \frac{\tau}{1 - e^{-\tau}}. \tag{2.19}$$

[12] http://www.apex-telescope.org/telescope/efficiency/

The last term in Eq. (2.19) is the optical depth correction factor C_τ. Adding the degeneracy of the upper state g_u we get the column density N from the Boltzmann distribution

$$\frac{N_u}{N} = \frac{g_u}{Z} e^{-\frac{E_u}{kT}}, \tag{2.20}$$

where Z is the partition function, while g_u is the upper state energy. We can replace units from v to ν in Eq. (2.19). Taking a logarithm of Eq. (2.20), assuming negligible influence of background temperature and optically thin emission we get to the operational version of Eq. (2.19) defining the rotational diagram method

$$\ln(N/Z) - \frac{E_u}{kT} = \ln \frac{\gamma \nu[\mathrm{MHz}] \int T_A[\mathrm{K}] \mathrm{d}\nu[\mathrm{MHz}]}{g_u \eta A_{\mathrm{ul}}[\mathrm{s}^{-1}] \nu^2[\mathrm{MHz}^2]}. \tag{2.21}$$

The constant $\gamma \sim 6.37\,[\mathrm{cm}^{-2}]$ carries unit conversion to MHz and incorporates change to column density in cm^{-2}. In the figures shown in this work, we will shorten the right hand side of Eq. (2.21) to

$$\ln \frac{N_u}{g_u}. \tag{2.22}$$

The partion functions, Z, were taken from *Splatalogue*[13] (Remijan et al. 2007) for most of the detected molecules. This web service gives partition functions calculated only on certain temperatures. The rotational part of the partition function carries a factor of $T^{3/2}$:

$$Z(T) = A T^{3/2} Z_{\mathrm{vib}}(T). \tag{2.23}$$

A better fit was made by approximating the vibrational partition function by an exponential. This approximation made fitting easier and fits well to the data, even though its actual form is complex (Kubo 1965):

$$Z(T) = A T^{3/2} e^{\alpha T}. \tag{2.24}$$

Its error is estimated as

$$M_Z = Z \sqrt{\left(\frac{M_A}{A}\right)^2 + (T M_\alpha)^2 + \left(\frac{3}{2T} + \alpha\right)^2 M_T^2}, \tag{2.25}$$

where M_A, M_α and M_T are errors in fit parameters A and α, and the temperature, respectively.

Column density, with its respective error, in units of cm^{-2} can thus be calculated:

$$N = Z e^{\ln(N/Z)} = Z e^x \tag{2.26}$$

$$M_N = N \sqrt{\frac{M_Z^2}{Z^2} + M_x^2}. \tag{2.27}$$

[13] www.splatalogue.net

In case the partion function was not available in the *Splatalogue* database, it was approximated by $Z(T) \sim Z_{\mathrm{rot}}(T)$. This approach was needed for e.g. methanol, with symmetry number $\sigma = 1$, giving:

$$Z \sim \sqrt{\pi} \left(\frac{k}{h}\right)^{3/2} \frac{10^{-9} T^{3/2}}{\sqrt{A[\mathrm{MHz}] B[\mathrm{MHz}] C[\mathrm{MHz}]}} \tag{2.28}$$

$$M_Z = Z \frac{3}{2} \frac{M_T}{T}. \tag{2.29}$$

A, B and C are rotational constants.

The H_2 densities required to thermalize the level populations vary from $10^8\,\mathrm{cm}^{-3}$ for $K = \pm 3$ levels to $10^6\,\mathrm{cm}^{-3}$ for $\Delta K = \pm 1$ ladders (Goldsmith & Langer 1999). The different transitions also have very different absorption coefficients, so that their optical depths vary considerably for a given molecular abundance. Hence, molecules were separated by quantum numbers and symmetry species. This expanded version of a diagram is called a population diagram.

2.3 Quantum numbers

The principal quantum number N, total angular momentum quantum number J, projection of the angular momentum on the principal axis K and vibrational quantum number ν are the simplest quantum numbers we encounter in molecular spectra. The general definition of the upper state degeneracy is (e.g. Mangum & Shirley 2015)

$$g_u = (2J_u + 1) g_K g_I, \tag{2.30}$$

where J_u is the total angular momentum of the upper state and g_K and g_I the K level degeneracy and the nuclear spin degeneracy, respectively. In cases where g_u could not be found in the literature, we calculated g_u as described below. Depending on the structure of the molecule, its quantum state definition might require some additional quantum numbers. For molecules like acetone and dimethyl ether (DME), the problem lies in two methyl groups, each capable of torsion. This type of molecules can be treated as a $C_{3v}^{-} \otimes C_{3v}^{+}$ group, each part of the direct product correspoding to difference or sum of methyl group position angles, respectively (Myers & Bright Wilson 1960). The C_{3v} group has three irreducible representations: A_1, A_2 and E. Symmetry species (of e.g. DME) are thus EE, EA_1, EA_2, A_1E etc. For simplicity and accordance with Splatalogue, we omit subscripts 1 and 2 (Clark et al. 1979). Both groups C_{3v}^{-} and C_{3v}^{+} give their respective quantum numbers, K_- and K_+. Splatalogue names them as K_a and K_c quantum numbers. They are projections of angular momentum on a and c principal axes of the Rho Axis Method Hamiltonian (Xu & Lovas 1997). We can classify transitions according to their parity for the upper and lower state. For example, transition $25_{1\,25} - 24_{2\,22}\,AA$ would be classified in two different ways: as an AA species and as an $oo - ee$ transition.

Methanol has one methyl group and therefore only A and E symmetry species. For this molecule Splatalogue gives, beside K_a and K_c quantum numbers, parities of the A state (Xu & Lovas 1997) and no sign for the E state. Examples are: $4_{3\,2} - 5_{2\,3}$ ++ for $A_+ - A_+$ and $16_{5,12} - 17_{4,13}$ for E. To simplify further discussion, we give Splatalogue quantum number codes for the detected molecules with examples in Table 2.1. The F quantum number is the total angular momentum: a sum of J and nuclear spin I. Quantum numbers were also used in determining the g_K and g_I degeneracies. We employed the corrections given in Table 2.2. This information is given in Turner (1991). For molecules with C_{3v} symmetry, g_I takes the form (Gordy & Cook 1984)

$$g_I = \begin{cases} \frac{\sigma}{3}\left(1 + \frac{2}{(2I+1)^2}\right) & K \in 3\mathbb{N} \\ \frac{\sigma}{3}\left(1 - \frac{1}{(2I+1)^2}\right) & K \notin 3\mathbb{N} \end{cases}. \tag{2.31}$$

The only C_{3v} molecule for which this analysis was necessary was methyl cyanide ($\sigma = 3$, $I = 1$). For methyl cyanide, we can approximate $\frac{1}{(2I+1)^2} \approx 0$ giving $g_I \approx 1$.

Table 2.1: The Splatalogue quantum number description with selected examples.

QN code	quantum numbers	examples
101	N	Thioformylium
102	N J	Thioxoethenylidene
202	N K	Methyl acetylene, methyl cyanide
303	N K_a K_c	Ethyl cyanide, ketene,
1202	J	Silicon Monoxide
1404	N K_a K_c v	Dimethyl ether, methyl formate

Table 2.2: K level degeneracies, g_K, and nuclear spin degeneracies, g_I, for selected types of molecules.

Type		g_K	g_I
2 Methyl groups	ee or oo; AA	6	1
2 Methyl groups	ee or oo; AE	2	1
2 Methyl groups	ee or oo; EA	4	1
2 Methyl groups	ee or oo; EE	16	1
2 Methyl groups	oe or eo; AA	10	1
2 Methyl groups	oe or eo; AE	6	1
2 Methyl groups	oe or eo; EA	4	1
2 Methyl groups	oe or eo; EE	16	1
1 Methyl group	A	1	2
1 Methyl group	E	2	1
C_{3v} symmetry	$K = 0$	1	1[a]
C_{3v} symmetry	$K \neq 0$	2	1[a]

[a] An approximation for methyl cyanide, refer to Eq. (2.31) for the whole expression.

2.4 *Velocities and line broadening*

When discussing velocities, we cannot simply take the barycenter of the Solar System as the rest frame (barycentric standard-of-rest) because the Sun has peculiar velocity compared to objects at the same distance from the Galactic Center. Data from which the standard solar motion has been eliminated are said to refer to the local standard of rest (LSR). This is a point coinciding with the position of the Sun and moving with the local circular velocity around the Galactic Center (Wilson et al. 2009). A spectral line can be shifted by a certain amount from that velocity. In calculating velocities care should be taken to choose the correct velocity definition. Here, we employ the so-called radio velocity convention[14]. The usual formula for relating radial velocities to frequencies in special relativity is (e.g. Carroll & Ostlie 2007).

$$\frac{\nu}{\nu_{ul}} = \sqrt{\frac{1 - v/c}{1 + v/c}}, \tag{2.32}$$

where ν is the observed frequency, and ν_{ul} is the laboratory frequency of a line. Expanding the square root we get

$$\frac{\nu}{\nu_{ul}} = 1 - \frac{v}{c} + O\left(\frac{v^2}{c^2}\right). \tag{2.33}$$

Solving for v we arrive at

$$v_{\rm radio} = c\frac{\nu_{ul} - \nu}{\nu_{ul}}. \tag{2.34}$$

The linewidth (here defined as the FWHM) transformed to m/s is

$$\Delta v = c\frac{\Delta\nu}{\nu_{ul}}. \tag{2.35}$$

As can be seen from Eq. (2.35), this convention is suitable because equal separations in frequency mean equal separations in velocity. We can hence create a velocity unit scale for spectra. It is also possible to estimate what fraction of the linewidth is due to thermal (Doppler) and natural line broadening. Converting Eq. (9.61) in Carroll & Ostlie (2007) to velocities and substituting numbers gives that natural line broadening is of the order

$$\Delta v_{\rm nat} \sim \frac{A_{ij}[{\rm s}^{-1}]}{\nu[100{\rm GHz}]}{\rm mm/s}. \tag{2.36}$$

Hence, the natural broadening is negligible compared to the observed widths of radio spectral lines observed from (high-mass) star-forming cores (e.g. see Table 1.2 for typical line widths in hot cores). If we define m as mass of the molecule, we can use the expression based solely on thermal broadening

$$R = \sqrt{\frac{2kT\ln 2}{m}}\frac{2}{\Delta v}, \tag{2.37}$$

[14] See https://www.iram.fr/IRAMFR/ARN/may95/node4.html for further discussion.

with its respective error

$$M_R = R\sqrt{\left(\frac{M_T}{2T}\right)^2 + \left(\frac{M_{\Delta v}}{\Delta v}\right)^2} \tag{2.38}$$

to estimate the ratio of thermal-to-observed line broadening. If this ratio is small, i.e. $R \ll 1$, collisional broadening or turbulence is present in the source. In the ISM, turbulent broadening is important (Larson 1981). The effects of gravitational contraction and star formation increase the line widths (Plume et al. 1997).

Observations towards the hot cores G327.3-0.6 and NGC 6334 I are described in the following chapter along with the methods used in the spectral line analysis.

3 Observations and data reduction

The observations of hot cores G327.3-0.6 and NGC 6334 I presented in this work were carried out with the *Atacama Pathfinder EXperiment*, or APEX, in Llano de Chajnantor, Northern Chile. The altitude of the site is $5105\,\mathrm{m}$, and the dish diameter is $12\,\mathrm{m}$. The instrument used was the *Swedish Heterodyne Facility Instrument* - SHeFI. The data are publicly available from the APEX data archive[15]. The observations toward G327.3-0.6 were taken as a part of the 081.F-9602(A) project, span the observed frequencies $213\,\mathrm{GHz}$ to $268\,\mathrm{GHz}$, $337 - 338\,\mathrm{GHz}$ and $350 - 351\,\mathrm{GHz}$ (Vassilev et al. 2008). The source NGC 6334 I was observed under the project O-091.F-9314A-2013 (unpublished) in the frequency range from 219 to $227\,\mathrm{GHz}$. For the hot core G327.3-0.6, the telescope was pointed toward the coordinates $(\alpha_{J2000}, \delta_{J2000}) = (15\,\mathrm{h}\,53\,\mathrm{m}\,08.19\,\mathrm{s}, -54°37'06.6'')$, while for NGC 6334 I the target position was at $(\alpha_{J2000}, \delta_{J2000}) = (17\,\mathrm{h}\,20\,\mathrm{m}\,53.44\,\mathrm{s}, -35°46'57.9'')$.

The spectral line data were reduced using the IRAM software package CLASS. A linear baseline was subtracted from the line-free parts of each individual spectrum with the BASE 1 command, with visible lines excluded by SET WINDOW. The spectra were then averaged to a single measurement for a given frequency band by weighting according to the integration time. An example of such a procedure's result is shown in Fig. 3.1, while the resulting spectra are shown in appendix A. The RMS noise was recorded as σ_{RMS}. The root -mean-square scatters, σ_{RMS}, plotted for every fre-

[15] http://www.apex-telescope.org/observing/archiving/

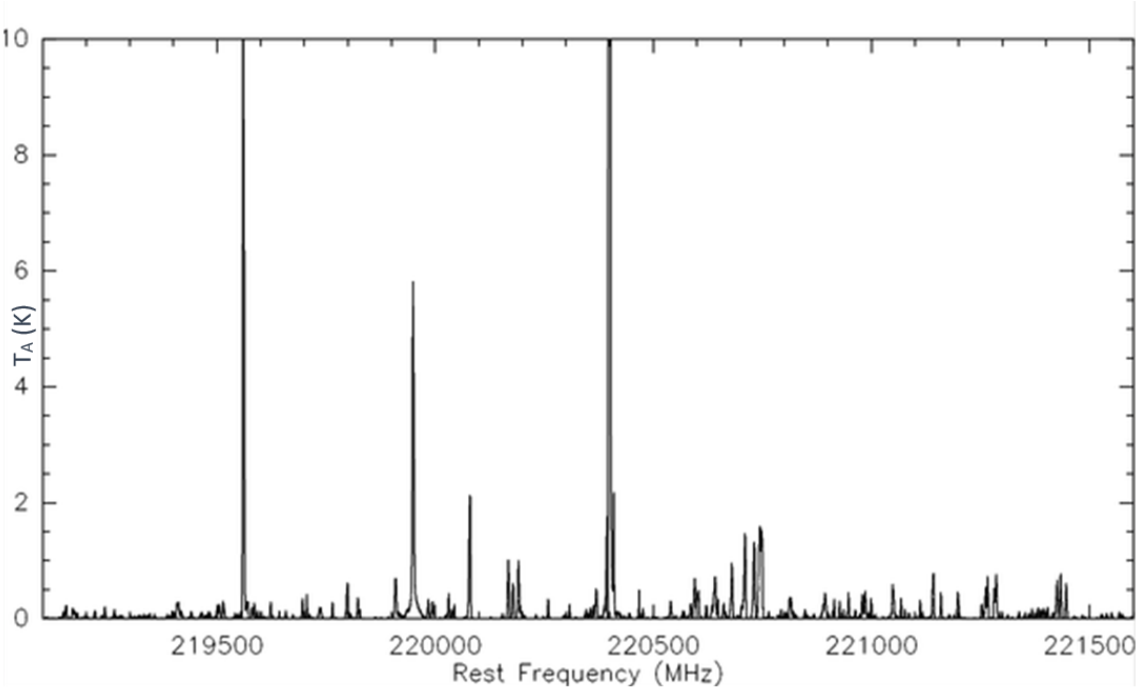

Figure 3.1: Spectra of NGC 6334 I in the frequency range [219,220] GHz after the baseline was subtracted.

Table 3.1: Results of the calculation of the upper state degeneracies for transitions for which Splatalogue does not tabulate them.

Name	Chemical formula	ν_{ul} (MHz)	Transition	g_u
G327.3-0.6				
Acetone	$(CH_3)_2CO$ $\nu = 0$	229127.3761	$12_{10\,2} - 11_{9\,2}$ EE	200
Methyl cyanide	CH_3CN $\nu = 0$	220594.4231	$12_6 - 11_6$	50
NGC 6334 I				
Acetone	$(CH_3)_2CO$ $\nu = 0$	220551.1144	$12_{8\,5} - 11_{7\,5}$ EE	200
Acetone	$(CH_3)_2CO$ $\nu = 0$	223732.8258	$12_{9\,4} - 11_{8\,4}$ EE	200
Acetone	$(CH_3)_2CO$ $\nu = 0$	224724.3324	$12_{10\,3} - 11_{9\,2}$ EA	50
Methyl cyanide	CH_3CN $\nu = 0$	220594.4231	$12_6 - 11_6$	50

quency range for both sources are shown in Fig. 3.2. Spectral lines were fitted with Gaussian profiles and exported for analysis as ASCII files. A total of 2848 lines were fitted for G327.3-0.6 and 636 lines for NGC 6334 I. A program was written in *Python* (see appendix F) for downloading spectral line data from the Splatalogue database. The program was based on Magnus Persson's Python script *Splatsearch.py*[16]. It gave 11640 line candidates for G327.3-0.6 and 2097 line candidates for NGC 6334 I. In this programming language, we also wrote a routine for further analysis and plotting. The spectroscopic databases used were the Cologne Database for Molecular Spectroscopy (CDMS; Müller et al. 2005) and Jet Propulsion Laboratory (JPL; Pickett et al. 1998) molecular spectroscopy database. The following cuts were made in the data. To avoid confusion, lines with multiple different molecular candidates were removed before plotting, as well as the lines whose $\sigma = T_A/\sigma_{\mathrm{RMS}}$ was less than 3 or their width or area relative errors were greater than 0.5.

Plots of all the transitions' velocity vs. σ are shown in Fig. 3.3. As shown in the figure, the weakest lines spread more over a large interval of velocites for small σ, justifying the $\sigma \geq 3$ criterion. We list the cases for which Splatalogue had no data on the upper state degeneracy in Table 3.1, along with calculated upper state degeneracies.

In the following chapter, we give the results of the rotational and population diagram analysis for the hot cores G327.3-0.6 and NGC 6334 I.

[16] http://vilhelmp.blogspot.com/2011/10/querying-splataloguenet-with-python.html

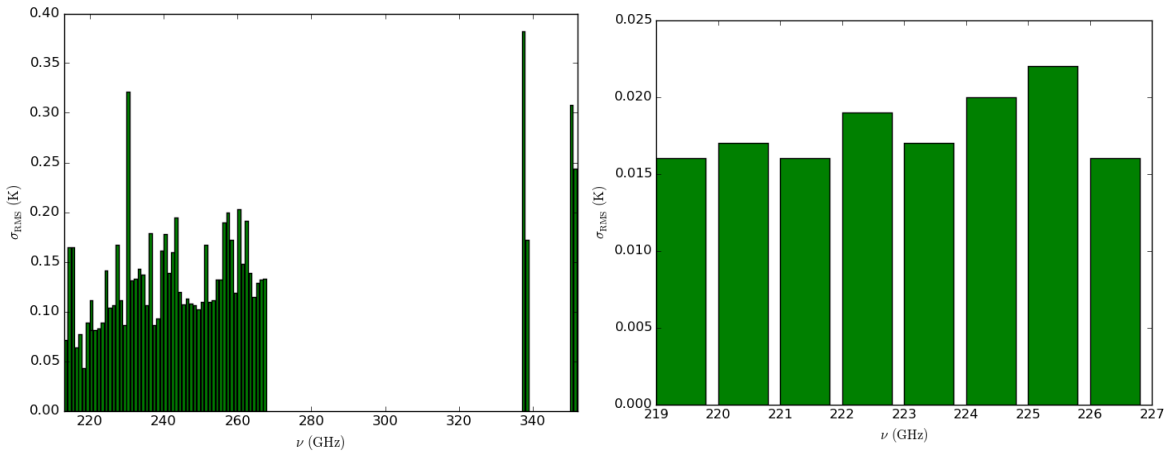

Figure 3.2: RMS noise levels versus frequency for G327.3-0.6 (left panel) and NGC 6334 I (right panel).

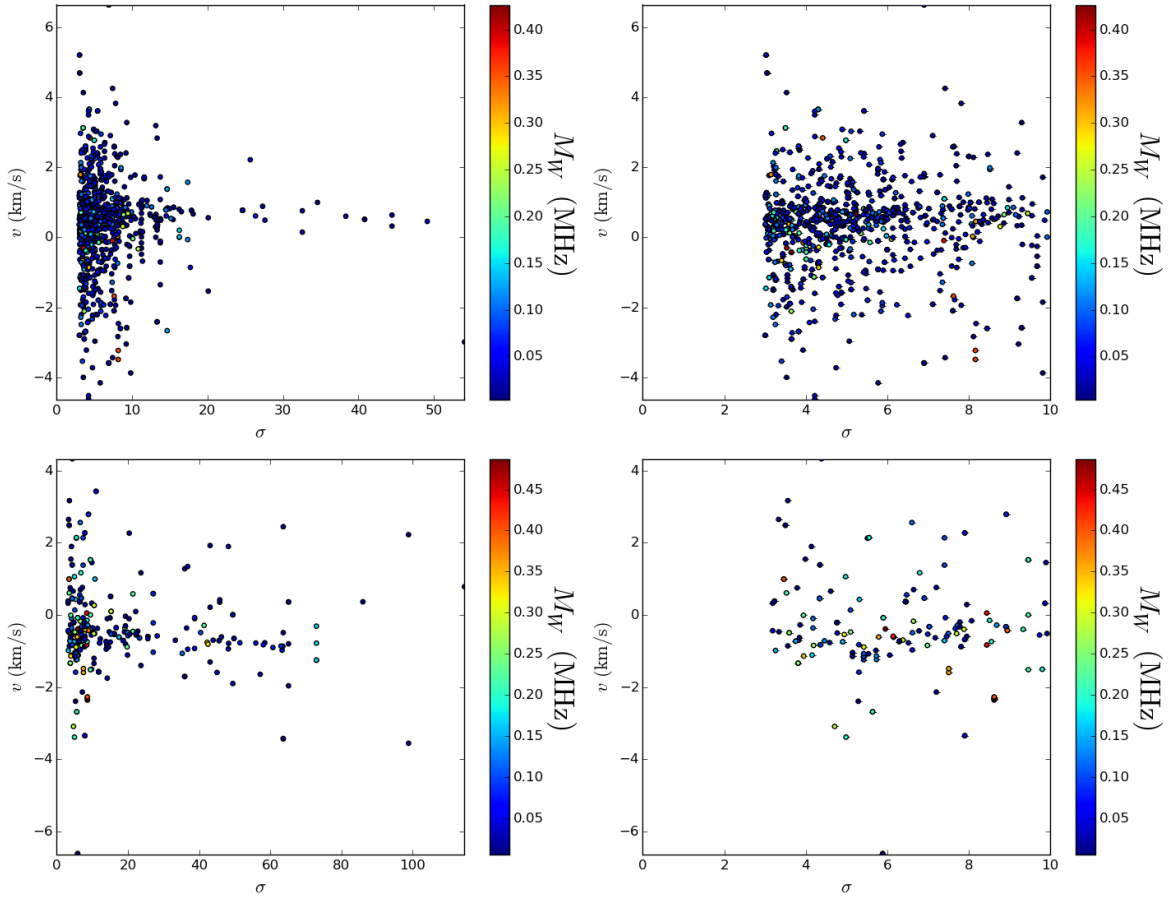

Figure 3.3: Line velocities plotted against σ with width errors M_W shown as a colorbar. The panels on the right are cropped to the range $\sigma \in [3, 10]$. The upper panels show plots for G327.3-0.6, the lower panels show plots for NGC 6334 I.

4 Results

In the analysis, it was necessary to remove transitions listed in Table 4.2. Without removing those points, rotational diagrams would not produce good fits to the data. However, not evey point in the rotational diagram could be removed. A reasonable criterion, in order not to remove points that could be due to non-LTE effects, was a cut based on velocity: the only points on the graph with velocities greater than 2 km/s or around -4 km/s that did not correspond to parts of the population diagrams that could be easily fitted. Upper state energy range was chosen to be from 0 to 450 K, except for acetone and methylamine for G327.3-0.6 and acetone and vinyl cyanide $CH_2CH^{13}CN$ for NGC6334 I, where a clear line was visible only up to 200 K, after which it became too scattered for the fit. The gas kinetic temperatures derived through the rotational diagram method are given in Table 4.1. The table has the Pearson coefficient (ρ) next to every species. In making this analysis, a threshold of $\rho > 0.5$ was employed and that had unphysical column density (i.e. higher than $10^{20}\,\mathrm{cm}^{-2}$) or temperatures (i.e. above 400 K) were omitted as well. The derived gas temperatures are in the range from 50 to 150 K, with exceptions of trans-ethanol (~ 350 K) for G327.3-0.6. Column densities are in a reasonable range of $10^{12} - 10^{17}\,\mathrm{cm}^{-2}$ for both sources. Distributions of partition functions are given in Fig. 4.1. Figures B.1-E.2 in appendices B and C show the rotational and population diagram method results for the sources G327.3-0.6 and NGC 6334 I, respectively. We give rotational and population diagrams for the target sources in appendices C and D (Figs. D.1-E.2). Figures C.1 and C.2 show the results of the population diagram analysis. Comparison of the two sources is given in Fig. 4.2. The results are discussed in the next chapter.

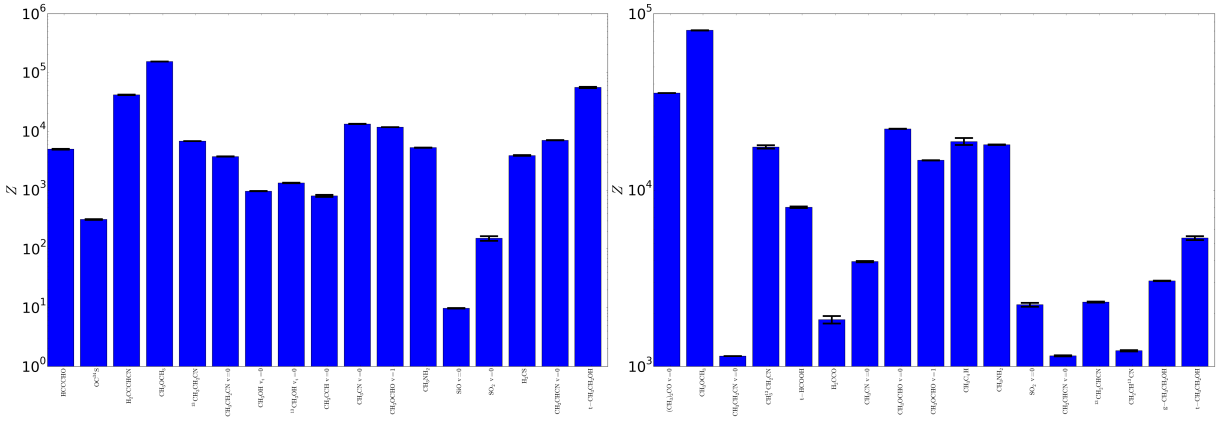

Figure 4.1: Distributions of partition functions for G327.3-0.6 (left panel) and NGC6334 I (right panel).

Table 4.1: Results of the rotational diagram analysis for both sources.

G327.3-0.6 - rotational diagrams									
Name	Chemical formula	Temperature (K)	Pearson	N (cm^{-2})	x_G[a]	x_L[a]	$v_{\rm LSR}$ (km/s)[b]	Δv (km/s)[c]	R (%)[d]
Carbonyl sulfide	$OC^{34}S$	96.2 ± 2.4	-1.0	$(5.2 \pm 0.2) \times 10^{14}$	$(1.61 \pm 0.05) \times 10^{-9}$	$(1.72 \pm 0.05) \times 10^{-8}$	-44.52 ± 0.03	5.05 ± 0.07	5.3 ± 0.1
Cyanoallene	$H_2CCCHCN$	105.3 ± 1.9	-1.0	$(2.7 \pm 0.2) \times 10^{15}$	$(8.3 \pm 0.6) \times 10^{-9}$	$(8.9 \pm 0.6) \times 10^{-8}$	-45.1 ± 0.6	6.0 ± 0.7	4.5 ± 0.5
Dimethyl ether	CH_3OCH_3	123.0 ± 0.1	-0.7	$(5.850 \pm 0.007) \times 10^{16}$	$(1.828 \pm 0.002) \times 10^{-7}$	$(1.950 \pm 0.002) \times 10^{-6}$	-45.1 ± 0.1	6.4 ± 0.1	5.5 ± 0.1
Trans-ethanol	$t - CH_3CH_2OH$	340 ± 20	-1.0	$(2.5 \pm 0.1) \times 10^{16}$	$(8.0 \pm 0.3) \times 10^{-8}$	$(8.5 \pm 0.4) \times 10^{-7}$	-44.0 ± 0.5	5.6 ± 0.6	10.3 ± 1.1
Ethyl cyanide	$CH_3CH_2CN\,\nu = 0$	64.75 ± 0.06	-0.9	$(1.059 \pm 0.002) \times 10^{15}$	$(3.309 \pm 0.008) \times 10^{-9}$	$(3.530 \pm 0.008) \times 10^{-8}$	-44.24 ± 0.05	6.07 ± 0.08	3.83 ± 0.05
Ethyl cyanide	$^{13}CH_3CH_2CN$	47.00 ± 0.07	-0.9	$(1.77 \pm 0.01) \times 10^{16}$	$(5.53 \pm 0.03) \times 10^{-8}$	$(5.90 \pm 0.04) \times 10^{-7}$	-44.5 ± 0.4	6.5 ± 0.6	3.0 ± 0.3
Methanol	$CH_3OH\,\nu_t = 0$	134.7 ± 0.2	-0.7	$(1.143 \pm 0.003) \times 10^{16}$	$(3.570 \pm 0.008) \times 10^{-8}$	$(3.808 \pm 0.009) \times 10^{-7}$	-44.45 ± 0.08	6.5 ± 0.1	6.8 ± 0.1
Methanol	$^{13}CH_3OH\,\nu_t = 0$	164.1 ± 1.0	-0.9	$(2.80 \pm 0.03) \times 10^{15}$	$(8.76 \pm 0.09) \times 10^{-9}$	$(9.3 \pm 0.1) \times 10^{-8}$	-44.6 ± 0.2	5.6 ± 0.2	8.5 ± 0.3
Methyl Acetylene	$CH_3CCH\,\nu = 0$	83.6 ± 6.8	-1.0	$(2.0 \pm 0.2) \times 10^{15}$	$(6.2 \pm 0.7) \times 10^{-9}$	$(6.6 \pm 0.8) \times 10^{-8}$	-44.61 ± 0.08	4.6 ± 0.1	6.7 ± 0.3
Methyl cyanide	$CH_3CN\,\nu = 0$	164.0 ± 2.8	-0.9	$(1.12 \pm 0.02) \times 10^{15}$	$(3.51 \pm 0.07) \times 10^{-9}$	$(3.74 \pm 0.08) \times 10^{-8}$	-44.3 ± 0.3	7.7 ± 0.6	5.6 ± 0.4
Methyl formate	$CH_3OCHO\,\nu = 1$	54.8 ± 0.1	-1.0	$(5.20 \pm 0.06) \times 10^{17}$	$(1.62 \pm 0.02) \times 10^{-6}$	$(1.73 \pm 0.02) \times 10^{-5}$	-44.8 ± 0.2	5.2 ± 0.2	3.9 ± 0.2
Methylamine	CH_3NH_2	36.6 ± 0.4	-1.0	$(1.30 \pm 0.05) \times 10^{16}$	$(4.1 \pm 0.2) \times 10^{-8}$	$(4.3 \pm 0.2) \times 10^{-7}$	-46.1 ± 0.8	5.0 ± 0.5	4.6 ± 0.4
2-Propynal	$HCCCHO$	107.4 ± 3.2	-0.9	$(5.1 \pm 0.4) \times 10^{16}$	$(1.6 \pm 0.1) \times 10^{-7}$	$(1.7 \pm 0.1) \times 10^{-6}$	-45.6 ± 0.8	6.1 ± 0.7	4.9 ± 0.6
Silicon Monoxide	$SiO\,\nu = 0$	19.5 ± 0.2	-1.0	$(1.45 \pm 0.04) \times 10^{13}$	$(4.5 \pm 0.1) \times 10^{-11}$	$(4.8 \pm 0.1) \times 10^{-10}$	-44.225 ± 0.002	9.2 ± 0.2	1.55 ± 0.03
Sulfur dioxide	$SO_2\,\nu = 0$	26.1 ± 4.7	-1.0	$(9.1 \pm 6.0) \times 10^{14}$	$(2.8 \pm 1.9) \times 10^{-9}$	$(3.0 \pm 2.0) \times 10^{-8}$	-43.8 ± 0.1	8.0 ± 0.3	1.7 ± 0.2
Thioformaldehyde	H_2CS	227.5 ± 6.1	-0.9	$(1.55 \pm 0.03) \times 10^{15}$	$(4.84 \pm 0.08) \times 10^{-9}$	$(5.16 \pm 0.08) \times 10^{-8}$	-44.8	5.8 ± 0.1	8.2 ± 0.2
Vinyl cyanide	$CH_2CHCN\,\nu = 0$	60.9 ± 0.1	-1.0	$(1.030 \pm 0.006) \times 10^{15}$	$(3.22 \pm 0.02) \times 10^{-9}$	$(3.43 \pm 0.02) \times 10^{-8}$	-44.3 ± 0.2	7.8 ± 0.3	2.9 ± 0.1
NGC 6334 I - rotational diagrams									
Name	Chemical formula	Temperature (K)	Pearson	N (cm^{-2})	x_o[a]	x_i[a]	$v_{\rm LSR}$ (km/s)[b]	Δv (km/s)[c]	R (%)[d]
Acetone	$(CH_3)_2CO\,\nu = 0$	25.89 ± 0.04	-0.9	$(2.31 \pm 0.02) \times 10^{16}$	$(2.3 \pm 1.8) \times 10^{-7}$	$(1.154 \pm 0.008) \times 10^{-7}$	-7.7 ± 0.2	5.3 ± 0.3	2.7 ± 0.2
Dimethyl ether	CH_3OCH_3	86.5 ± 0.1	-0.7	$(3.583 \pm 0.006) \times 10^{16}$	$(3.6 \pm 2.9) \times 10^{-7}$	$(1.792 \pm 0.003) \times 10^{-7}$	-7.4 ± 0.2	5.5 ± 0.2	5.4 ± 0.2
Gauche-ethanol	$g - CH_3CH_2OH$	56.4 ± 0.3	-1.0	$(2.00 \pm 0.04) \times 10^{16}$	$(2.0 \pm 1.6) \times 10^{-7}$	$(1.00 \pm 0.02) \times 10^{-7}$	-7.8 ± 0.4	8.2 ± 0.7	2.9 ± 0.2
Trans-ethanol	$t - CH_3CH_2OH$	80.9 ± 4.1	-1.0	$(2.28 \pm 0.09) \times 10^{16}$	$(2.3 \pm 1.8) \times 10^{-7}$	$(1.14 \pm 0.05) \times 10^{-7}$	-6.7	7.1 ± 1.2	4.0 ± 0.7
Ethyl cyanide	$CH_3CH_2CN\,\nu = 0$	29.44 ± 0.04	-1.0	$(3.31 \pm 0.02) \times 10^{15}$	$(3.3 \pm 2.6) \times 10^{-8}$	$(1.65 \pm 0.01) \times 10^{-8}$	-6.8 ± 0.1	4.7 ± 0.2	3.3 ± 0.1
Ethyl cyanide	$CH_3^{13}CH_2CN$	88.7 ± 3.9	-1.0	$(1.0 \pm 0.2) \times 10^{17}$	$(1.0 \pm 0.8) \times 10^{-6}$	$(4.8 \pm 0.9) \times 10^{-7}$	-6.9	3.3 ± 0.1	8.1 ± 0.3
Formic Acid	$t - HCOOH$	280.0 ± 5.8	-0.9	$(5.29 \pm 0.07) \times 10^{14}$	$(5.3 \pm 4.2) \times 10^{-9}$	$(2.65 \pm 0.04) \times 10^{-9}$	-8.09 ± 0.09	4.8 ± 0.3	11.1 ± 0.6
Ketene	H_2CCO	98.3 ± 9.5	-1.0	$(2.3 \pm 0.3) \times 10^{14}$	$(2.3 \pm 1.9) \times 10^{-9}$	$(1.2 \pm 0.1) \times 10^{-9}$	-7.3 ± 0.2	5.17 ± 0.08	6.4 ± 0.3
Methylamine	CH_3NH_2	82.9 ± 0.6	-0.8	$(3.62 \pm 0.03) \times 10^{15}$	$(3.6 \pm 2.9) \times 10^{-8}$	$(1.81 \pm 0.01) \times 10^{-8}$	-6.1 ± 0.9	6.3 ± 0.8	5.6 ± 0.7
Methyl diacetylene	CH_3C_4H	170 ± 20	-1.0	$(4.2 \pm 0.8) \times 10^{14}$	$(4.2 \pm 3.5) \times 10^{-9}$	$(2.1 \pm 0.4) \times 10^{-9}$	-7.2 ± 1.0	4.2 ± 0.2	8.2 ± 0.6
Methyl cyanide	$CH_3CN\,\nu = 0$	79.2 ± 1.4	-1.0	$(7.7 \pm 0.1) \times 10^{14}$	$(7.7 \pm 6.2) \times 10^{-9}$	$(3.87 \pm 0.07) \times 10^{-9}$	-7.5 ± 0.7	7.5 ± 1.2	4.0 ± 0.6
Methyl formate	$CH_3OCHO\,\nu = 0$	81.9 ± 0.2	-0.9	$(1.784 \pm 0.008) \times 10^{16}$	$(1.8 \pm 1.4) \times 10^{-7}$	$(8.92 \pm 0.04) \times 10^{-8}$	-7.55 ± 0.07	4.3 ± 0.1	5.9 ± 0.2
Methyl formate	$CH_3OCHO\,\nu = 1$	63.1 ± 0.2	-1.0	$(8.9 \pm 0.1) \times 10^{16}$	$(8.9 \pm 7.2) \times 10^{-7}$	$(4.47 \pm 0.06) \times 10^{-7}$	-7.3 ± 0.1	4.5 ± 0.2	4.9 ± 0.2
Sulfur dioxide	$SO_2\,\nu = 0$	157.1 ± 8.0	-0.9	$(8.5 \pm 0.4) \times 10^{14}$	$(8.5 \pm 6.8) \times 10^{-9}$	$(4.3 \pm 0.2) \times 10^{-9}$	-7.9 ± 0.1	5.4 ± 0.5	6.2 ± 0.6
Vinyl cyanide	$CH_2CHCN\,\nu = 0$	19.0 ± 0.3	-0.9	$(2.9 \pm 0.2) \times 10^{15}$	$(2.9 \pm 2.4) \times 10^{-8}$	$(1.5 \pm 0.1) \times 10^{-8}$	-3.9 ± 0.2	7.5 ± 0.3	1.72 ± 0.06
Vinyl cyanide	$^{13}CH_2CHCN$	28.0 ± 0.4	-0.8	$(4.5 \pm 0.2) \times 10^{14}$	$(4.5 \pm 3.6) \times 10^{-9}$	$(2.27 \pm 0.08) \times 10^{-9}$	-7.0	6.3 ± 1.2	2.5 ± 0.5
Vinyl cyanide	$CH_2CH^{13}CN$	18.7 ± 0.3	-1.0	$(2.3 \pm 0.2) \times 10^{15}$	$(2.3 \pm 1.8) \times 10^{-8}$	$(1.1 \pm 0.1) \times 10^{-8}$	-6.1 ± 0.6	6.1 ± 1.0	2.1 ± 0.3

[a] Abundances based on the column densities of hydrogen from Leurini et al. (2013) (L) and Gibb et al. (2000) (G) for G327.3-0.3 and i for the inner, and o for the outer envelope in NGC 6334 I. [b] Velocities calculated with respect to the LSR. [c] Average line widths for a molecule. [d] R ratios averaged over all detected lines of a molecule.

Table 4.2: Points removed during analysis.

Name	Chemical formula	T (K)	$\ln N_u/g_u$	transition
G327.3-0.6				
Dimethyl ether	CH_3OCH_3	393.15	21.33	28(4,25)-27(5,22)AA eo-oe
Dimethyl ether	CH_3OCH_3	393.15	20.4	28(4,25)-27(5,22)EE eo-oe
Dimethyl ether	CH_3OCH_3	393.15	23.16	28(4,25)-27(5,22)EA eo-oe
Dimethyl ether	CH_3OCH_3	393.15	22.35	28(4,25)-27(5,22)AE eo-oe
Dimethyl ether	CH_3OCH_3	265.92	25.163	22(5,17)-23(2,22)EE oo-ee
Dimethyl ether	CH_3OCH_3	159.03	26.35	16(5,12)-17(2,15)AA oe-eo
Methanol	$^{13}CH_3OH\,\nu_t = 0$	103.93	32.72	8(2,6)-8(-1,8) ee-oe
Ethyl cyanide	$CH_3CH_2CN\,\nu = 0$	321.32	27.7	29(11,19)-30(10,20)oo-ee
Ethyl cyanide	$CH_3CH_2CN\,\nu = 0$	321.32	27.7	29(11,19)-30(10,20)oo-ee
Ethyl cyanide	$CH_3CH_2CN\,\nu = 0$	321.32	27.7	29(11,18)-30(10,21)oe-eo
NGC 6334 I				
Gauche-ethanol	$g - CH_3CH_2OH$	187.15	29.22	15(5,10)-15(4,11),$\nu_t = 0 - 0$ oe-eo
Gauche-ethanol	$g - CH_3CH_2OH$	279.71	29.52	21(5,17)-21(4,18),$\nu_t = 0 - 0$ oo-ee
Gauche-ethanol	$g - CH_3CH_2OH$	358.92	28.72	26(3,24)-26(2,25),$\nu_t = 0 - 0$ oe-eo
Gauche-ethanol	$g - CH_3CH_2OH$	262.18	29.38	20(5,16)-20(4,17),$\nu_t = 0 - 0$ oe-eo
Gauche-ethanol	$g - CH_3CH_2OH$	229.66	28.97	18(5,13)-18(4,14),$\nu_t = 0 - 0$ oo-ee
Gauche-ethanol	$g - CH_3CH_2OH$	358.92	28.72	26(3,24)-26(2,25),$\nu_t = 0 - 0$ oe-eo

Table 4.3: Results of the population diagram analysis for both sources.

G327.3-0.6 - population diagrams									
Name	Chemical formula	Temperature (K)	Pearson	N (cm^{-2})	x_G[a]	x_L[a]	$v_{\rm LSR}$ (km/s)[b]	Δv (km/s)[c]	R (%)[d]
Acetone	$(CH_3)_2CO\,\nu=0$ oo − oe	350 ± 160	-1.0	$(3.7 \pm 1.0) \times 10^{16}$	$(1.2 \pm 0.3) \times 10^{-7}$	$(1.2 \pm 0.3) \times 10^{-6}$	-44.8 ± 0.1	4.7 ± 0.4	11.3 ± 2.7
Acetone	$(CH_3)_2CO\,\nu=0$ AE	280 ± 20	-1.0	$(1.70 \pm 0.07) \times 10^{17}$	$(5.3 \pm 0.2) \times 10^{-7}$	$(5.7 \pm 0.2) \times 10^{-6}$	-45.1 ± 0.3	5.0 ± 0.3	9.5 ± 0.6
Dimethyl ether	CH_3OCH_3 ee − oo	118.4 ± 0.4	-0.7	$(6.77 \pm 0.02) \times 10^{16}$	$(2.116 \pm 0.007) \times 10^{-7}$	$(2.258 \pm 0.007) \times 10^{-6}$	-45.1 ± 0.4	6.3 ± 0.3	5.5 ± 0.3
Dimethyl ether	CH_3OCH_3 oo − ee	145.9 ± 0.3	-0.6	$(7.60 \pm 0.01) \times 10^{16}$	$(2.375 \pm 0.004) \times 10^{-7}$	$(2.533 \pm 0.004) \times 10^{-6}$	-45.2 ± 0.2	6.7 ± 0.2	5.7 ± 0.2
Dimethyl ether	CH_3OCH_3 eo − oe	111.5 ± 0.7	-0.7	$(4.31 \pm 0.03) \times 10^{16}$	$(1.347 \pm 0.009) \times 10^{-7}$	$(1.44 \pm 0.01) \times 10^{-6}$	-45.0 ± 0.5	7.1 ± 0.2	4.7 ± 0.2
Dimethyl ether	CH_3OCH_3 oe − eo	105.1 ± 0.2	-0.7	$(4.01 \pm 0.01) \times 10^{16}$	$(1.252 \pm 0.003) \times 10^{-7}$	$(1.335 \pm 0.003) \times 10^{-6}$	-45.1 ± 0.2	6.0 ± 0.2	5.4 ± 0.2
Dimethyl ether	CH_3OCH_3 AA	140.8 ± 0.3	-0.6	$(5.40 \pm 0.01) \times 10^{16}$	$(1.688 \pm 0.004) \times 10^{-7}$	$(1.800 \pm 0.005) \times 10^{-6}$	-43.9 ± 0.3	6.2 ± 0.2	6.1 ± 0.2
Dimethyl ether	CH_3OCH_3 EA	143.0 ± 0.4	-0.7	$(1.340 \pm 0.004) \times 10^{17}$	$(4.19 \pm 0.01) \times 10^{-7}$	$(4.47 \pm 0.01) \times 10^{-6}$	-45.8 ± 0.3	6.5 ± 0.2	5.9 ± 0.2
Dimethyl ether	CH_3OCH_3 AE	128.1 ± 0.4	-0.7	$(1.367 \pm 0.004) \times 10^{17}$	$(4.27 \pm 0.01) \times 10^{-7}$	$(4.56 \pm 0.01) \times 10^{-6}$	-46.0 ± 0.3	6.6 ± 0.3	5.4 ± 0.2
Dimethyl ether	CH_3OCH_3 EE	121.4 ± 0.2	-0.7	$(2.479 \pm 0.006) \times 10^{16}$	$(7.75 \pm 0.02) \times 10^{-8}$	$(8.26 \pm 0.02) \times 10^{-7}$	-44.8 ± 0.1	6.3 ± 0.2	5.5 ± 0.2
Ethyl cyanide	$CH_3CH_2CN\,\nu=0$ ee − oo	195.3 ± 2.9	-0.9	$(1.37 \pm 0.02) \times 10^{16}$	$(4.27 \pm 0.07) \times 10^{-8}$	$(4.56 \pm 0.07) \times 10^{-7}$	-44.3 ± 0.1	5.2 ± 0.1	7.7 ± 0.2
Ethyl cyanide	$CH_3CH_2CN\,\nu=0$ oo − ee	261.7 ± 8.4	-0.8	$(3.57 \pm 0.06) \times 10^{16}$	$(1.11 \pm 0.02) \times 10^{-7}$	$(1.19 \pm 0.02) \times 10^{-6}$	-45.1 ± 0.3	5.4 ± 0.2	8.6 ± 0.4
Ethyl cyanide	$CH_3CH_2CN\,\nu=0$ eo − oe	145.8 ± 0.9	-0.9	$(7.42 \pm 0.05) \times 10^{15}$	$(2.32 \pm 0.02) \times 10^{-8}$	$(2.47 \pm 0.02) \times 10^{-7}$	-44.1 ± 0.1	5.7 ± 0.2	6.1 ± 0.2
Ethyl cyanide	$^{13}CH_3CH_2CN$ ee − eo	18.0 ± 0.2	-1.0	$(6.0 \pm 0.7) \times 10^{18}$	$(1.9 \pm 0.2) \times 10^{-5}$	0.00020 ± 0.00002	-46.3 ± 1.1	6.6 ± 1.1	1.8 ± 0.3
Methanol	$^{13}CH_3OH\,\nu_t=0$ −−	190 ± 10	-0.9	$(3.1 \pm 0.2) \times 10^{15}$	$(9.8 \pm 0.8) \times 10^{-9}$	$(1.05 \pm 0.08) \times 10^{-7}$	-44.2 ± 0.5	6.5 ± 0.8	8.0 ± 1.0
Methanol	$^{13}CH_3OH\,\nu_t=0$ +−	96.0 ± 0.7	-0.9	$(2.14 \pm 0.03) \times 10^{15}$	$(6.7 \pm 0.1) \times 10^{-9}$	$(7.1 \pm 0.1) \times 10^{-8}$	-44.4 ± 0.1	5.2 ± 0.2	7.1 ± 0.3
Methanol	$^{13}CH_3OH\,\nu_t=0$ −+	222.1 ± 6.4	-0.9	$(2.9 \pm 0.2) \times 10^{15}$	$(9.0 \pm 0.6) \times 10^{-9}$	$(9.6 \pm 0.6) \times 10^{-8}$	-44.5 ± 0.3	5.9 ± 0.6	9.5 ± 0.9
Methanol	$CH_3OH\,\nu_t=0$	98.4 ± 0.2	-0.7	$(1.064 \pm 0.004) \times 10^{16}$	$(3.32 \pm 0.01) \times 10^{-8}$	$(3.55 \pm 0.01) \times 10^{-7}$	-44.5 ± 0.1	6.3 ± 0.2	5.9 ± 0.2
Methanol	$CH_3OH\,\nu_t=0$ ++	218.0 ± 0.8	-0.8	$(1.81 \pm 0.01) \times 10^{16}$	$(5.67 \pm 0.04) \times 10^{-8}$	$(6.04 \pm 0.04) \times 10^{-7}$	-44.4 ± 0.3	6.5 ± 0.3	8.7 ± 0.4
Methanol	$CH_3OH\,\nu_t=0$ −−	118.0 ± 1.0	-0.8	$(9.2 \pm 0.1) \times 10^{15}$	$(2.87 \pm 0.04) \times 10^{-8}$	$(3.06 \pm 0.04) \times 10^{-7}$	-44.5 ± 0.1	6.5 ± 0.2	6.4 ± 0.2
Methanol	$CH_3OH\,\nu_t=0$ +−	148.4 ± 0.7	-0.9	$(5.43 \pm 0.05) \times 10^{15}$	$(1.70 \pm 0.02) \times 10^{-8}$	$(1.81 \pm 0.02) \times 10^{-7}$	-44.33 ± 0.08	6.5 ± 0.2	7.1 ± 0.2
Methanol	$CH_3OH\,\nu_t=0$ −+	129.4 ± 0.8	-0.9	$(5.55 \pm 0.06) \times 10^{15}$	$(1.73 \pm 0.02) \times 10^{-8}$	$(1.85 \pm 0.02) \times 10^{-7}$	-44.5 ± 0.1	7.1 ± 0.2	6.1 ± 0.2
Methanol	$^{13}CH_3OH\,\nu_t=0$ ++	85.3 ± 3.0	-1.0	$(2.9 \pm 0.2) \times 10^{15}$	$(9.0 \pm 0.8) \times 10^{-9}$	$(9.7 \pm 0.8) \times 10^{-8}$	-44.4 ± 0.5	5.5 ± 0.6	6.3 ± 0.7
Methyl formate	$CH_3OCHO\,\nu=0$ oe − eo	201.9 ± 4.8	-1.0	$(9.0 \pm 0.2) \times 10^{16}$	$(2.81 \pm 0.06) \times 10^{-7}$	$(3.00 \pm 0.06) \times 10^{-6}$	-45.4 ± 0.5	6.3 ± 0.2	6.2 ± 0.2
Methyl formate	$CH_3OCHO\,\nu=0$ ee − oo	163.9 ± 5.4	-1.0	$(7.3 \pm 0.2) \times 10^{16}$	$(2.27 \pm 0.08) \times 10^{-7}$	$(2.42 \pm 0.08) \times 10^{-6}$	-44.9	5.7 ± 0.4	6.2 ± 0.4
Methyl formate	$CH_3OCHO\,\nu=0$ oo − ee	73.6 ± 1.7	-0.9	$(8.6 \pm 0.4) \times 10^{16}$	$(2.7 \pm 0.1) \times 10^{-7}$	$(2.9 \pm 0.1) \times 10^{-6}$	-44.8	6.0 ± 0.5	3.9 ± 0.3
Methyl formate	$CH_3OCHO\,\nu=0$ eo − oe	197.9 ± 3.4	-1.0	$(2.78 \pm 0.05) \times 10^{17}$	$(8.7 \pm 0.2) \times 10^{-7}$	$(9.3 \pm 0.2) \times 10^{-6}$	-45.2 ± 0.5	5.5 ± 0.7	7.0 ± 0.9
Methyl formate	$CH_3OCHO\,\nu=1$ ee − oo	38.9 ± 0.4	-1.0	$(2.6 \pm 0.2) \times 10^{19}$	$(8.0 \pm 0.6) \times 10^{-5}$	0.00085 ± 0.00007	-45.6 ± 0.9	6.5 ± 1.0	2.7 ± 0.4
Methyl formate	$CH_3OCHO\,\nu=1$ eo − oe	49.9 ± 0.3	-1.0	$(1.27 \pm 0.04) \times 10^{18}$	$(4.0 \pm 0.1) \times 10^{-6}$	$(4.2 \pm 0.1) \times 10^{-5}$	-45.5 ± 0.6	5.2 ± 0.3	3.7 ± 0.2
Methyl formate	$CH_3OCHO\,\nu=1$ A	67.6 ± 0.2	-1.0	$(1.64 \pm 0.02) \times 10^{17}$	$(5.13 \pm 0.07) \times 10^{-7}$	$(5.47 \pm 0.07) \times 10^{-6}$	-44.9	4.9 ± 0.2	4.6 ± 0.2
Methyl formate	$CH_3OCHO\,\nu=1$ E	156.2 ± 5.7	-1.0	$(2.4 \pm 0.2) \times 10^{17}$	$(7.5 \pm 0.6) \times 10^{-7}$	$(8.0 \pm 0.6) \times 10^{-6}$	-44.6 ± 0.3	5.6 ± 0.4	6.2 ± 0.5
2-Propynal	HCCCHO eo − ee	17.5 ± 0.5	-0.7	$(5.6 \pm 0.7) \times 10^{17}$	$(1.8 \pm 0.2) \times 10^{-6}$	$(1.9 \pm 0.2) \times 10^{-5}$	-44.9	5.3 ± 0.9	2.3 ± 0.4
Thioformaldehyde	H_2CS oo − oe	178.6 ± 6.7	-0.9	$(1.45 \pm 0.04) \times 10^{15}$	$(4.5 \pm 0.1) \times 10^{-9}$	$(4.8 \pm 0.1) \times 10^{-8}$	-44.9	6.1 ± 0.2	7.0 ± 0.3
Vinyl cyanide	$CH_2CHCN\,\nu=0$ oe − oo	24.60 ± 0.07	-1.0	$(9.7 \pm 0.3) \times 10^{16}$	$(3.02 \pm 0.08) \times 10^{-7}$	$(3.22 \pm 0.09) \times 10^{-6}$	-44.3 ± 0.5	8.4 ± 0.7	1.7 ± 0.2
Vinyl cyanide	$CH_2CHCN\,\nu=0$ ee − eo	66.2 ± 0.2	-1.0	$(8.24 \pm 0.09) \times 10^{14}$	$(2.58 \pm 0.03) \times 10^{-9}$	$(2.75 \pm 0.03) \times 10^{-8}$	-43.9 ± 0.3	7.4 ± 0.7	3.2 ± 0.3
Vinyl cyanide	$CH_2CHCN\,\nu=0$ eo − ee	45.2 ± 0.3	-1.0	$(4.5 \pm 0.2) \times 10^{15}$	$(1.42 \pm 0.06) \times 10^{-8}$	$(1.51 \pm 0.06) \times 10^{-7}$	-44.6 ± 0.4	7.6 ± 0.7	2.6 ± 0.3
Vinyl cyanide	$CH_2CHCN\,\nu=0$ oo − oe	84.2 ± 0.7	-1.0	$(5.5 \pm 0.1) \times 10^{14}$	$(1.72 \pm 0.03) \times 10^{-9}$	$(1.84 \pm 0.04) \times 10^{-8}$	-44.4 ± 0.3	8.2 ± 0.7	3.3 ± 0.3
NGC 6334 I - population diagrams									
Name	Chemical formula	Temperature (K)	Pearson	N (cm^{-2})	x_o[a]	x_i[a]	$v_{\rm LSR}$ (km/s)[b]	Δv (km/s)[c]	R (%)[d]
Acetone	$(CH_3)_2CO\,\nu=0$ EE	11.90 ± 0.01	-0.9	$(1.24 \pm 0.01) \times 10^{17}$	$(1.2 \pm 1.0) \times 10^{-6}$	$(6.19 \pm 0.05) \times 10^{-7}$	-7.4 ± 0.2	4.9 ± 0.6	2.0 ± 0.2
Acetone	$(CH_3)_2CO\,\nu=0$ AA	12.59 ± 0.05	-0.9	$(3.31 \pm 0.09) \times 10^{16}$	$(3.3 \pm 2.6) \times 10^{-7}$	$(1.65 \pm 0.05) \times 10^{-7}$	-6.9	5.4 ± 1.1	1.8 ± 0.4
Acetone	$(CH_3)_2CO\,\nu=0$ ee − oo	50.1 ± 0.7	-0.9	$(1.81 \pm 0.06) \times 10^{17}$	$(1.8 \pm 1.5) \times 10^{-6}$	$(9.1 \pm 0.3) \times 10^{-7}$	-7.5 ± 0.5	5.9 ± 1.5	3.4 ± 0.8
Dimethyl ether	CH_3OCH_3 oe − eo	185.9 ± 8.1	-0.9	$(4.4 \pm 0.4) \times 10^{16}$	$(4.4 \pm 3.5) \times 10^{-7}$	$(2.2 \pm 0.2) \times 10^{-7}$	-7.5 ± 0.2	5.4 ± 0.3	8.0 ± 0.5
Dimethyl ether	CH_3OCH_3 oo − ee	123.6 ± 0.8	-0.9	$(4.99 \pm 0.04) \times 10^{16}$	$(5.0 \pm 4.0) \times 10^{-7}$	$(2.50 \pm 0.02) \times 10^{-7}$	-7.3 ± 0.3	4.6 ± 0.3	7.6 ± 0.5
Dimethyl ether	CH_3OCH_3 EE	88.4 ± 0.2	-0.7	$(1.707 \pm 0.006) \times 10^{16}$	$(1.7 \pm 1.4) \times 10^{-7}$	$(8.54 \pm 0.03) \times 10^{-8}$	-7.6 ± 0.2	5.8 ± 0.4	5.1 ± 0.4
Dimethyl ether	CH_3OCH_3 AA	113.8 ± 0.3	-0.7	$(4.16 \pm 0.01) \times 10^{16}$	$(4.2 \pm 3.3) \times 10^{-7}$	$(2.082 \pm 0.007) \times 10^{-7}$	-7.1 ± 0.5	5.5 ± 0.5	6.2 ± 0.5
Dimethyl ether	CH_3OCH_3 EA	62.5 ± 0.3	-0.9	$(4.63 \pm 0.03) \times 10^{16}$	$(4.6 \pm 3.7) \times 10^{-7}$	$(2.31 \pm 0.01) \times 10^{-7}$	-7.4 ± 0.5	5.3 ± 0.5	4.7 ± 0.5
Ethyl cyanide	$CH_3CH_2CN\,\nu=0$ ee − eo	270.0 ± 9.2	-1.0	$(2.23 \pm 0.06) \times 10^{14}$	$(2.2 \pm 1.8) \times 10^{-9}$	$(1.12 \pm 0.03) \times 10^{-9}$	-6.75 ± 0.06	5.2 ± 0.2	9.2 ± 0.3
Ethyl cyanide	$CH_3CH_2CN\,\nu=0$ eo − ee	51.1 ± 1.7	-1.0	$(2.3 \pm 0.4) \times 10^{15}$	$(2.3 \pm 1.9) \times 10^{-8}$	$(1.1 \pm 0.2) \times 10^{-8}$	-6.5 ± 0.1	4.5 ± 0.2	4.6 ± 0.2
Methyl formate	$CH_3OCHO\,\nu=0$ oe − eo	109.0 ± 3.4	-1.0	$(1.5 \pm 0.1) \times 10^{16}$	$(1.5 \pm 1.2) \times 10^{-7}$	$(7.4 \pm 0.6) \times 10^{-8}$	-7.62 ± 0.04	3.9 ± 0.3	7.5 ± 0.6
Methyl formate	$CH_3OCHO\,\nu=0$ ee − oo	100.3 ± 3.0	-0.8	$(2.09 \pm 0.04) \times 10^{16}$	$(2.1 \pm 1.7) \times 10^{-7}$	$(1.05 \pm 0.02) \times 10^{-7}$	-7.7 ± 0.1	3.6 ± 0.2	7.7 ± 0.5
Methyl formate	$CH_3OCHO\,\nu=0$ oo − oe	46.0 ± 0.1	-0.9	$(3.35 \pm 0.02) \times 10^{16}$	$(3.3 \pm 2.7) \times 10^{-7}$	$(1.67 \pm 0.01) \times 10^{-7}$	-7.6 ± 0.2	5.0 ± 0.3	3.8 ± 0.2
Methyl formate	$CH_3OCHO\,\nu=0$ oo − ee	132.3 ± 3.4	-0.9	$(2.0 \pm 0.1) \times 10^{16}$	$(2.0 \pm 1.6) \times 10^{-7}$	$(9.9 \pm 0.5) \times 10^{-8}$	-7.38 ± 0.09	4.0 ± 0.1	8.0 ± 0.2
Methyl formate	$CH_3OCHO\,\nu=0$ eo − oe	75.6 ± 0.7	-0.9	$(1.39 \pm 0.02) \times 10^{16}$	$(1.4 \pm 1.1) \times 10^{-7}$	$(6.94 \pm 0.09) \times 10^{-8}$	-7.61 ± 0.08	3.8 ± 0.3	6.4 ± 0.5
Methyl formate	$CH_3OCHO\,\nu=0$ A	77.5 ± 0.2	-0.9	$(1.956 \pm 0.009) \times 10^{16}$	$(2.0 \pm 1.6) \times 10^{-7}$	$(9.78 \pm 0.05) \times 10^{-8}$	-7.62 ± 0.09	4.4 ± 0.2	5.6 ± 0.2
Methyl formate	$CH_3OCHO\,\nu=1$ oo − oe	173.2 ± 2.9	-1.0	$(1.23 \pm 0.04) \times 10^{16}$	$(1.2 \pm 1.0) \times 10^{-7}$	$(6.1 \pm 0.2) \times 10^{-8}$	-7.5 ± 0.2	4.5 ± 0.4	8.1 ± 0.7
Methyl formate	$CH_3OCHO\,\nu=1$ oo − ee	75.5 ± 8.6	-1.0	$(2.7 \pm 1.3) \times 10^{17}$	$(2.7 \pm 2.5) \times 10^{-6}$	$(1.3 \pm 0.6) \times 10^{-6}$	-6.2 ± 0.6	4.6 ± 0.6	5.2 ± 0.7
Methyl formate	$CH_3OCHO\,\nu=1$ A	75.0 ± 0.5	-1.0	$(6.0 \pm 0.2) \times 10^{16}$	$(6.0 \pm 4.8) \times 10^{-7}$	$(3.01 \pm 0.09) \times 10^{-7}$	-7.3 ± 0.2	4.6 ± 0.2	5.2 ± 0.2
Methyl formate	$CH_3OCHO\,\nu=1$ E	53.1 ± 0.1	-1.0	$(1.46 \pm 0.02) \times 10^{17}$	$(1.5 \pm 1.2) \times 10^{-6}$	$(7.3 \pm 0.1) \times 10^{-7}$	-7.3 ± 0.2	4.3 ± 0.3	4.7 ± 0.3

[a] Abundances based on the column densities of hydrogen from Leurini et al. (2013) (L) and Gibb et al. (2000) (G) for G327.3-0.3 and i for the inner, and o for the outer envelope in NGC 6334 I. [b] Velocities calculated with respect to the LSR. [c] Average line widths for a molecule. [d] R ratios averaged over all detected lines of a molecule.

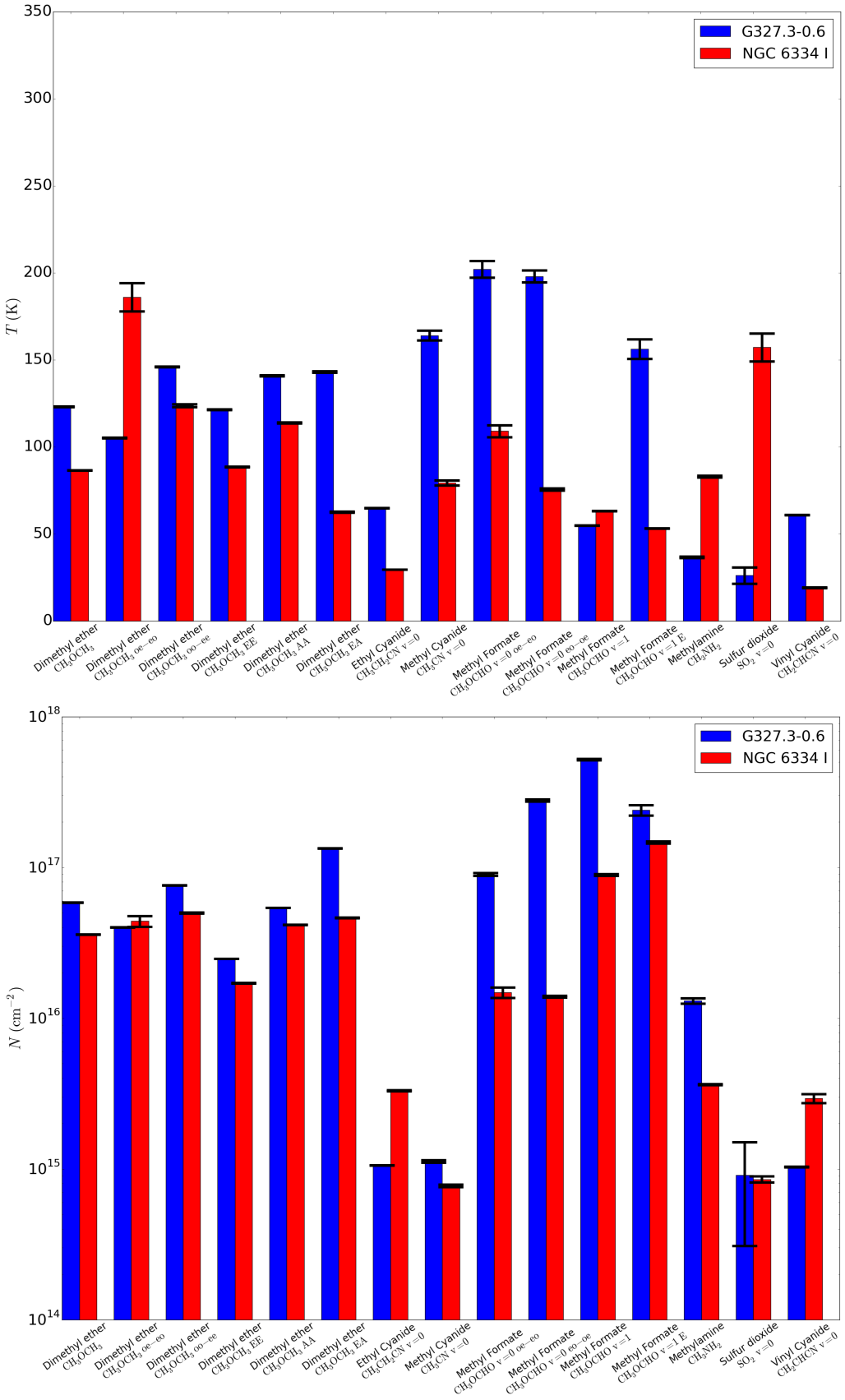

Figure 4.2: Comparison of the results using rotational and populational diagrams for both sources.

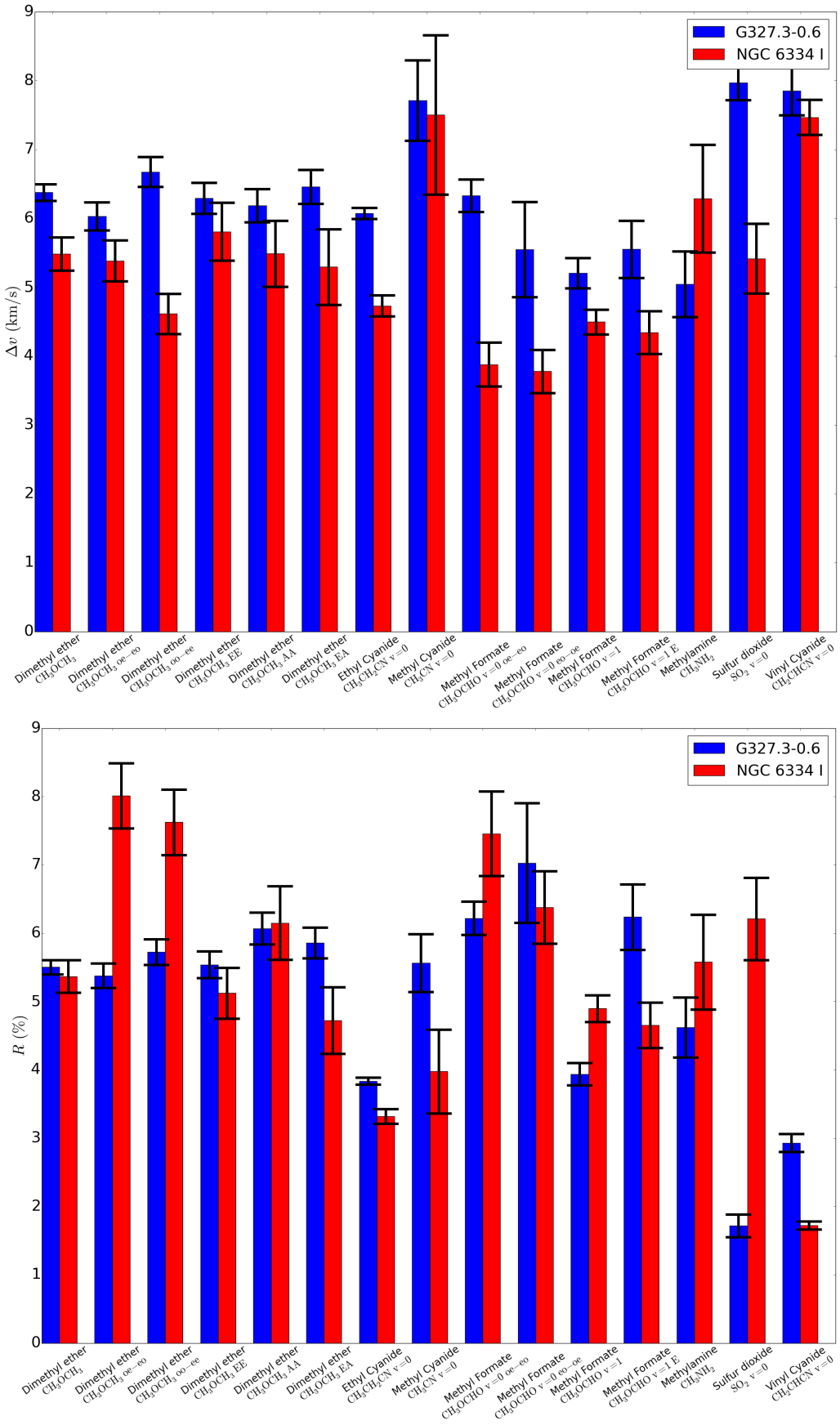

Figure 4.2: (*Cont.*) Comparison of the results using rotational and populational diagrams for both sources.

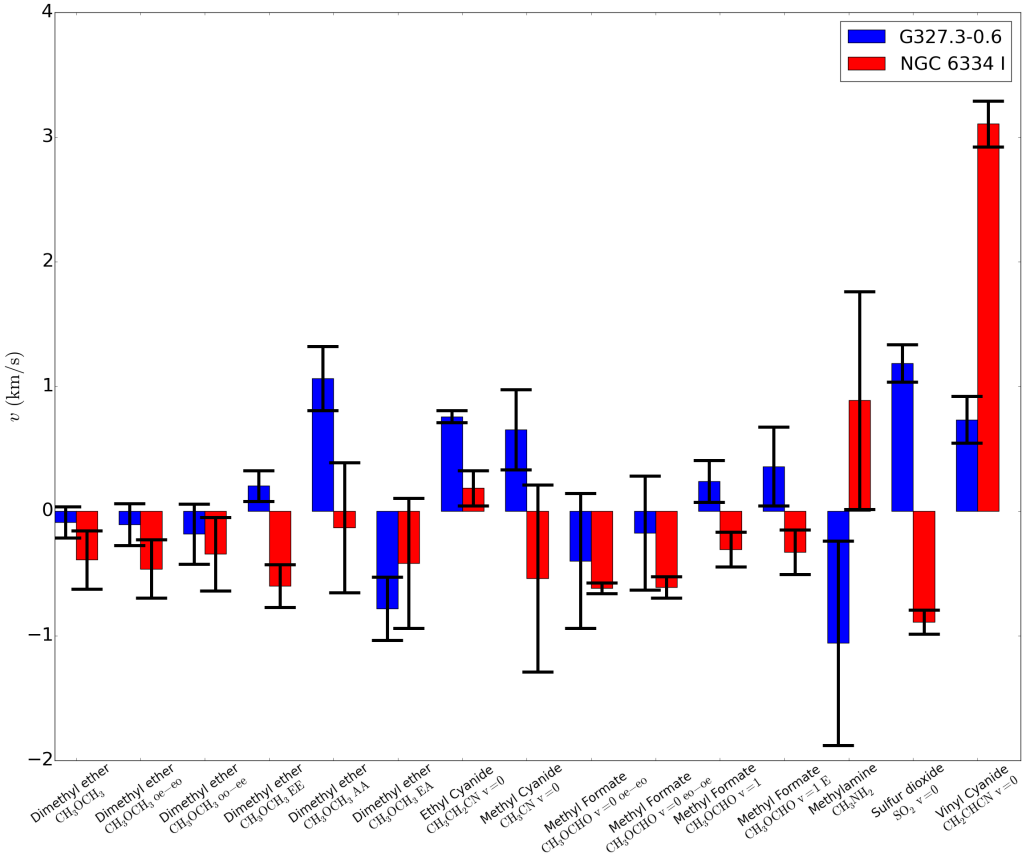

Figure 4.2: (*Cont.*) Comparison of the results using rotational and populational diagrams for both sources.

5 Discussion

As shown in Fig. 4.2, the temperatures and molecular column densities do not vary much between the two target hot cores, save for temperatures of sulfur dioxide, vinyl cyanide and methyl formate. Line widths and R ratios are similar in both sources because the R ratio is connected to temperature by Eq. (2.37). A notable exception is sulfur dioxide with a narrower linewidth in the colder gas of G327.3-0.6. If we look at the last panel in Fig. 4.2, we see that the only two cases of a greater difference to the LSR velocity of the whole source is vinyl cyanide in NGC 6334 I (but it has a smaller number of points in the rotational diagram) and dimethyl ether EE (in NGC 6334 I) and AA (in G327.3-0.6).

For molecules where literature values were not available for our target sources, we have compared the sources' temperatures and column densities with the following sources: Sgr B2, OMC-1, TMC-1, NGC 7129, Orion IRc2, Orion KL and NGC 6334 F.

5.1 Acetone

In Orion KL hot core acetone was determined to be at temperatures $100 - 150$ K and column density $\sim 10^{16}$ cm^{-2} (Peng et al. 2013; Friedel et al. 2005). This molecule was problematic to fit because of the scatter.

G327.3-0.6: We have fitted two different species: AE, and oo-oe. Their temperatures are in the range 200-350 K. The corresponding column densities are of the same order of magnitude with those detected towards the hot core in Orion KL, but the temperatures are higher than expected.

NGC 6334 I: Acetone rotational lines were also observed toward NGC 6334 I. EE, AA and ee-oo species, as well as the rotational diagram indicate acetone's temperature to be less than 50 K, which is unexpected for a hot core, but can be attributed to large a scatter in the data.

5.2 Carbonyl Sulfide

In G327.3-0.6, Gibb et al. (2000) found OC^{34}S at a gas temperature of 106 K, and at a column density of 3.3×10^{14} cm^{-2}, which are comparable to our values.

5.3 Cyanoallene

In G327.3-0.6 we have found cyanoallene at ~ 100 K and 10^{15} cm^{-2}. For comparison, Lovas et al. (2006) derived a three orders of magnitude lower column density of 10^{12} cm^{-2} towards the low-mass star-forming region TMC-1 by assuming a rotational temperature of 4 K. The direct comparison is not feasible because TMC-1 is a low-mass star-forming region.

5.4 Dimethyl Ether

G327.3-0.6: Gibb et al. (2000) derived a gas kinetic temperature of 82^{+8}_{-7} K, and a column density of $1.15^{+0.1}_{-0.1} \times 10^{17}$ cm^{-2} based on their observations with the SEST telescope. On the other hand, Bisschop et al. (2013), who also used APEX observations, derived the values of 105 K for the gas kinetic temperature and a column density of $5.5^{+0.1}_{-0.1} 10^{17}$ cm^{-2}. The values derived in the present work agree within an order of magnitude for the column densities, and within 50 K for the gas temperature for all symmetry species.
NGC 6334 I: Schilke et al. (2006) found two components with differing line widths. The component with smaller line width (3 km/s) has a gas temperature of 200 K, and column density of 2.0×10^{18} cm^{-2}, while the greater line width component (5 km/s) has a gas temperature of 50 K and column density of 1.5×10^{16} cm^{-2}. Our line widths are in the range $4.5 - 6$ km/s and do not follow this discrepancy.

5.5 Ethanol

G327.3-0.6: Gibb et al. (2000) found ethanol at a gas kinetic temperature of 66^{+11}_{-8} K and at a column density of 8.32×10^{14} cm^{-2}. We have found trans-ethanol at ~ 300 K and at 10^{16} cm^{-2}. This species has one of the highest differences of velocity compared to the systemic LSR velocity (with a high error as well), the only higher being SO_2 at 26 K. On the other hand, we can conclude that the possible culprit for the discrepancy in temperature might be a result of the large scatter in data for this species.
NGC 6334 I: We have found trans- and gauche-ethanol around 50-80 K and at $\sim 2 \times 10^{16}$ cm^{-2}. The line width of gauche-ethanol is 1 km/s broader than for trans-ethanol. Gauche-ethanol is also more blueshifted. The temperature difference and the difference in line widths might be due to a smaller number of data points for trans-ethanol. Otherwise, it could mean that both components of ethanol do not coexist at the same location. If we allow multiple different molecular candidates for the same line, we get the line width of 7.6 ± 0.9 km/s and a gas kinetic temperature of ~ 40 K, indicating that this difference between gauche and trans ethanol might just be a result of a small number of points for trans ethanol.

5.6 Ethyl Cyanide

G327.3-0.6: Gibb et al. (2000) found only the high temperature component 208^{+11}_{-9} K; $2.48^{+0.2}_{-0.2} \times 10^{15}$ cm^{-2}. Schilke et al. (2006) measured two distinct temperature components at 50 K and 200 K with differing column densities of 8×10^{15} cm^{-2} and 3×10^{17} cm^{-2}, respectively. For this source we have found three components: eo-oe at 145 K and $\sim 7 \times 10^{15}$ cm^{-2}, ee-oo at 195 K; $\sim 10^{16}$ cm^{-2} and oo-ee at 260 K; $\sim 3 \times 10^{16}$ cm^{-2}. We have found $^{13}CH_3CH_2CN$ at 50 K; and $\sim 1.8 \times 10^{16}$ cm^{-2} .

The detected ee-eo transition has too few data points for a proper rotational diagram analysis. The ratio $CH_3CH_2CN/^{13}CH_3CH_2CN$ is in the range from 0.4 to 2. A ratio less than unity is surprising but might be due to a relatively large scatter in the CH_3CH_2CN data. Another interesting property of this species is that there were components in the range of 500-1000 K. They were excluded, but can be seen in Fig. E.1 in Appendix E.

NGC 6334 I: Schilke et al. (2006) have measured 150 K; 2.0×10^{15} cm^{-2}. We found two components: one at 50 K ($\sim 2 \times 10^{15}$ cm^{-2}) and the other at $\sim$ 270 K ($\sim 2 \times 10^{14}$ cm^{-2}). The ratio $CH_3CH_2CN/CH_3{}^{13}CH_2CN < 1$ is low, but considering the ^{13}C isotopologue was detected only for 3 points, it again has too few data points for a proper rotational diagram analysis.

5.7 Formic Acid

Gibb et al. (2000) found formic acid in G327.3-0.6 to be at a temperature of 71^{+64}_{-22} K and column density of $8.51^{+7.9}_{-2.5} \times 10^{13}$ cm^{-2}. We have detected t-HCOOH only in NGC 6334 I. It is at a higher temperature (280 K) and has an order of magnitude higher column density.

5.8 Ketene

While we did not detect ketene in G327.3-0.6, we will use Gibb et al. (2000)'s result as a comparison for NGC 6334 I. The authors derived a gas temperature of 72^{+29}_{-16} K and a column density of $2.19^{+0.4}_{-0.3} \times 10^{15}$ cm^{-2}. We find ketene in NGC 6334 I in similar temperature and an order of magnitude lower column density.

5.9 Methanol

In G327.3-0.6 Gibb et al. (2000) detected both CH_3OH and $^{13}CH_3OH$ with 180^{+14}_{-11} K; $1.68^{+0.1}_{-0.1} \times 10^{16}$ cm^{-2} and 93^{+11}_{-10} K; $1.70^{+0.2}_{-0.2} \times 10^{15}$ cm^{-2}, respectively (C/^{13}C$\sim$10). We have found methanol and its isotopologue in G327.3-0.6 with the temperature range from 100 to 200 K, and with column densities of $10^{15} - 10^{16}$ cm^{-2}. Comparing the lowest temperature components we find $CH_3OH/^{13}CH_3OH$=1.4. On the other hand the highest temperature components give C/^{13}C=6.2.

5.10 Methyl Acetylene

In G327.3-0.6 Gibb et al. (2000) found methyl acetylene to be at a gas kinetic temperature of 72^{+29}_{-16} K and a column density of $2.19^{+0.4}_{-0.3} \times 10^{15}\,\mathrm{cm}^{-2}$, which is similar to our results for G327.3-0.6. Methyl acetylene was not detected in NGC 6334 I.

5.11 *Methylamine*

Gibb et al. (2000) argue that G327.3-0.6 is rich in amines, but give lower limits only on CH_2NH. For G327.3-0.6 we have found a good fit for methylamine at 30 K; $\sim 10^{16}$ cm^{-2} and for NGC 6334 I at 80 K; $\sim 4 \times 10^{15}$ cm^{-2}.

5.12 *Methyl Cyanide*

G327.3-0.6: Gibb et al. (2000) report a gas temperature of 162^{+15}_{-14} K and a column density of $1.74^{+0.8}_{-0.3} \times 10^{18}$cm^{-2}, while Schilke et al. (2006) found 300 K; 5.0×10^{17} cm^{-2}. We find methyl cyanide at ~ 160 K but at $\sim 1 \times 10^{15}$ cm^{-2}. This discrepancy could be attributed to relatively large scatter in the data for this molecule.
NGC 6334 I: Schilke et al. (2006) found methyl cyanide at a gas temperature of 200 K and column density of 1.5×10^{17} cm^{-2}. For this source, we find methyl cyanide at ~ 80 K and at $8 \sim 10^{14}$ cm^{-2}. As in the case of G327.3-0.6, this discrepancy could be attributed to relatively large scatter in the data.

5.13 *Methyl Diacetylene*

Methyl diacetylene has been detected in TMC-1 with a column density of 2×10^{13} cm^{-2} (Loren et al. 1984). Our fit for NGC 6334 I is an order of magnitude higher in column density, but is based only on a small number of data points and the fact that TMC-1 is a low-mass star forming region. Methyl diacetylene was not detected in G327.3-0.6.

5.14 *Methyl Formate*

G327.3-0.6: Gibb et al. (2000) found 375^{+62}_{-50} K; $1.62^{+0.3}_{-0.2} \times 10^{17}$ cm^{-2}, while Schilke et al. (2006) give 150 K; 2.0×10^{18} cm^{-2}. Methyl formate shows clumping (see Appendix E) in rotational diagrams that is not present in the population diagram.
NGC 6334 I: Schilke et al. (2006) found 200 K; 1.0×10^{18} cm^{-2}.

For both sources we have found methyl formate in its ground and torsionally excited state ($\nu = 1$), but in a range of column densities of $10^{16} - 10^{19}$ cm^{-2} and in a range of temperatures of 50-200 K.

5.15 *2-Propynal*

Irvine et al. (1988) derived a column density of 10^{12}cm^{-2} towards TMC-1. Irvine et al. (1988) and Loomis et al. (2015) give 10^{13}cm^{-2} for Sgr B2(N). We have found a scattered fit in G327.3-0.6 at ~ 100 K and $\sim 5 \times 10^{16}$ cm^{-2} and 18 K; $\sim 5 \times 10^{17}$ cm^{-2} for the detected eo-ee transition. This is a somewhat dubious detection based on high column densities compared to expected $\sim 10^{14}$ cm^{-2} on ice grains (Zhou et al. 2008) and literature value for Sgr B2(N). Propynal was not detected in NGC 6334 I.

5.16 Silicon Monoxide

For G327.3-0.6, Gibb et al. (2000) give only a lower limit of 8.7×10^{12} cm^{-2}, which is consistent with our value of $\sim 1.5 \times 10^{13}$ cm^{-2}, but it should be noted that only a few transitions of SiO were detected, and hence the derived column density has a relatively high uncertainty. Silicon monoxide was not detected in NGC 6334 I, which is to be expected because there is only one transition of SiO at the observed frequency range (at ~ 217105 MHz).

5.17 Sulfur Dioxide

G327.3-0.6: Gibb et al. (2000) report temperature of 130^{+80}_{-34} K and column density of $7.41^{+5.5}_{-2.0} \times 10^{14}$ cm^{-2}, while Schilke et al. (2006) found 250 K and 2.0×10^{18} cm^{-2}, differing in four orders of magnitude in column density. We have found sulfur dioxide at low temperature ~ 30 K and with column density closer to Gibb et al. (2000)'s but with a large error.
NGC 6334 I: Schilke et al. (2006) report a gas temperature of 150 K and a column density of 2.0×10^{17} cm^{-2}. We get temperatures near this value ~ 160 K, derived a low column density of $\sim 9 \times 10^{14}$ cm^{-2}.

5.18 Thioformaldehyde

For G327.3-0.6, Gibb et al. (2000) found thioformaldehyde at a gas temperature of 53^{+12}_{-8} K and a column density of $3.98^{+0.7}_{-0.6} \times 10^{14}$ cm^{-2}. We have found thioformaldehyde at a higher temperature of ~ 200 K, but at a comparable column density $\sim 10^{15}$ cm^{-2}. Thioformaldehyde was not detected in NGC 6334 I, which is to be expected because there is only one transition of thioformaldehyde at the observed frequency range (at ~ 218803 MHz).

5.19 Vinyl Cyanide

G327.3-0.6: Gibb et al. (2000) derived the values of 131^{+15}_{-18} K, $2.61^{+1.0}_{-0.7} \times 10^{18}$ cm^{-2}. We have found vinyl cyanide at a lower temperature ($\sim 20-80$ K) and lower column density ~ 70 K; $\sim 10^{14} - 10^{16}$ cm^{-2}.
NGC 6334 I: We have found vinyl cyanide along with its two isotopomers $^{13}CH_2CHCN$ and $CH_2CH^{13}CN$ at low temperatures 20-30 K and comparable column densities of $10^{14} - 10^{15}$ cm^{-2}. The ratio $CH_2CHCN/^{13}CH_2CHCN$ is approximately 6.4, and for $CH_2CHCN/CH_2CH^{13}CN$ it is smaller, namely 1.3.

6 Conclusion

We have analyzed the millimeter-wavelength APEX spectra of two hot cores G327.3-0.6 and NGC 6334 I. The derived temperatures and column densities correspond to those found in the literature for most molecules. In some cases, the determination of accurate gas temperatures and column densities is hampered by the large scatter in the rotational diagrams, implying non-LTE and/or optical depth effects (Goldsmith & Langer 1999). A method that eased the process was the use of separate fits for transitions based on different parities and symmetry states. On one hand, this procedure helped in reducing scatter, but on the other hand exacerbated the uncertainty because of the small number of points for many molecules. Except for methanol in G327.3-0.6, a clear cut influence of finite optical depth was not seen. In these sources, we have found molecular candidates in good agreement with literature: acetone, carbonyl sulfide, dimethyl ether, ethanol, ethyl cyanide, formic acid, ketene, methanol, methyl acetylene, methylamine, methyl cyanide, methyl formate, sulfur dioxide and vinyl cyanide along with some of their most common isotopologues. This plethora of complex molecular species identified in the target sources clearly illustrates the chemical richness of the hot core stage in high-mass star formation.

Appendices

Appendix A Spectra

A.1 Spectra of G327.3-0.6

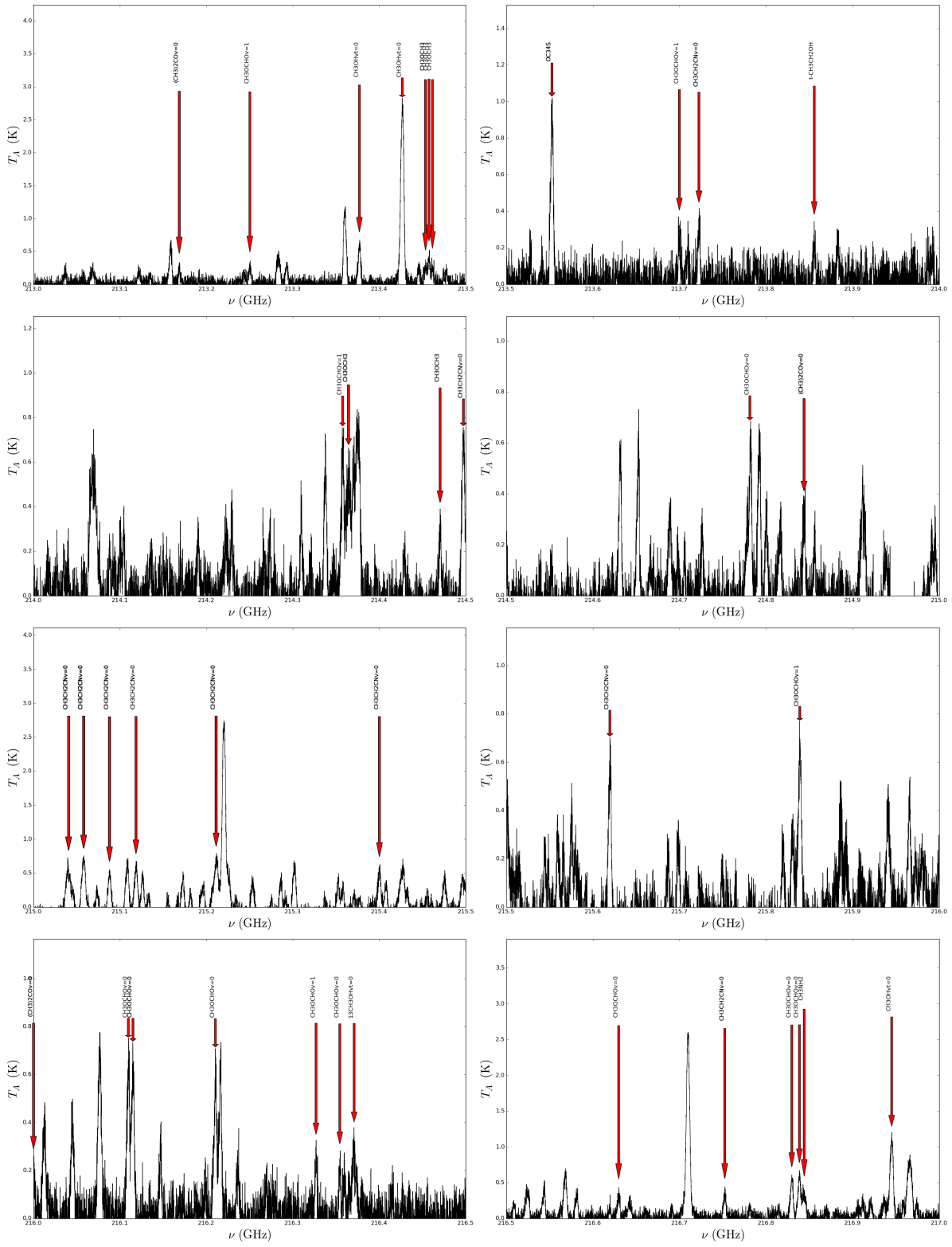

Figure A.1: Spectra of G327.3-0.6.

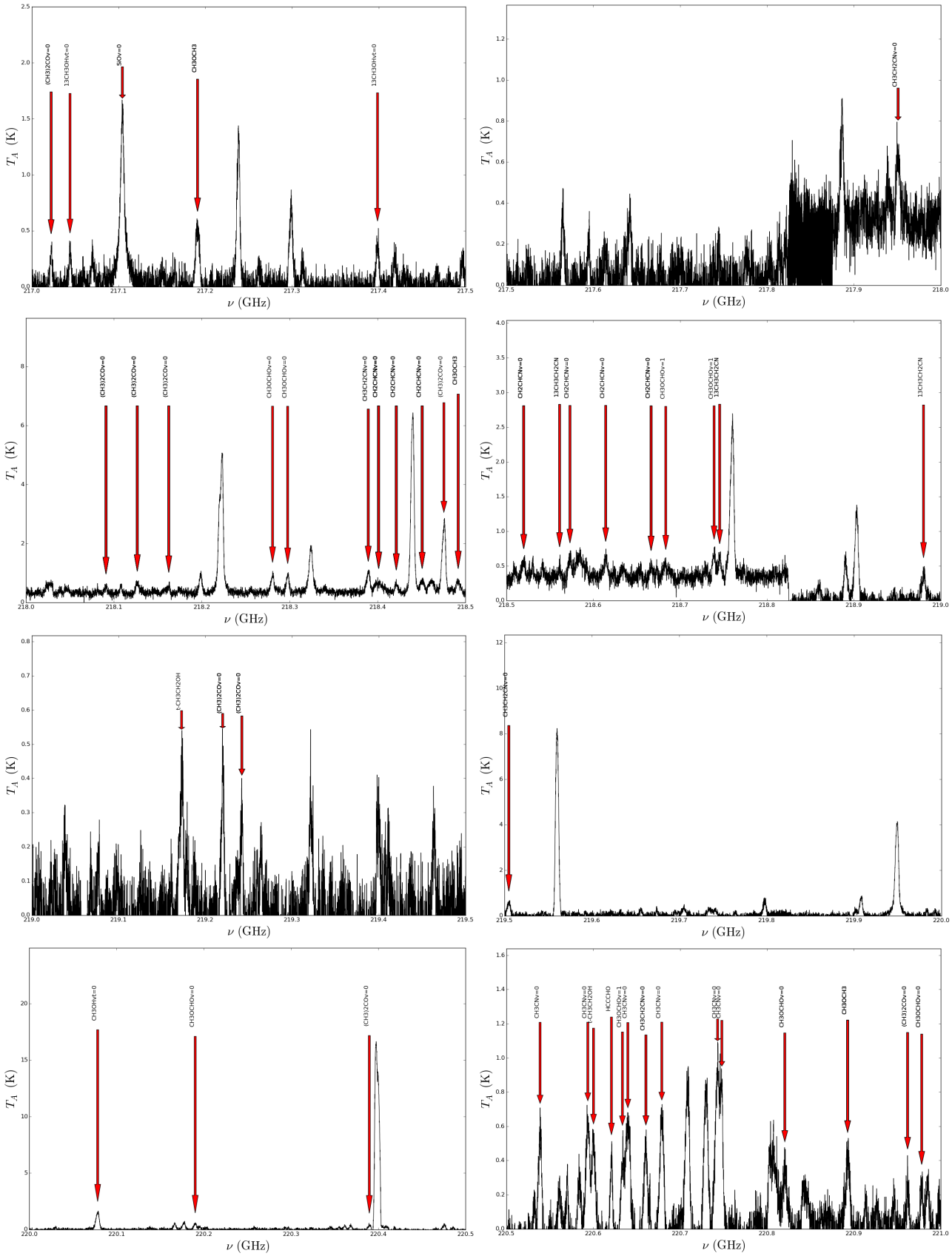

Figure A.1: (*Cont.*) Spectra of G327.3-0.6.

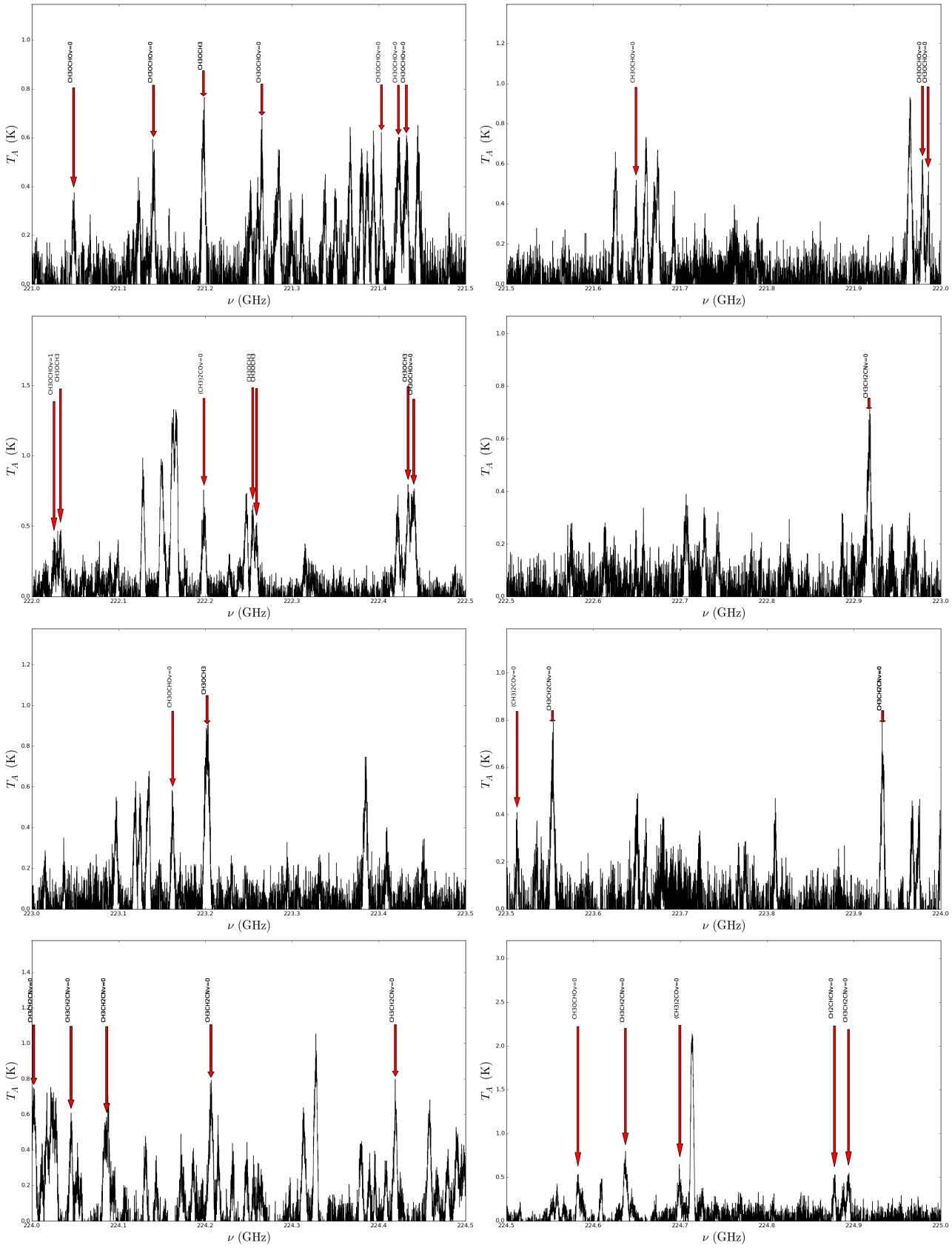

Figure A.1: (*Cont.*) Spectra of G327.3-0.6.

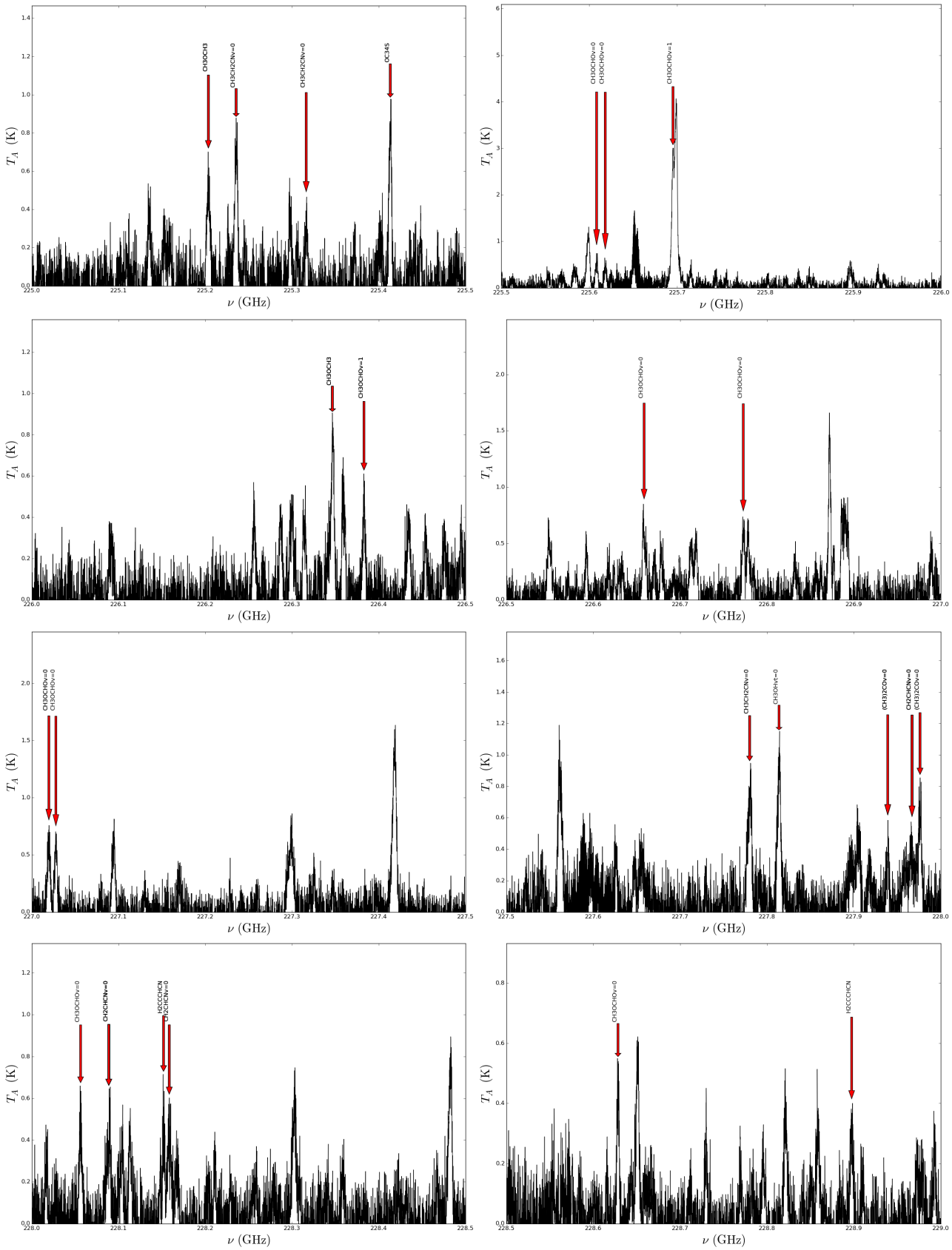

Figure A.1: (*Cont.*) Spectra of G327.3-0.6.

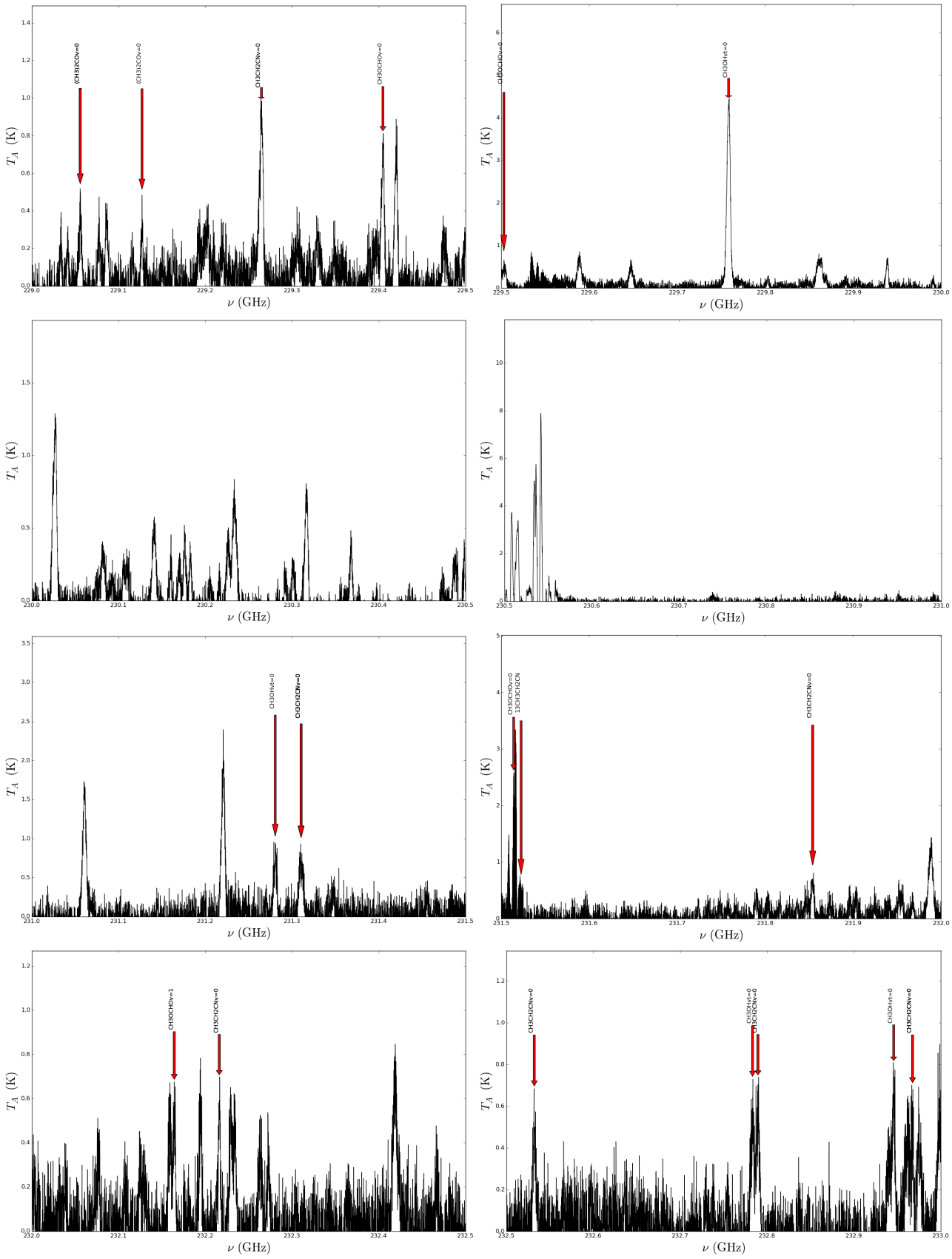

Figure A.1: (*Cont.*) Spectra of G327.3-0.6.

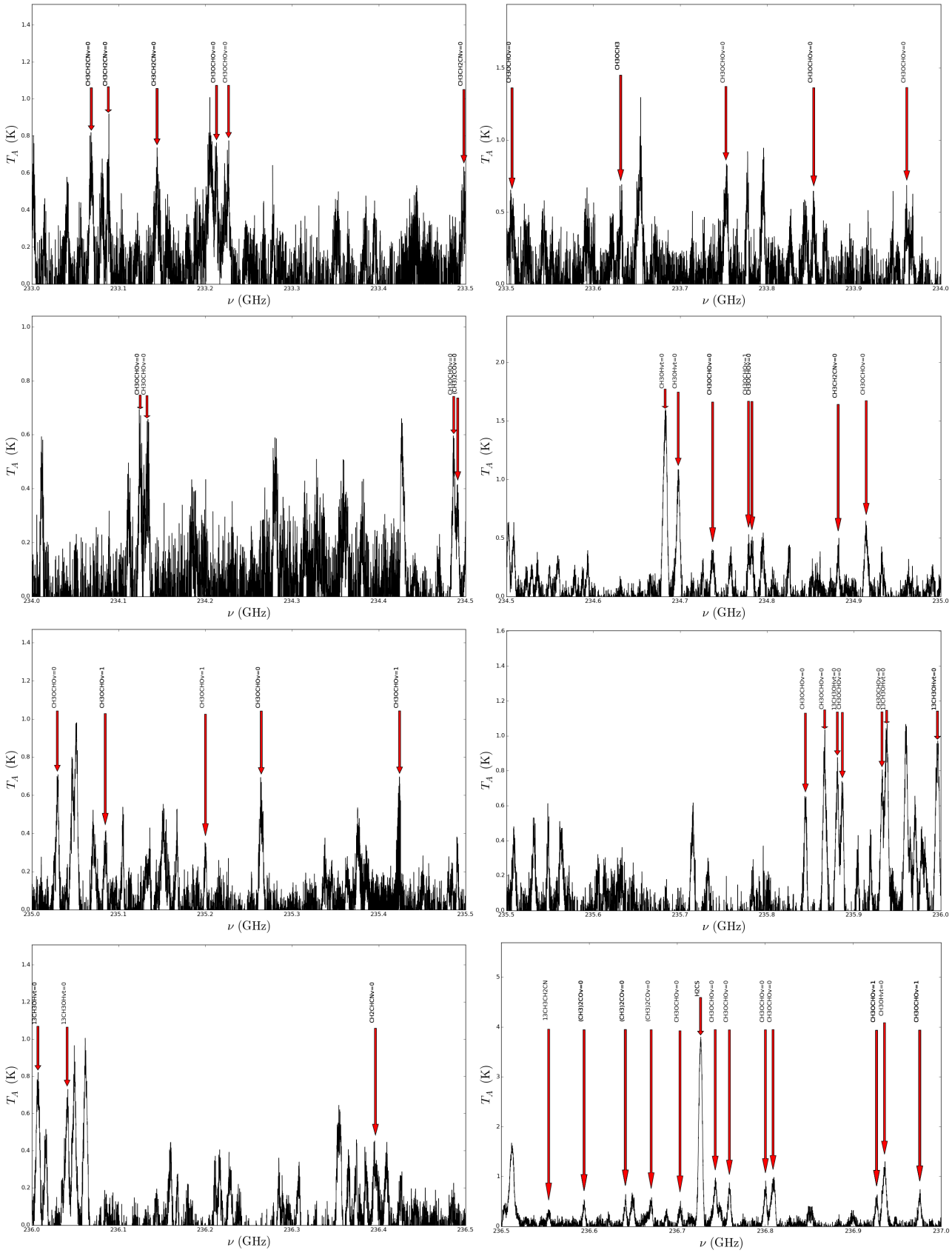

Figure A.1: (*Cont.*) Spectra of G327.3-0.6.

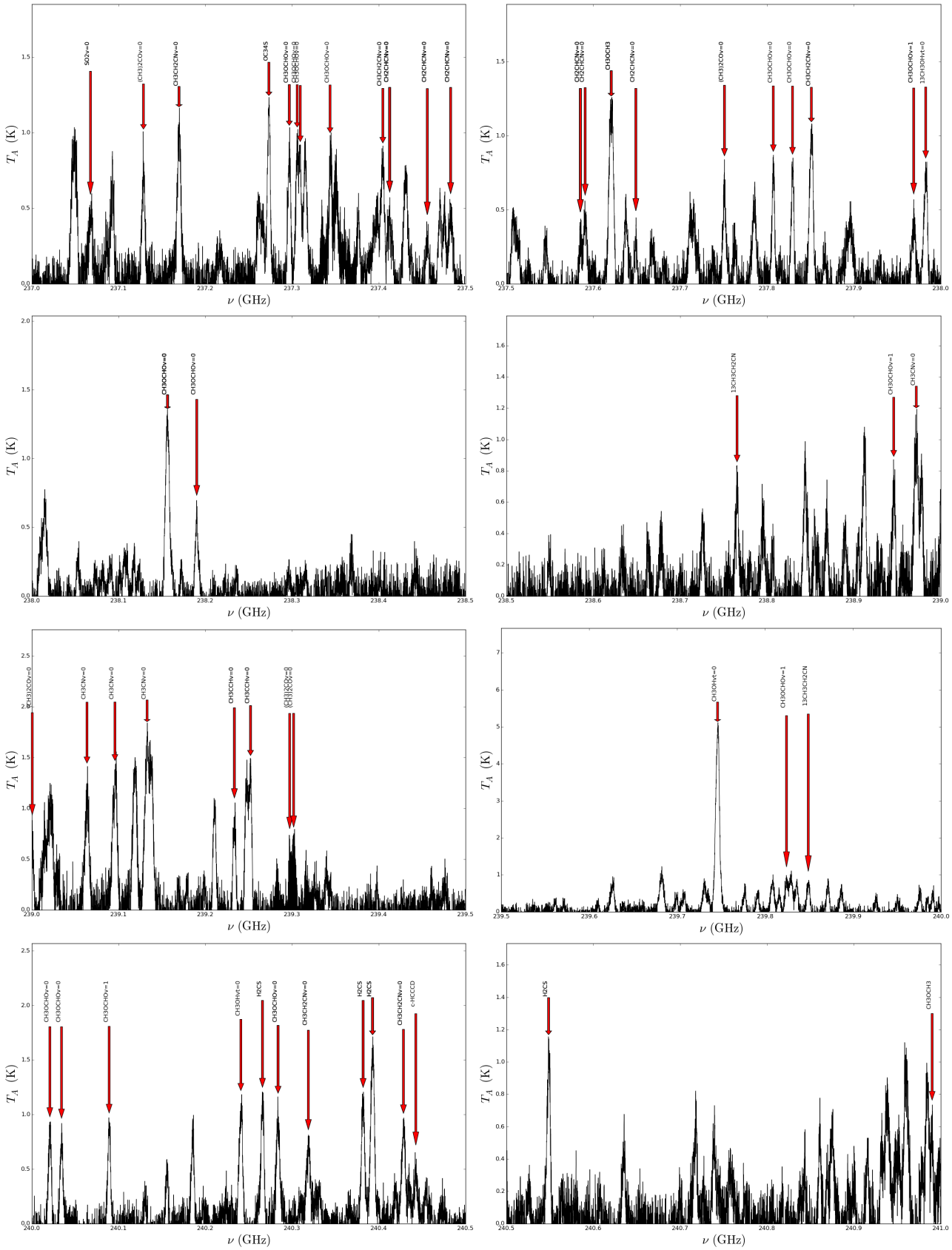

Figure A.1: (*Cont.*) Spectra of G327.3-0.6.

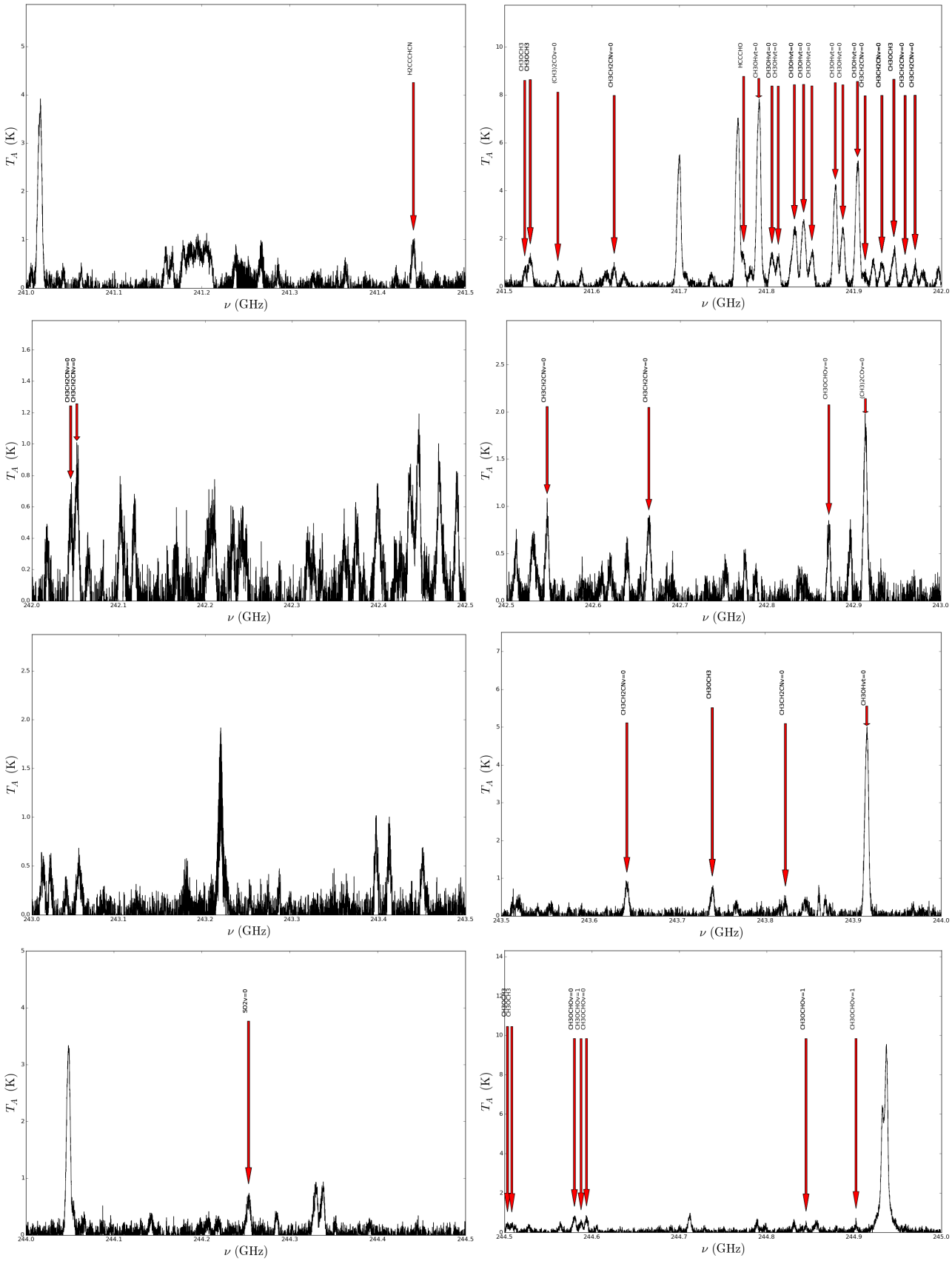

Figure A.1: (*Cont.*) Spectra of G327.3-0.6.

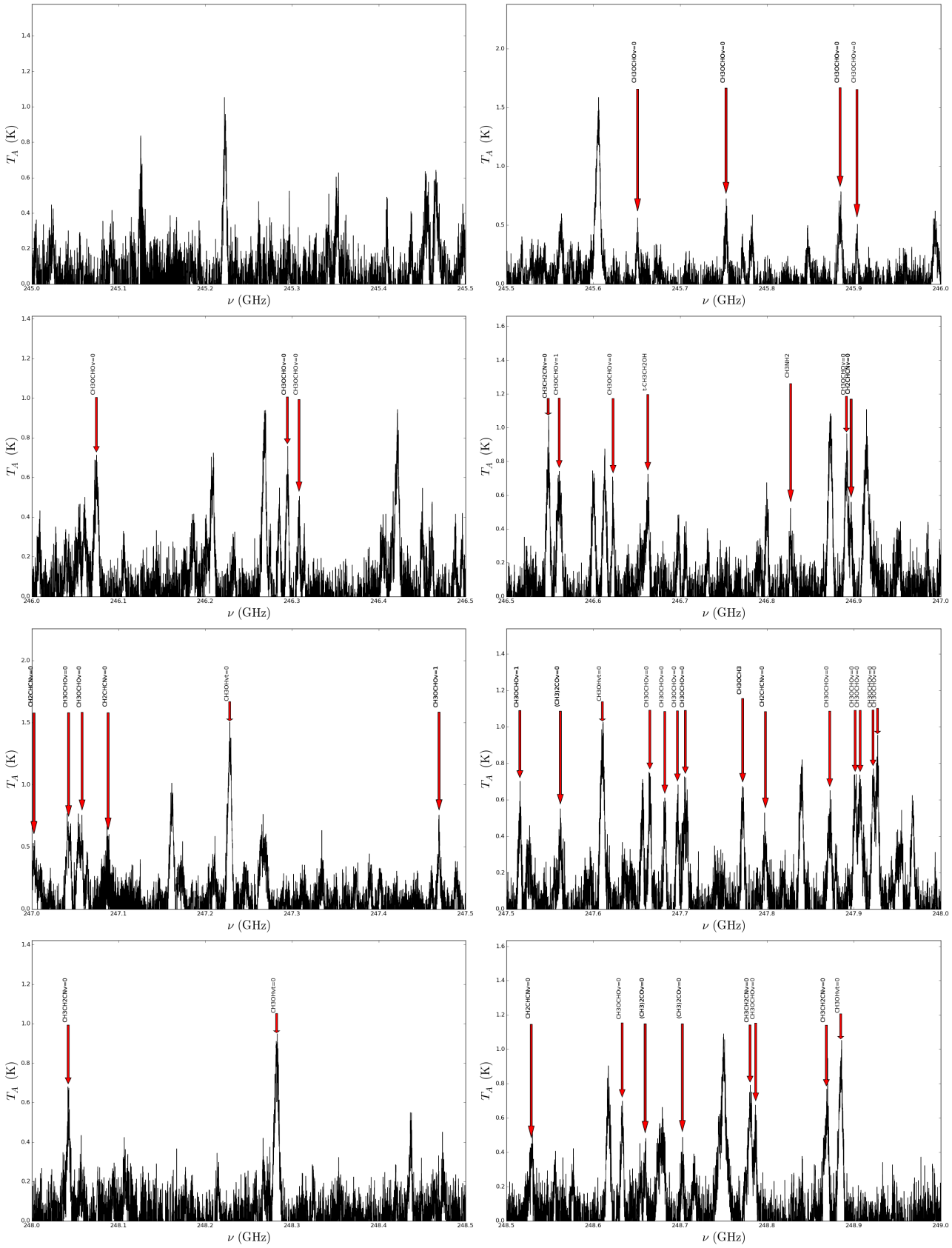

Figure A.1: (*Cont.*) Spectra of G327.3-0.6.

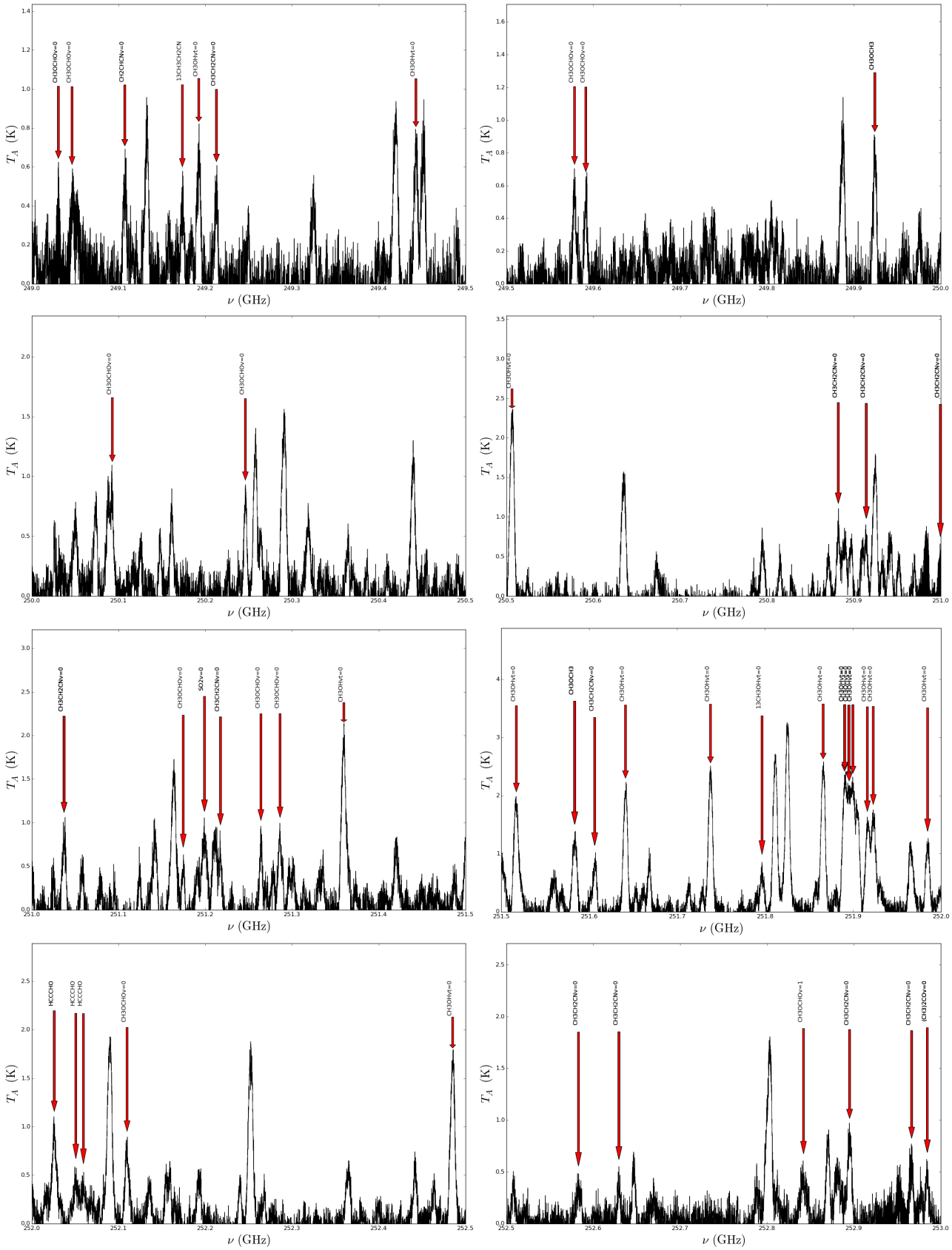

Figure A.1: (*Cont.*) Spectra of G327.3-0.6.

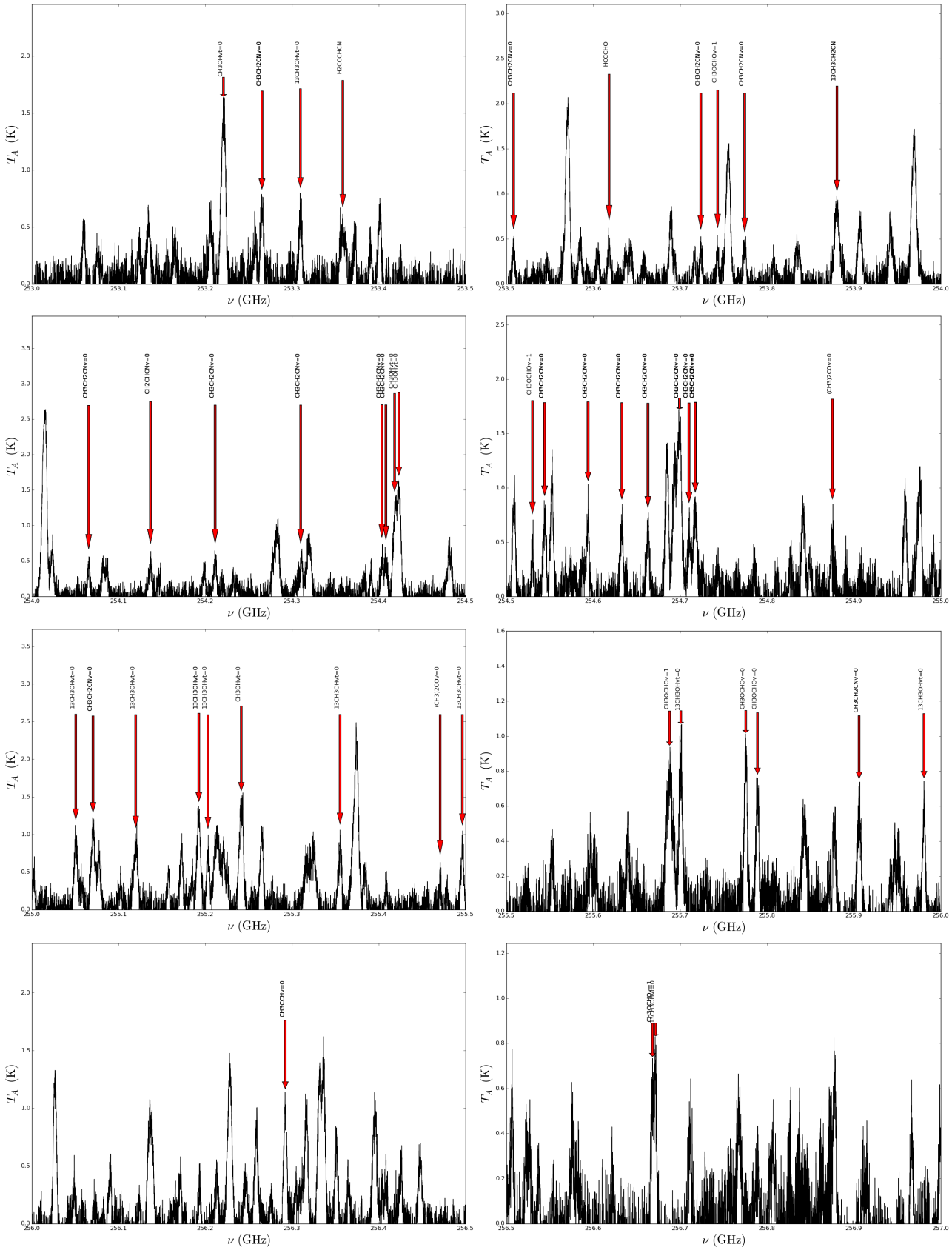

Figure A.1: (*Cont.*) Spectra of G327.3-0.6.

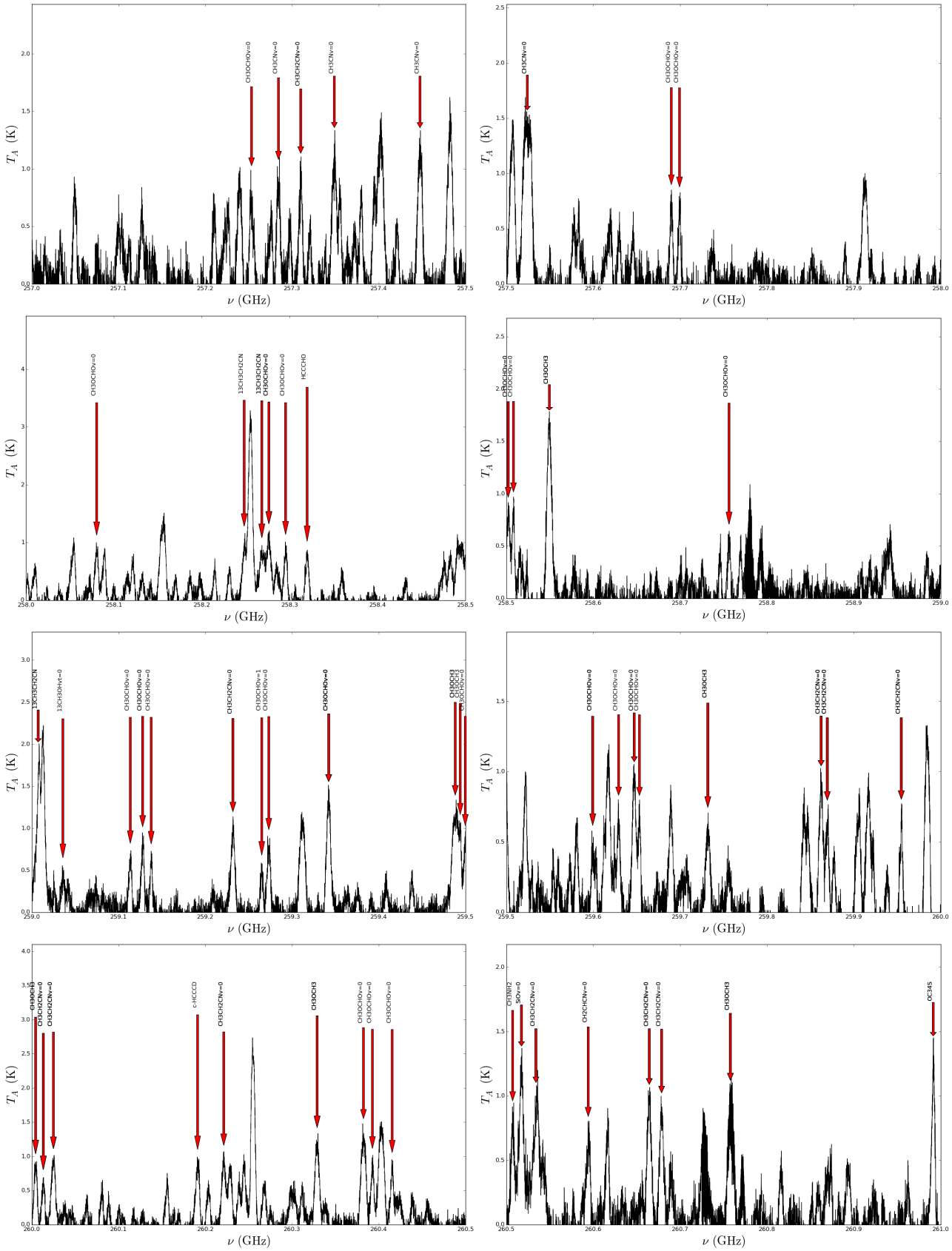

Figure A.1: (*Cont.*) Spectra of G327.3-0.6.

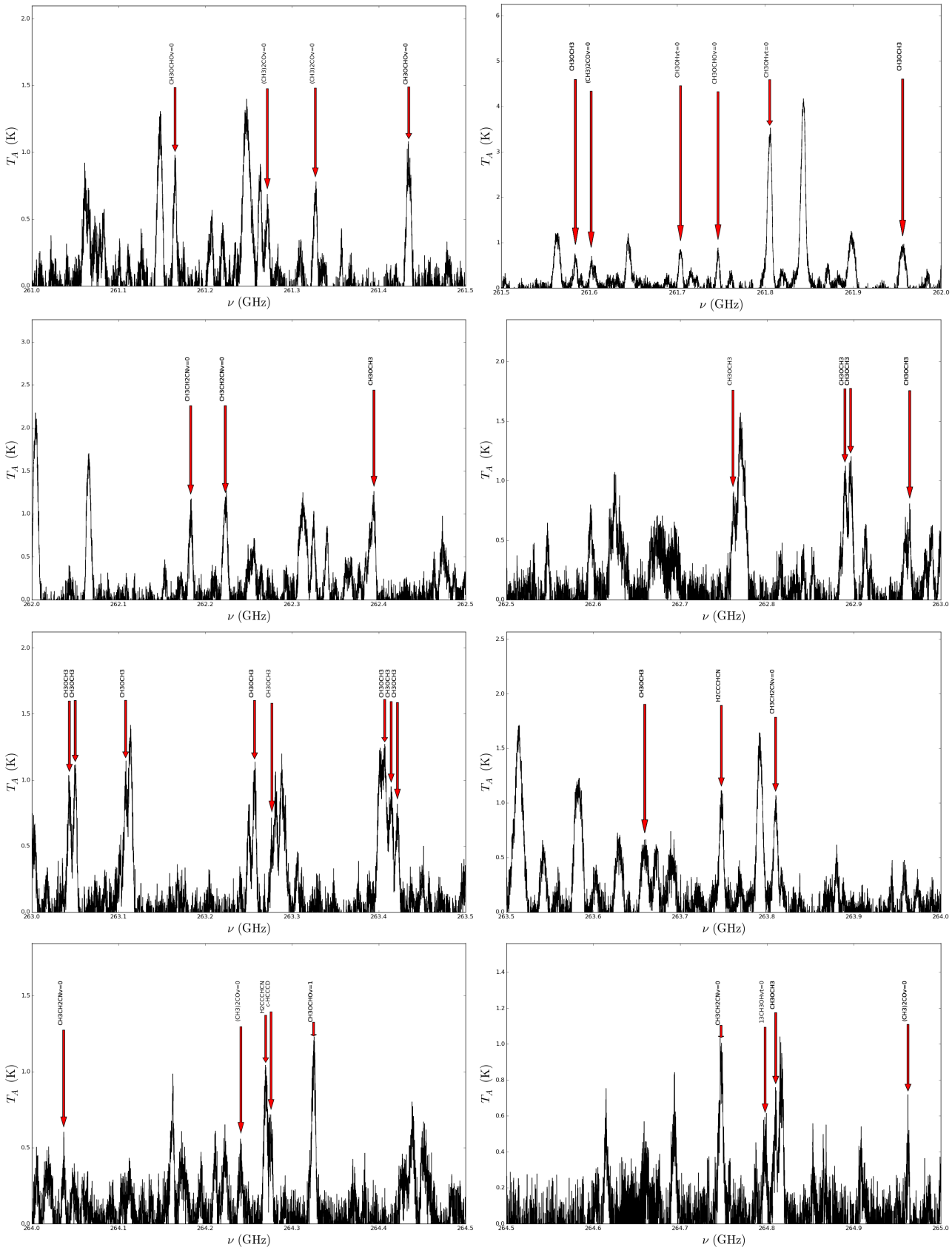

Figure A.1: (*Cont.*) Spectra of G327.3-0.6.

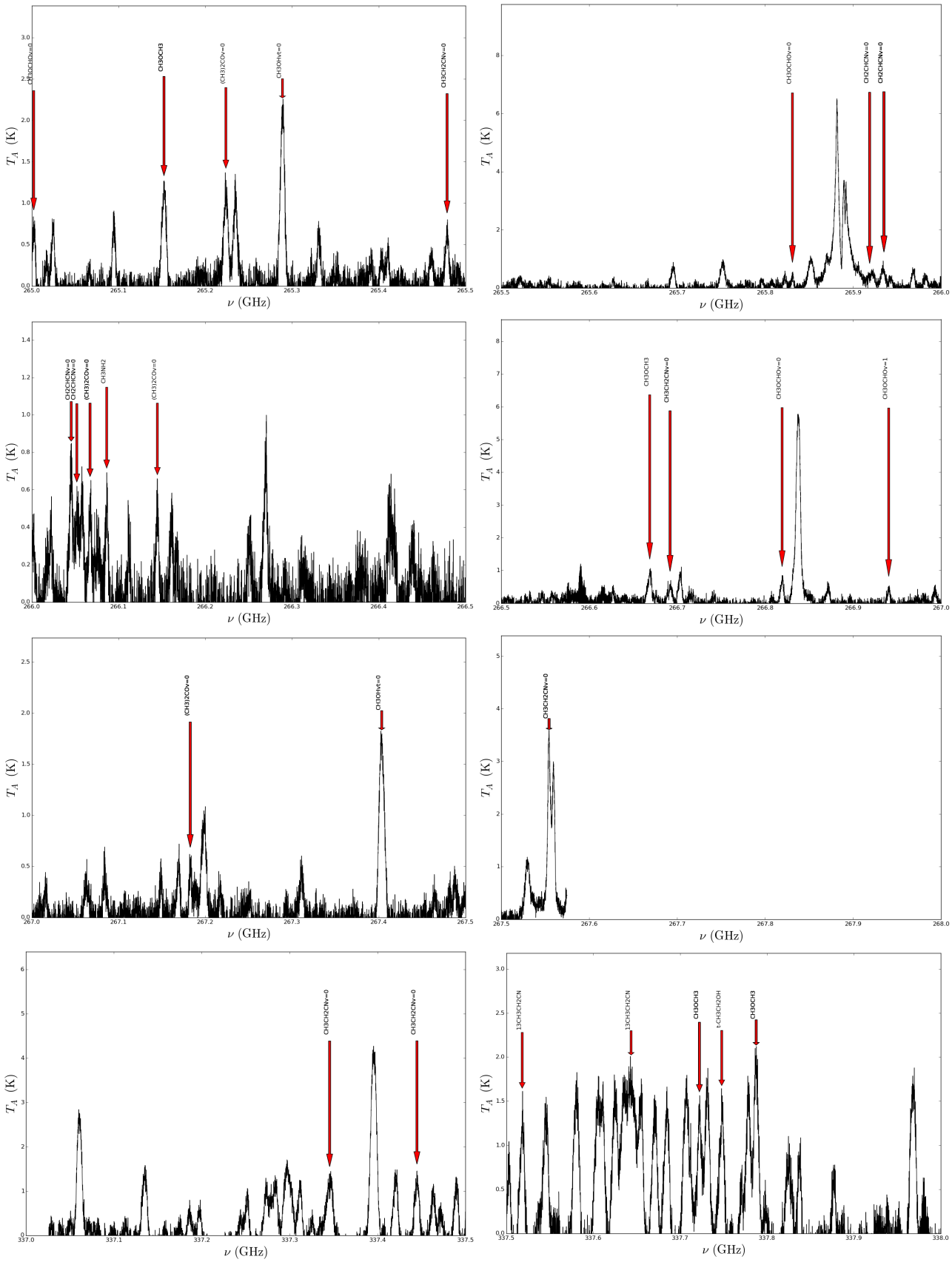

Figure A.1: (*Cont.*) Spectra of G327.3-0.6.

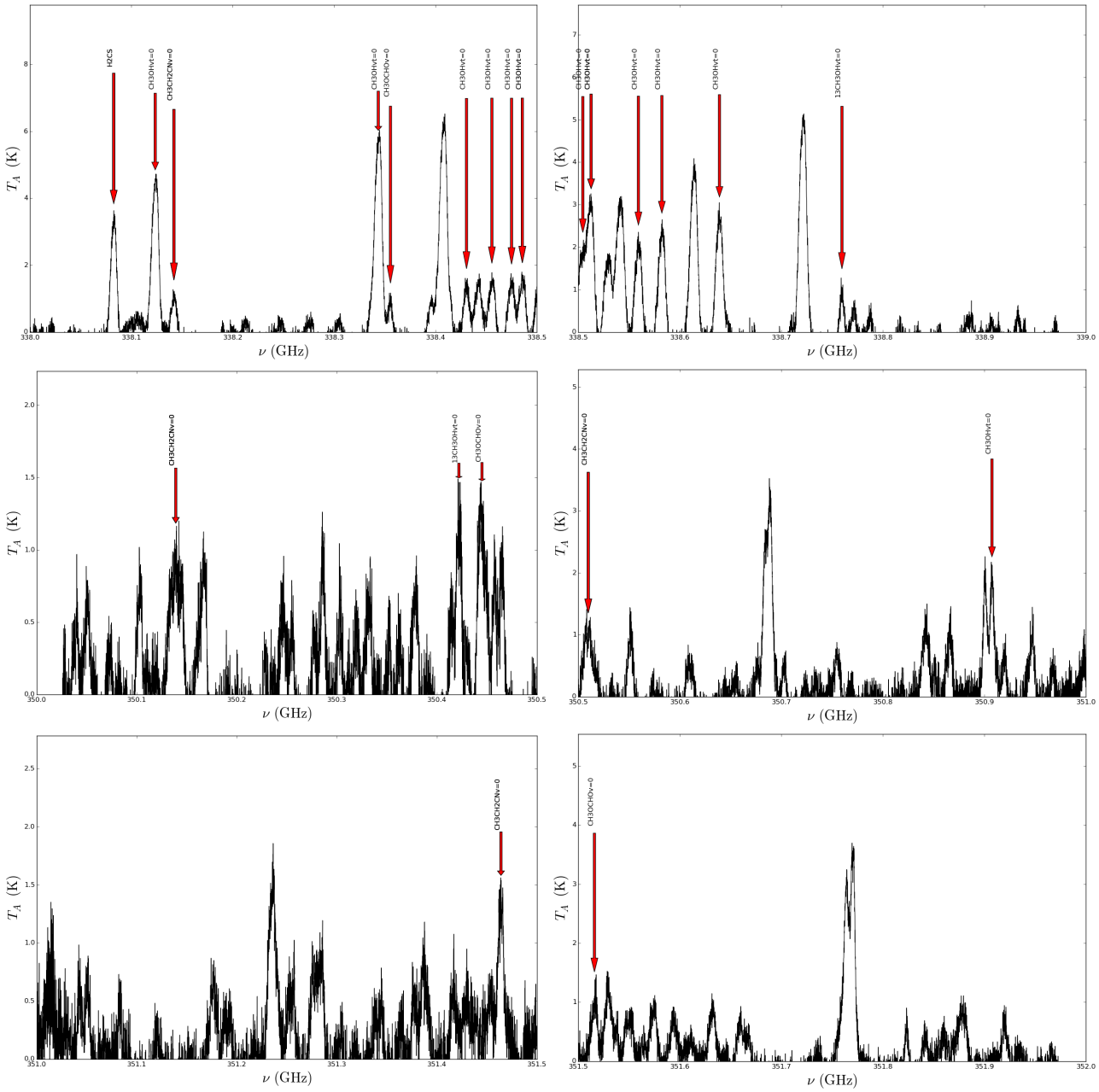

Figure A.1: (*Cont.*) Spectra of G327.3-0.6.

A.2 Spectra of NGC 6334 I

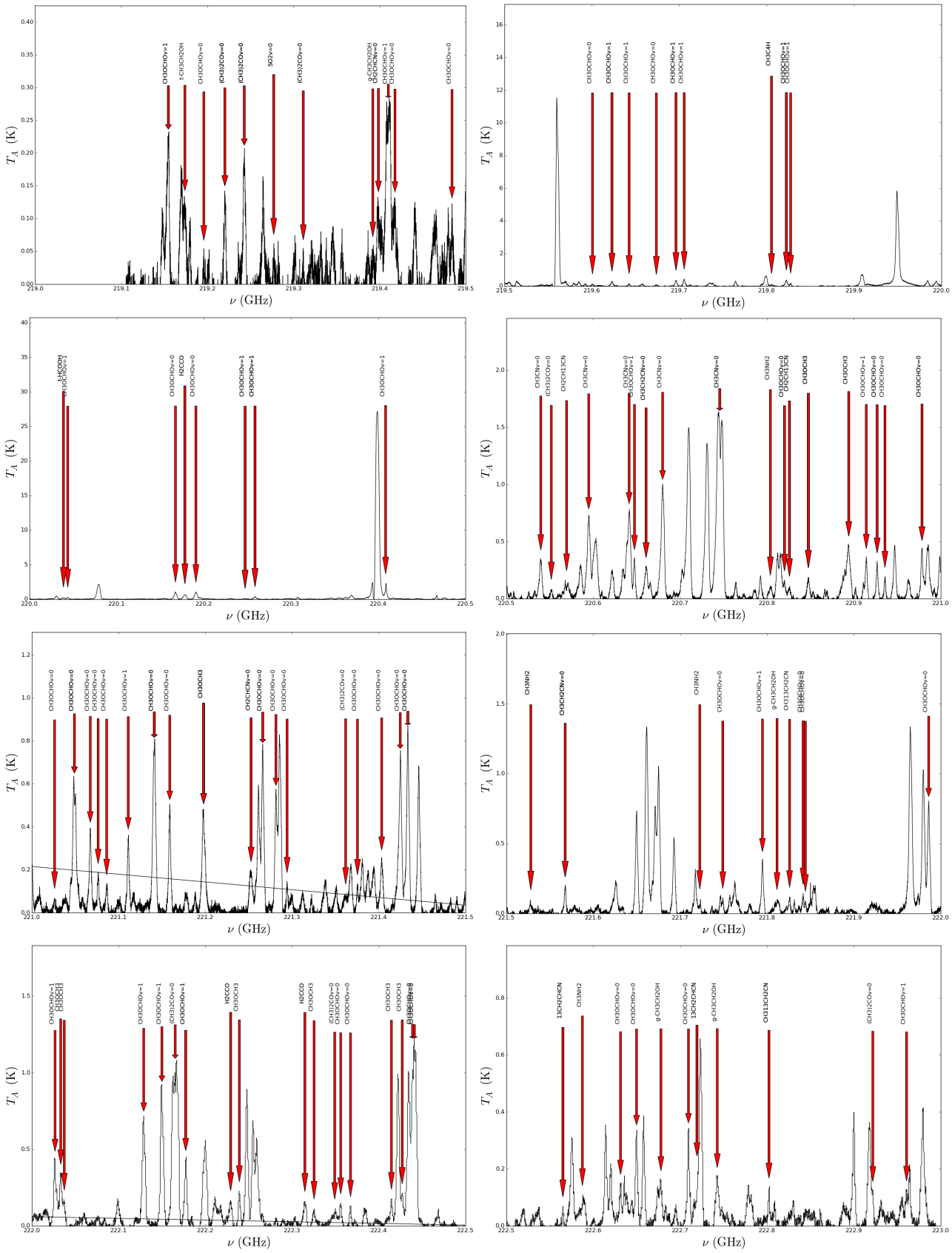

Figure A.2: Spectra of NGC 6334 I.

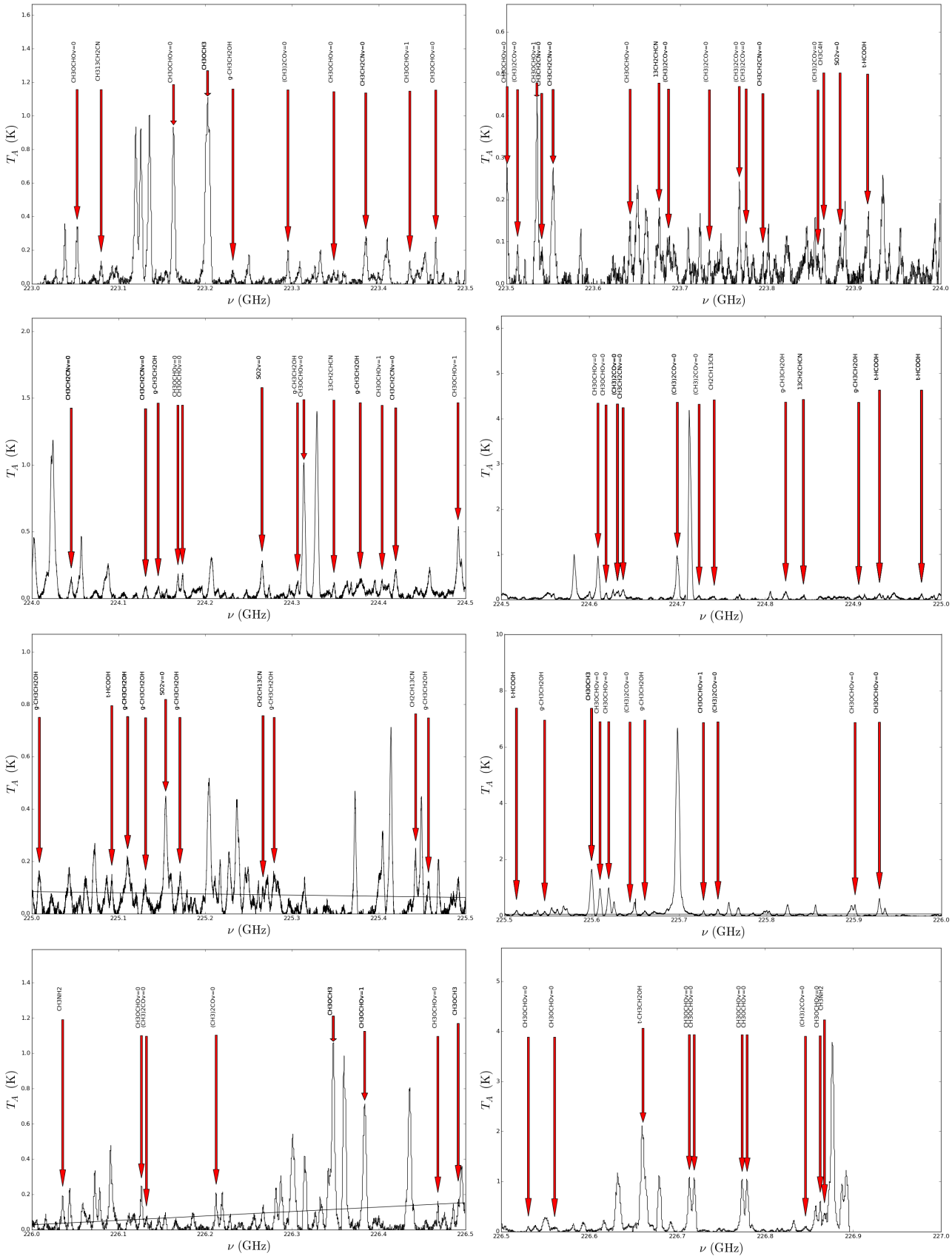

Figure A.2: (*Cont.*) Spectra of NGC 6334 I.

Appendix B Bar plots for rotational diagrams

B.1 Results for G327.3-0.6

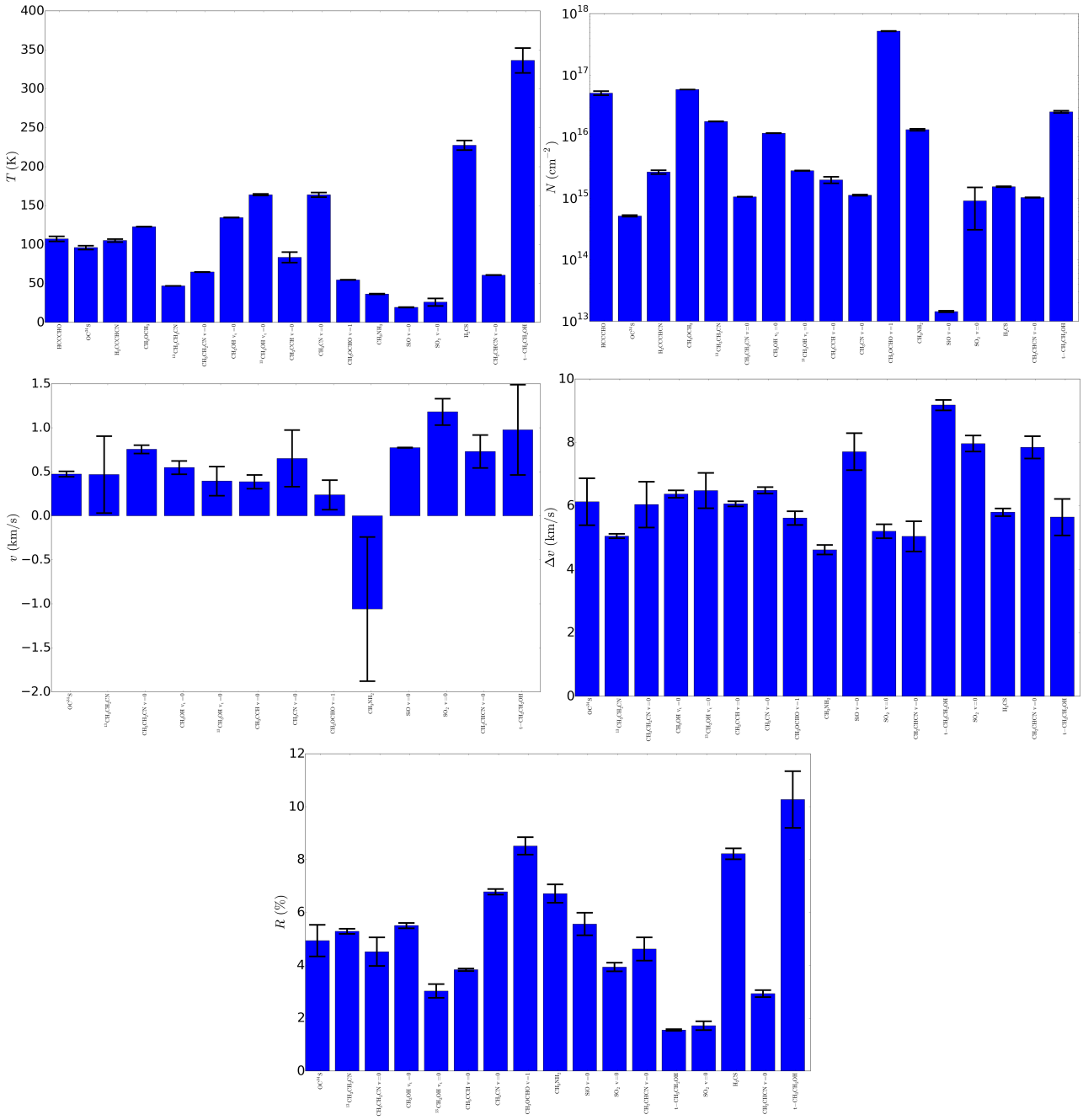

Figure B.1: Bar plots of results of the rotational diagram method for G327.3-0.6 (see Table 4.1 for data).

B.2 Results for NGC 6334 I

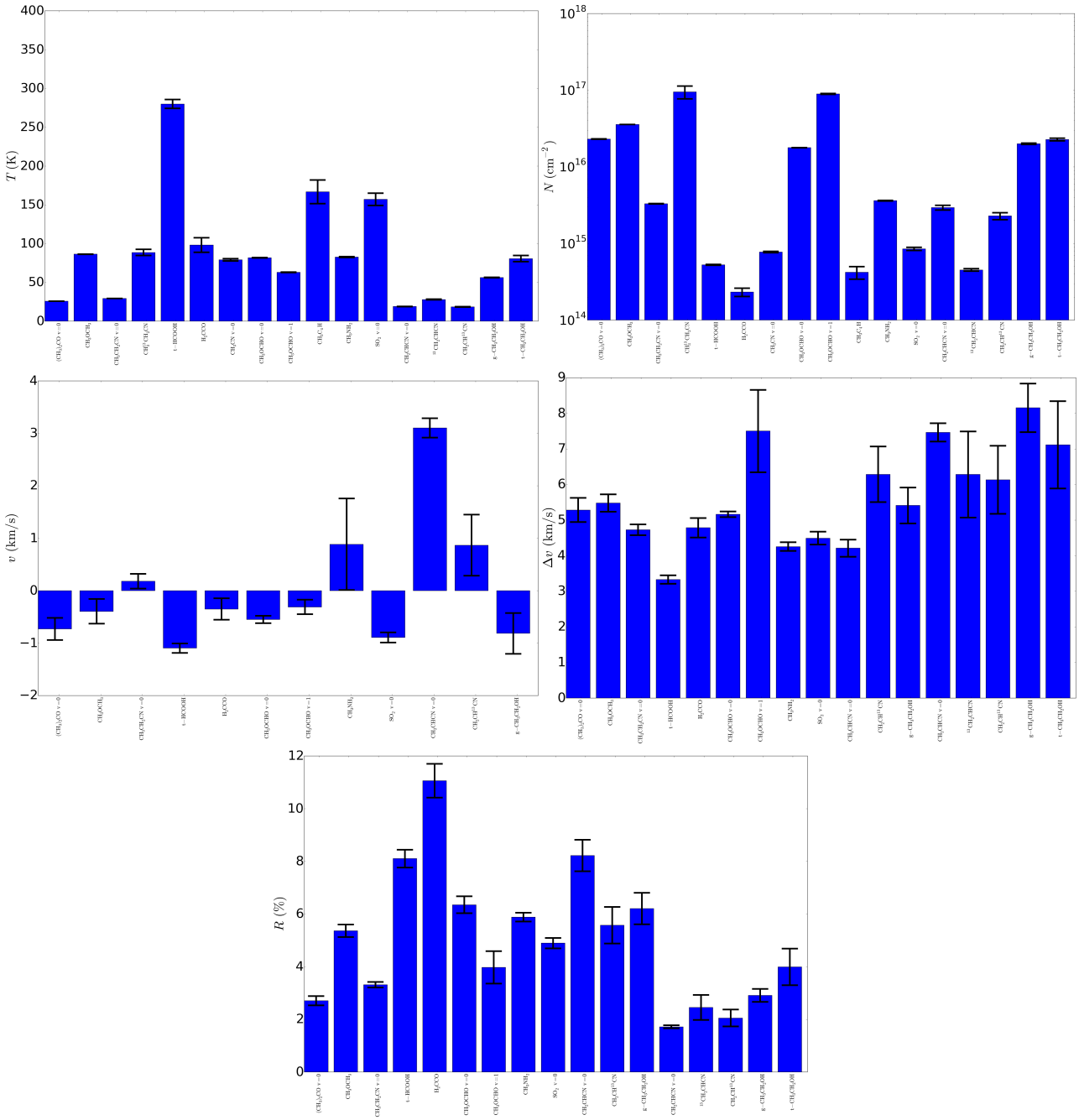

Figure B.2: Bar plots of results of the rotational diagram method for NGC 6334 I (see Table 4.1 for data).

Appendix C Bar plots for population diagrams

C.1 Results for G327.3-0.6

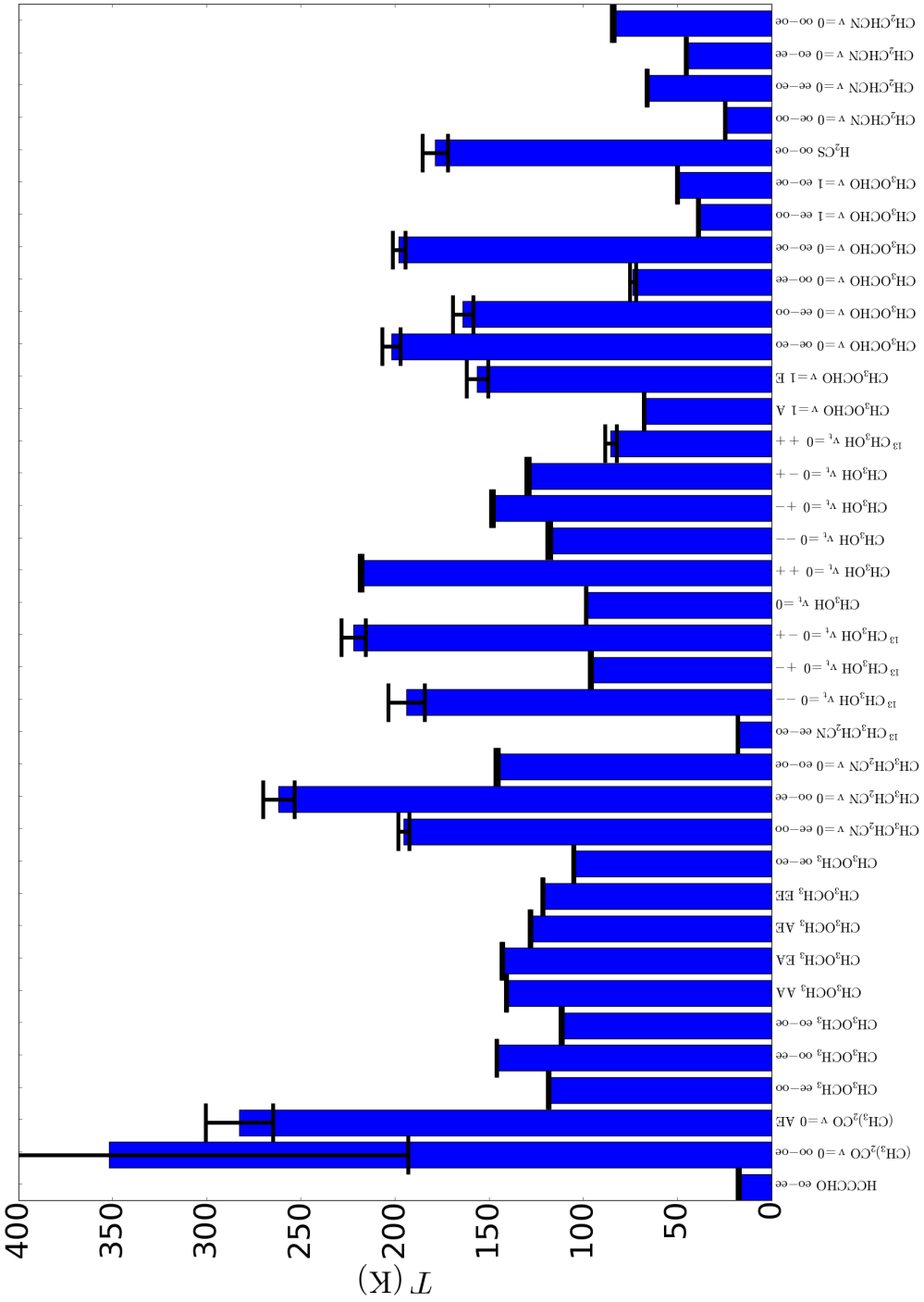

Figure C.1: Bar plots of results of the population diagram method (see Table 4.3 for data) for G327.3-0.6.

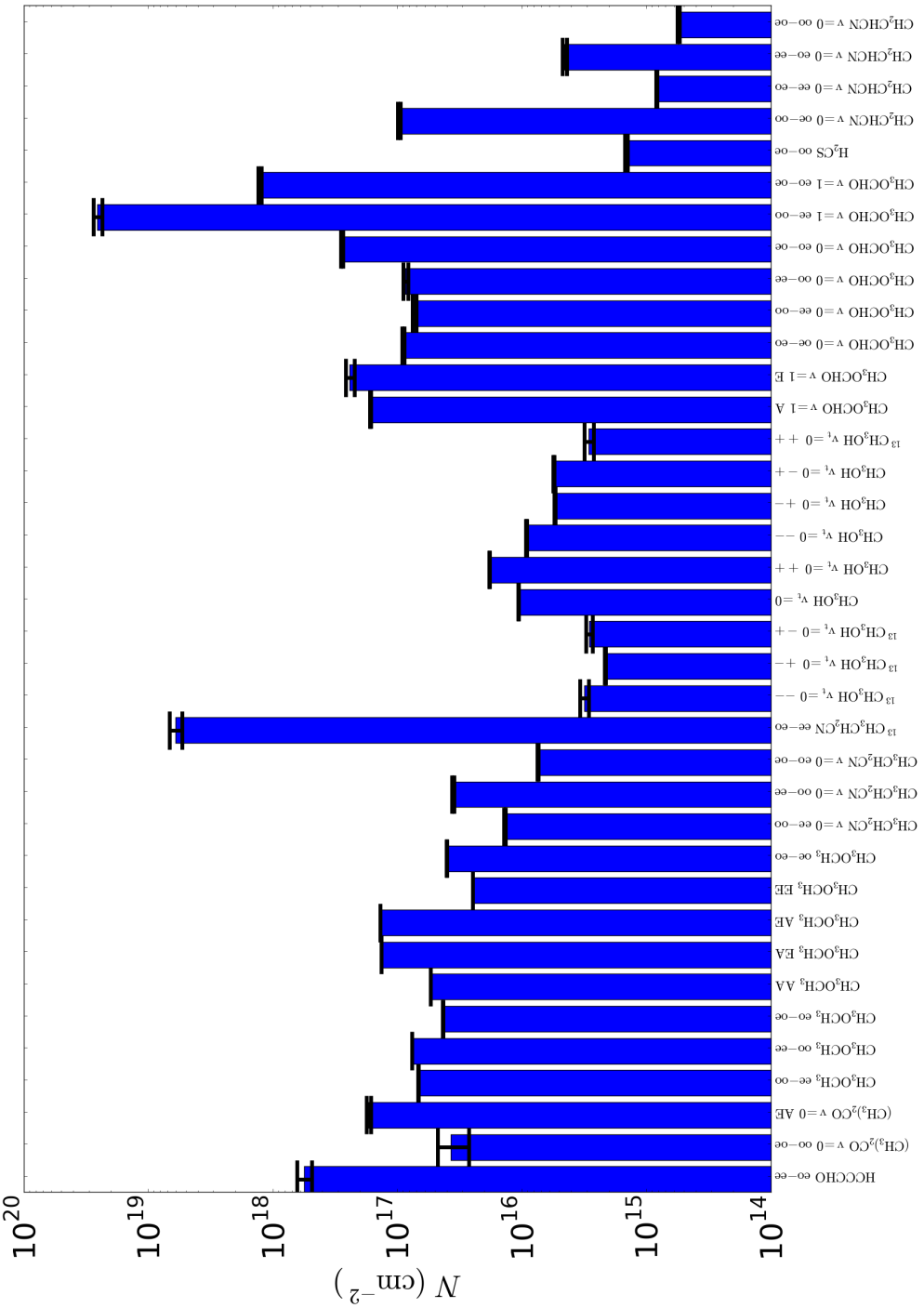

Figure C.1: (*Cont.*) Bar plots of results of the population diagram method (see Table 4.3 for data) for G327.3-0.6.

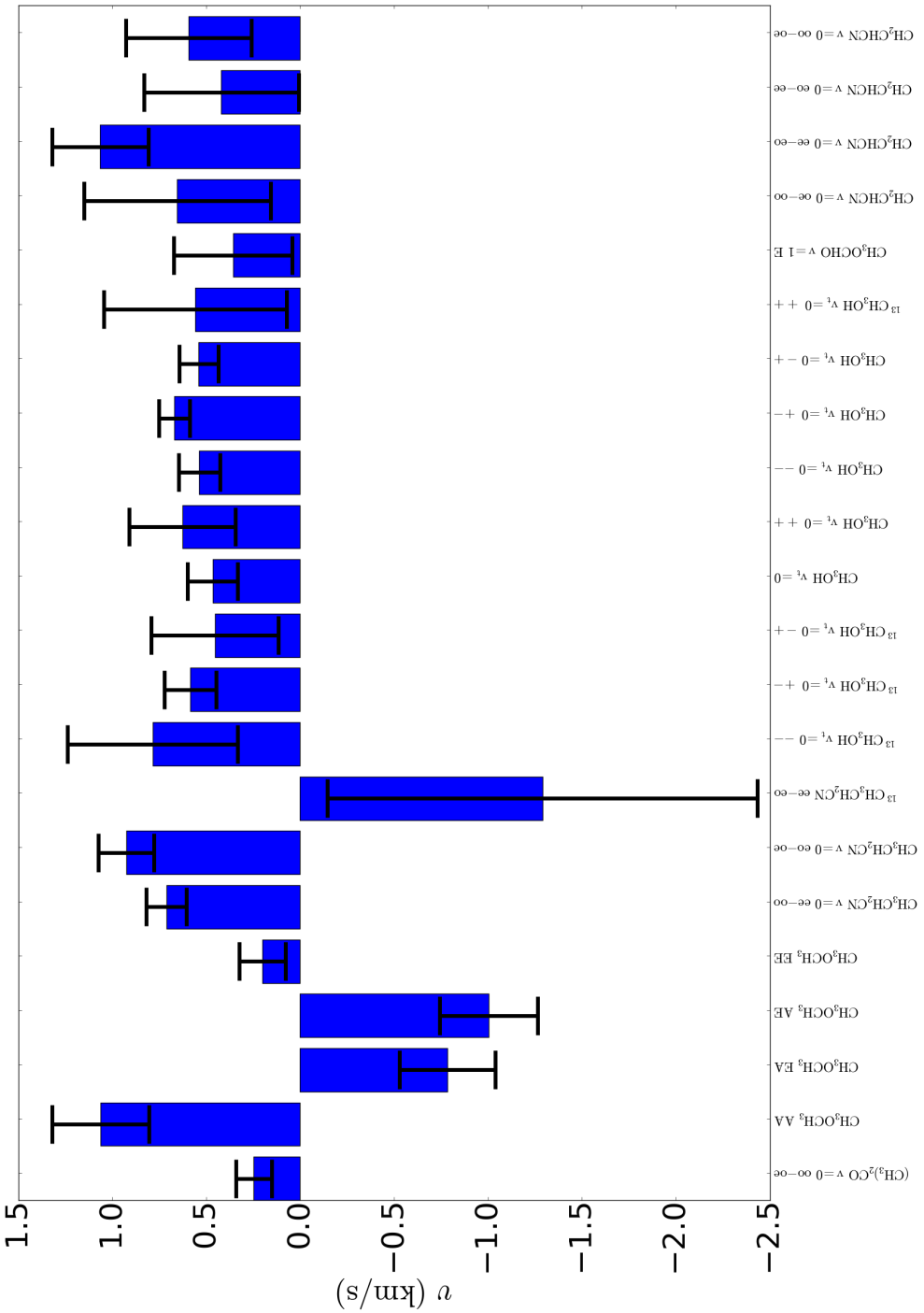

Figure C.1: (*Cont.*) Bar plots of results of the population diagram method (see Table 4.3 for data) for G327.3-0.6.

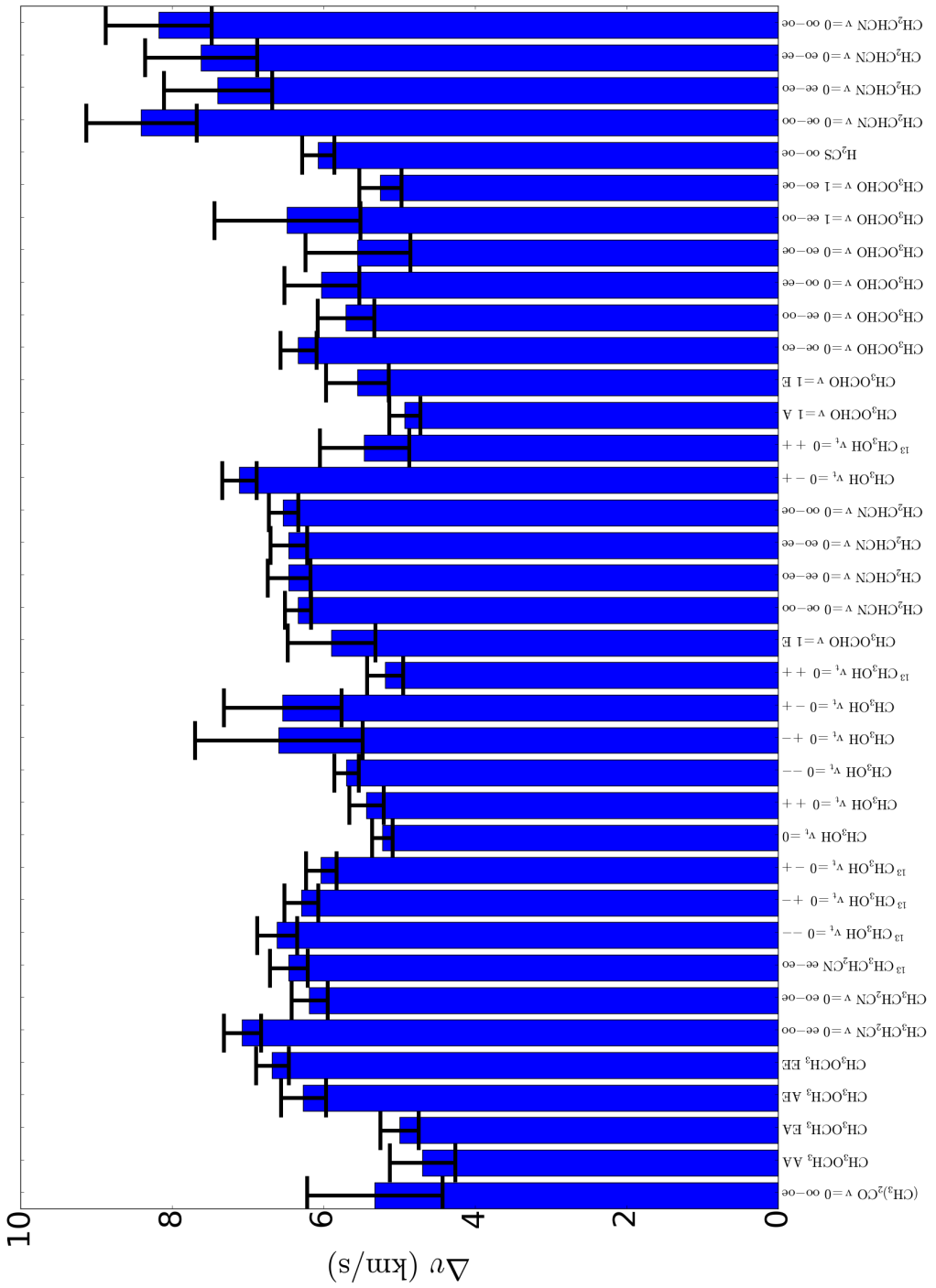

Figure C.1: (*Cont.*) Bar plots of results of the population diagram method (see Table 4.3 for data) for G327.3-0.6.

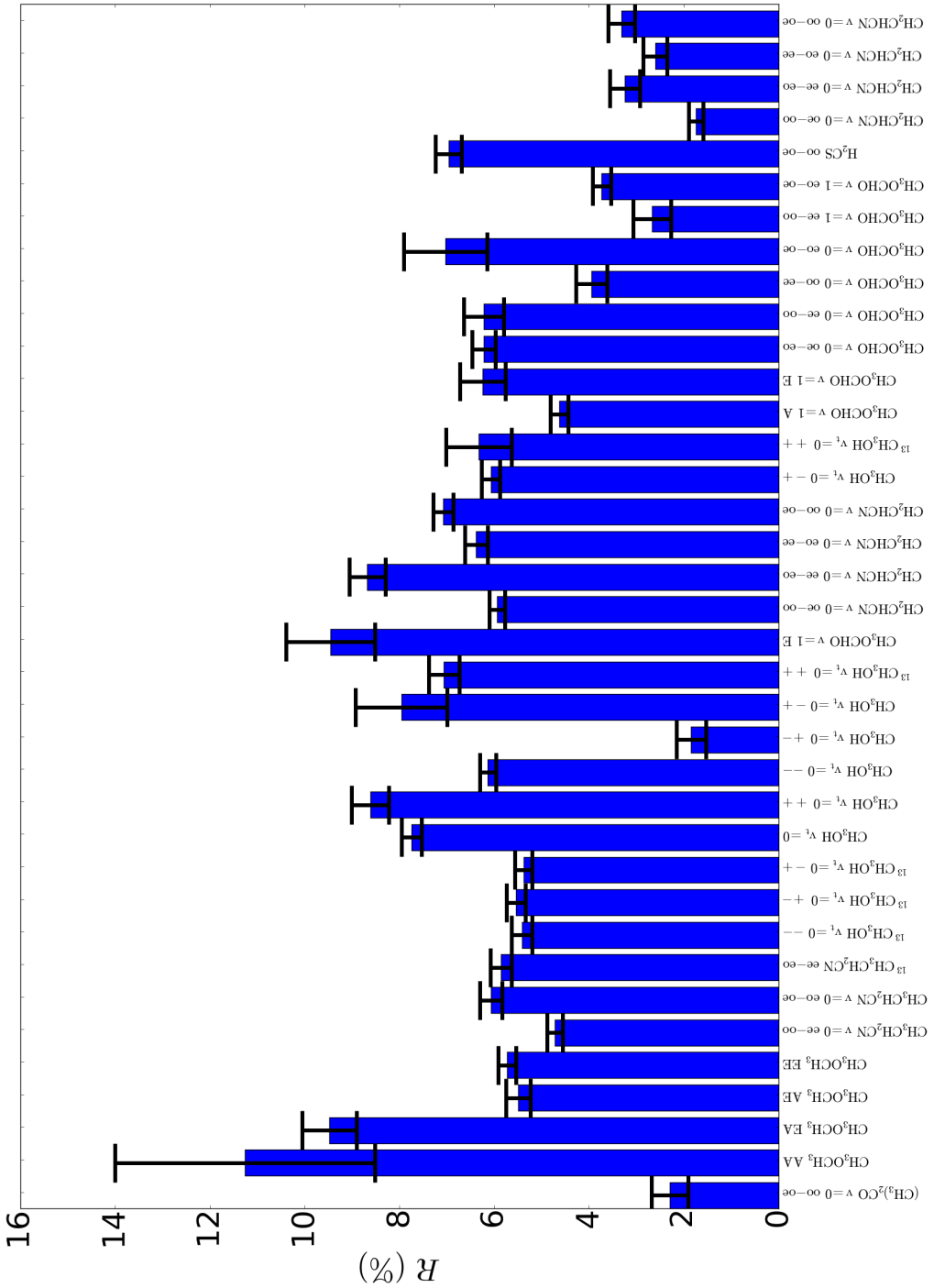

Figure C.1: (*Cont.*) Bar plots of results of the population diagram method (see Table 4.3 for data) for G327.3-0.6.

C.2 Results for NGC 6334 I

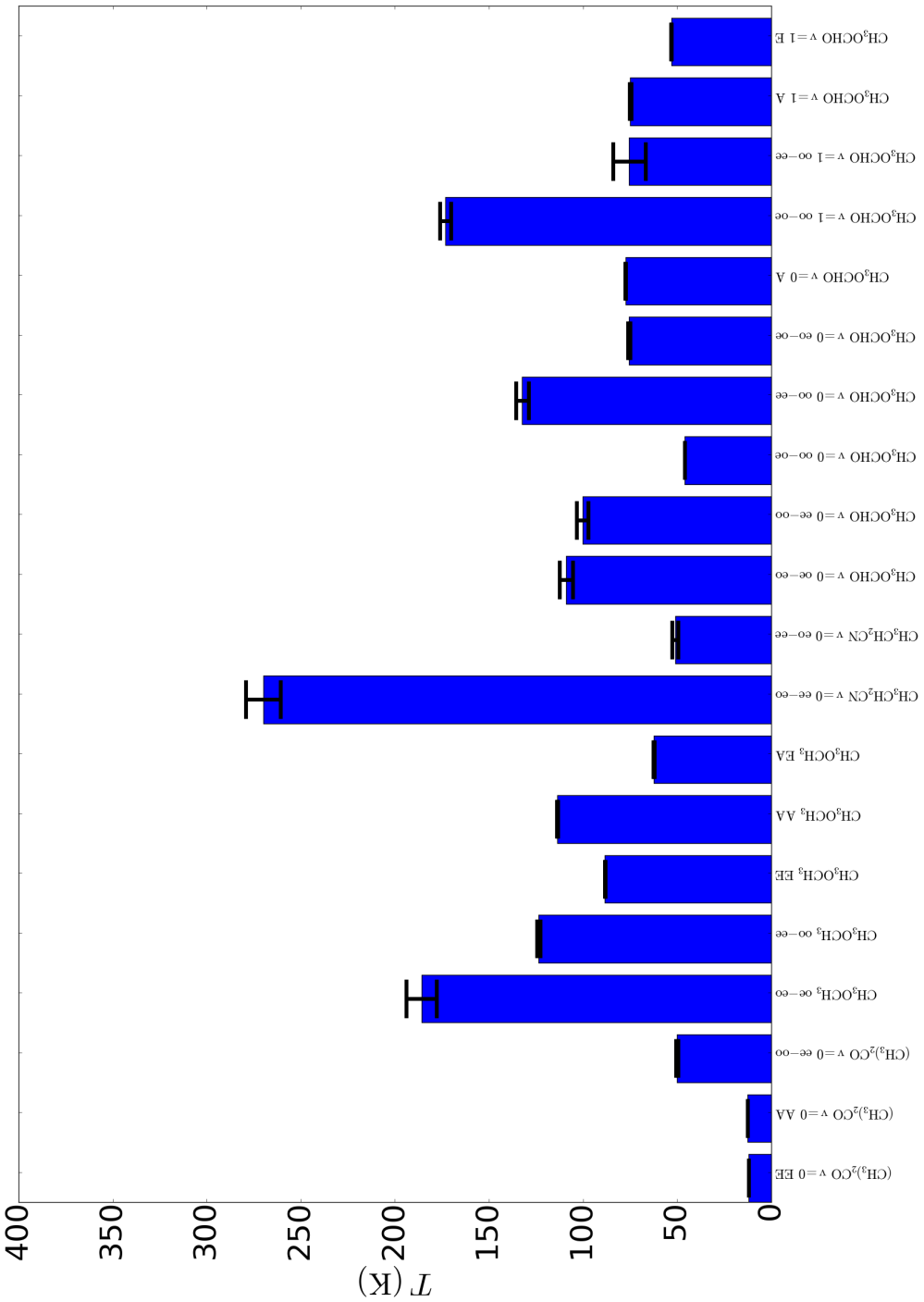

Figure C.2: Bar plots of results of the population diagram method (see Table 4.3 for data) for NGC 6334 I.

Figure C.2: (*Cont.*) Bar plots of results of the population diagram method (see Table reftab:popdiag for data) for NGC 6334 I.

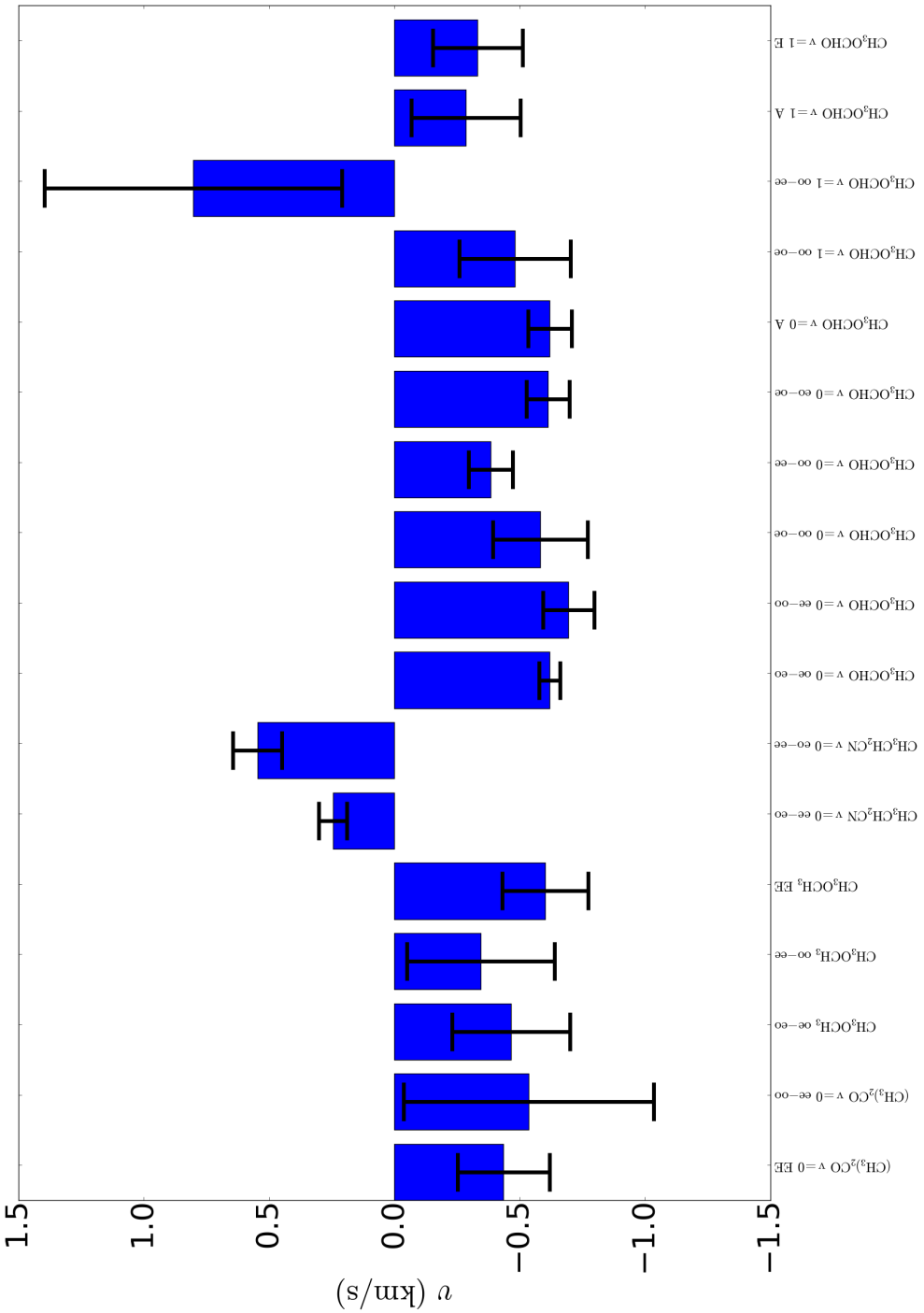

Figure C.2: (*Cont.*) Bar plots of results of the population diagram method (see Table 4.3 for data) for NGC 6334 I.

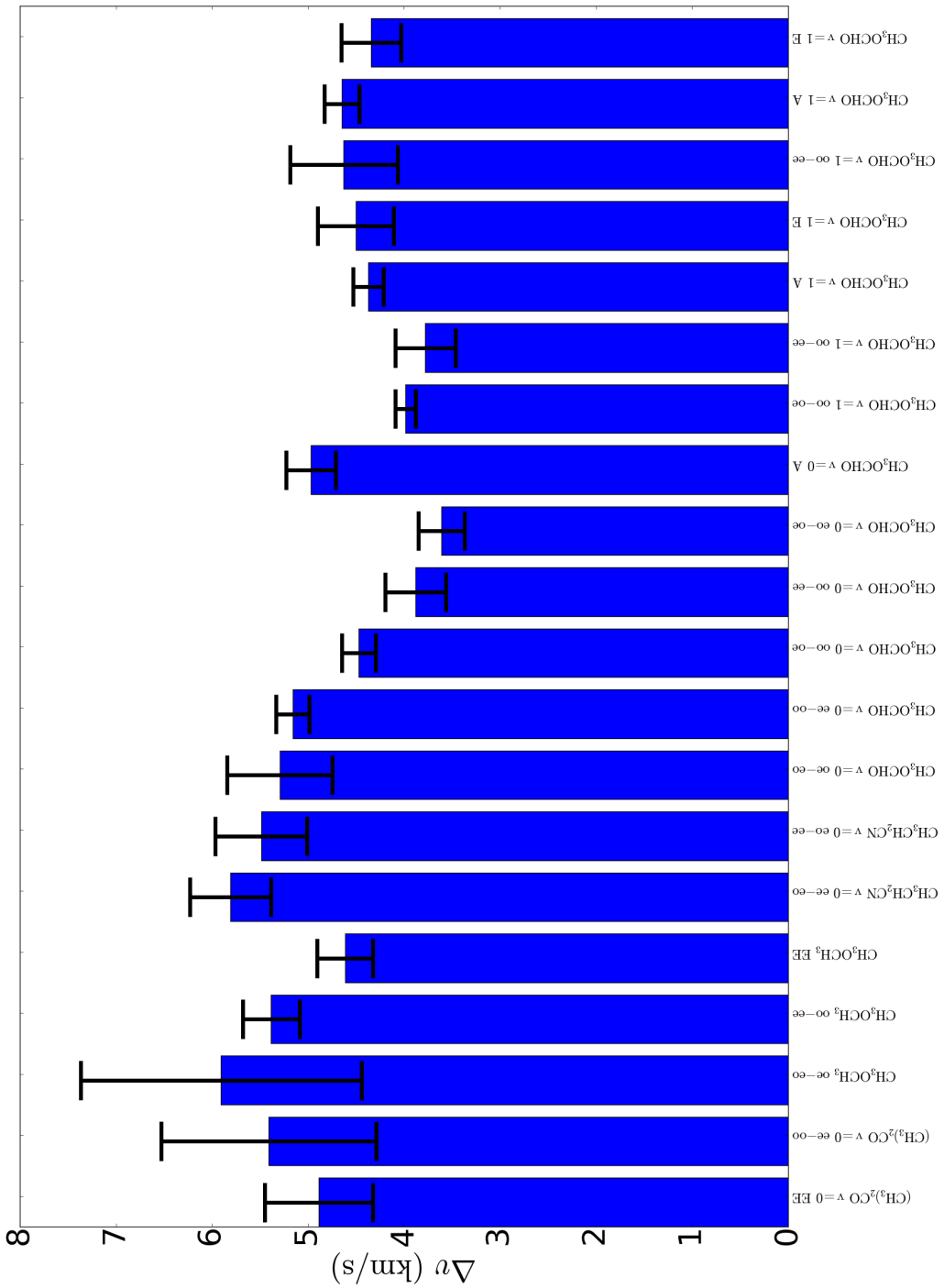

Figure C.2: (*Cont.*) Bar plots of results of the population diagram method (see Table 4.3for data) for NGC 6334 I.

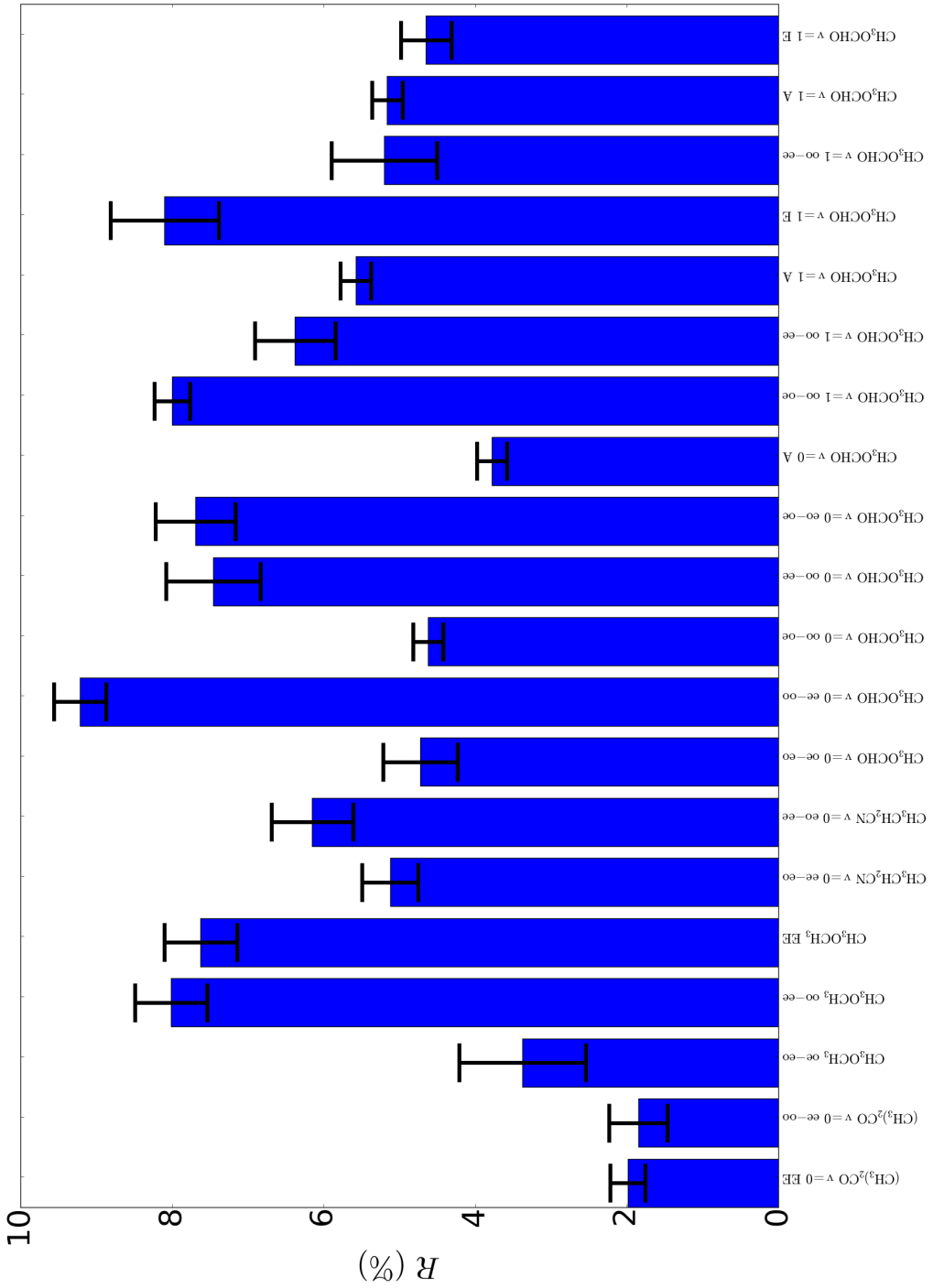

Figure C.2: (*Cont.*) Bar plots of results of the population diagram method (see Table 4.3 for data) for NGC 6334 I.

Appendix D Rotational diagrams

D.1 Rotational diagrams for G327.3-0.6

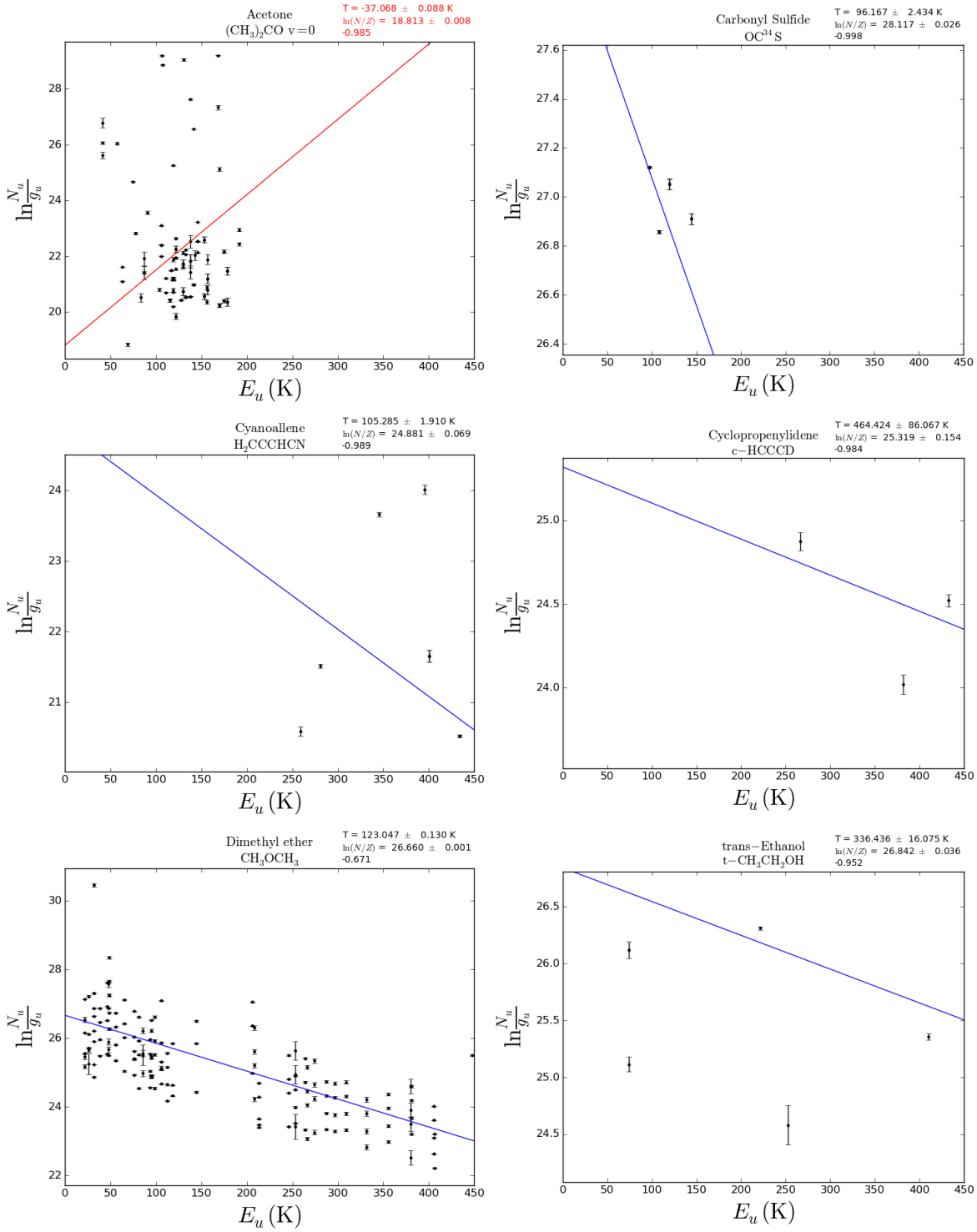

Figure D.1: Rotational diagrams for G327.3-0.6

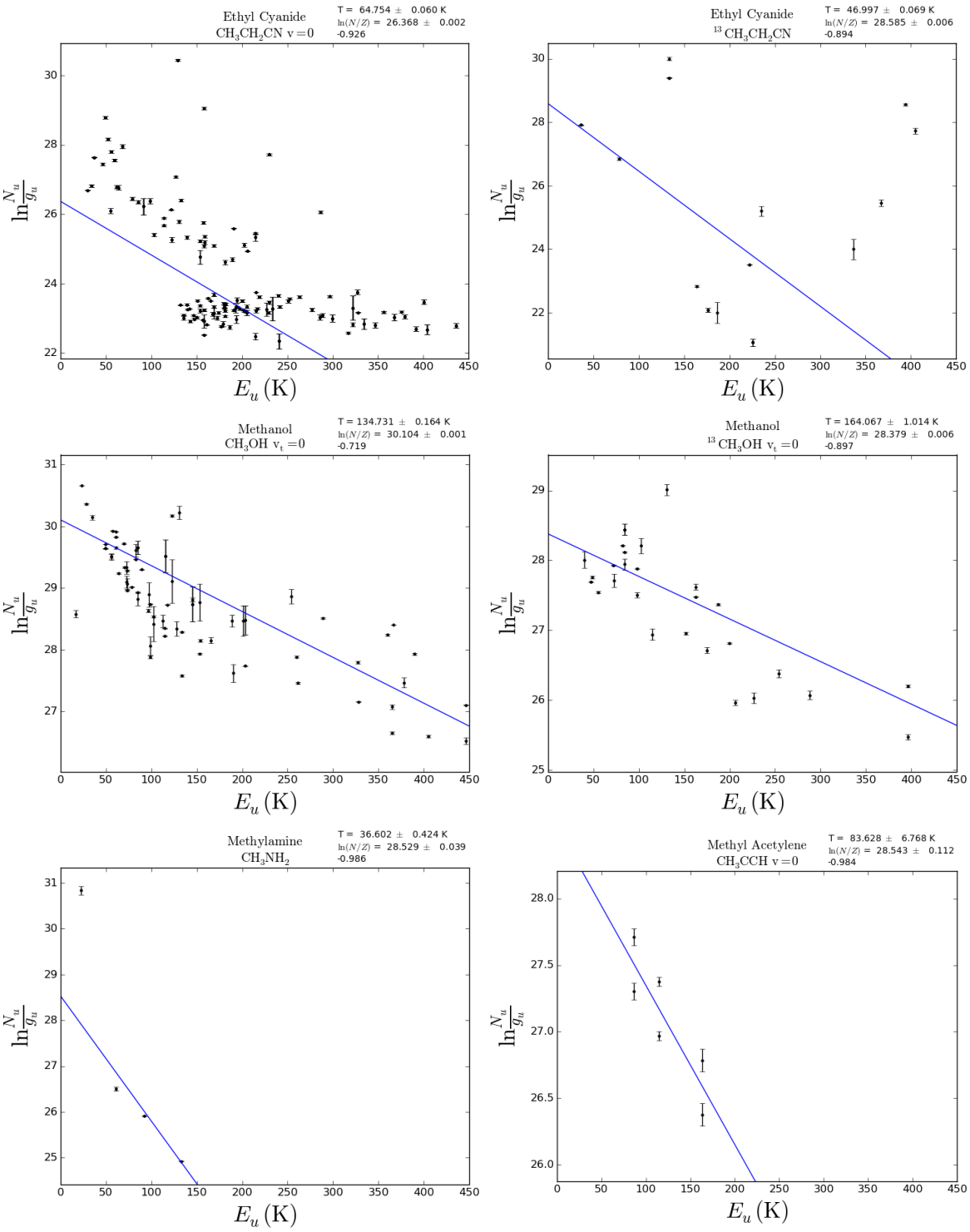

Figure D.1: (*Cont.*) Rotational diagrams for G327.3-0.6

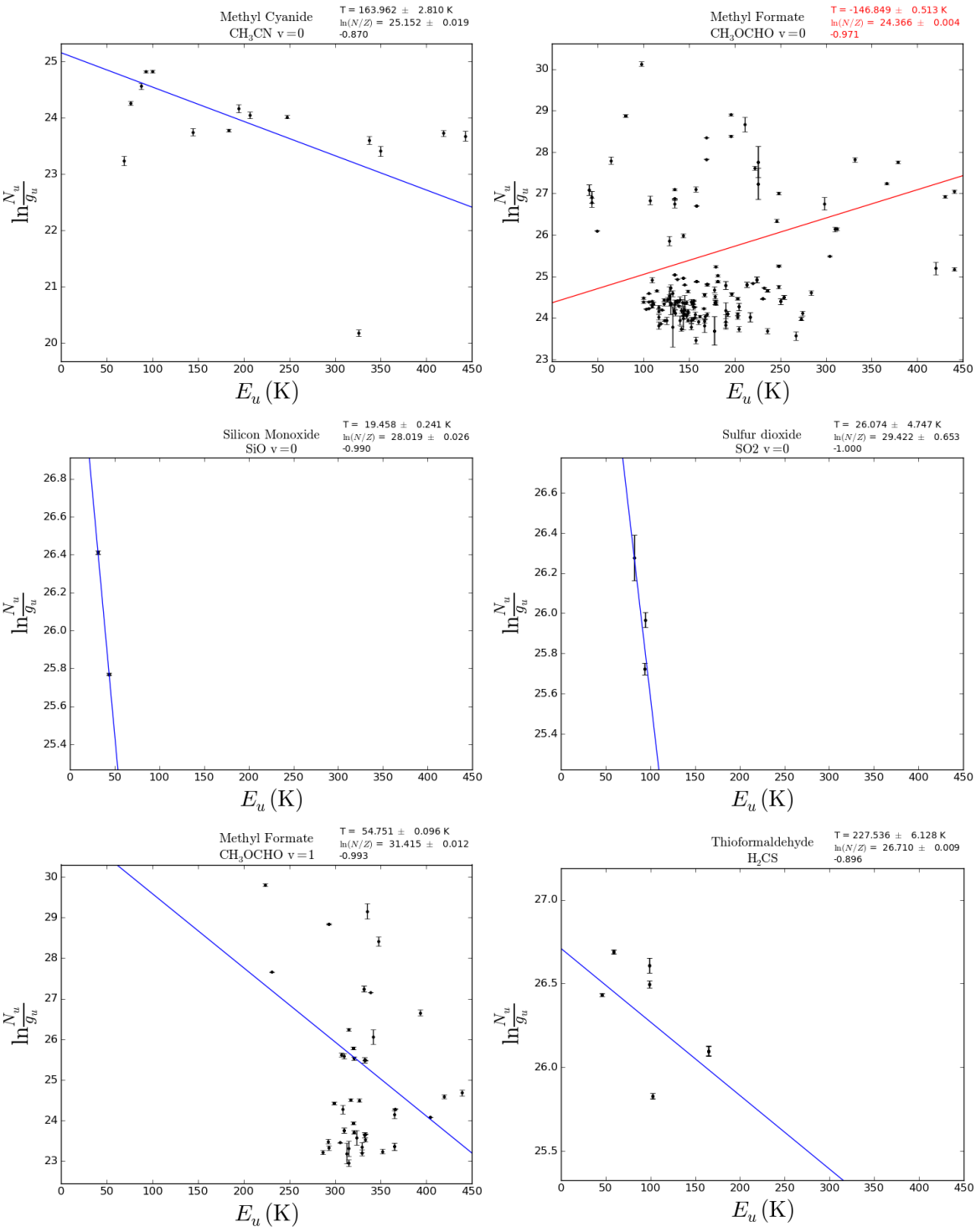

Figure D.1: (*Cont.*) Rotational diagrams for G327.3-0.6

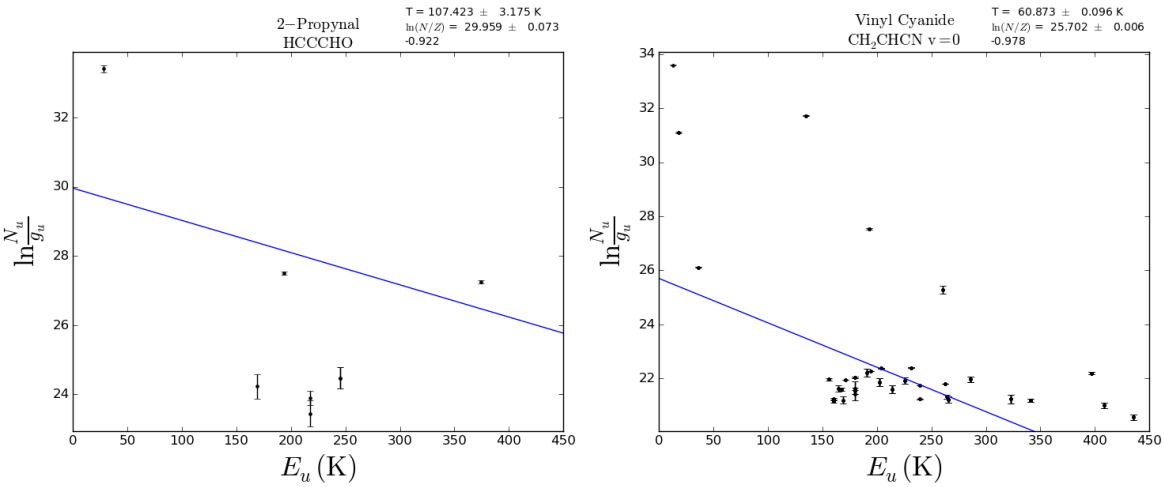

Figure D.1: (*Cont.*) Rotational diagrams for G327.3-0.6

D.2 Rotational diagrams for NGC 6334 I

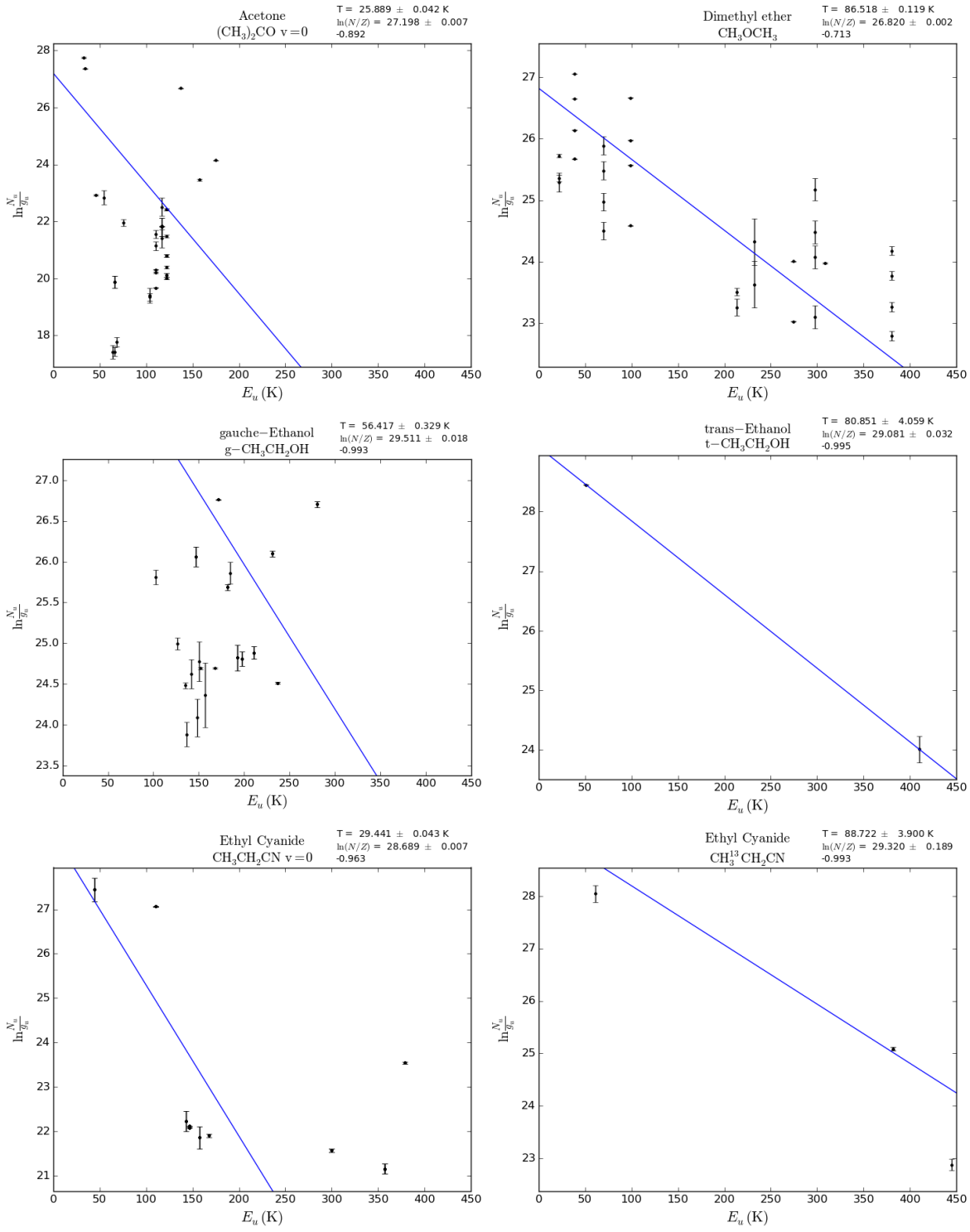

Figure D.2: Rotational diagrams for NGC 6334 I

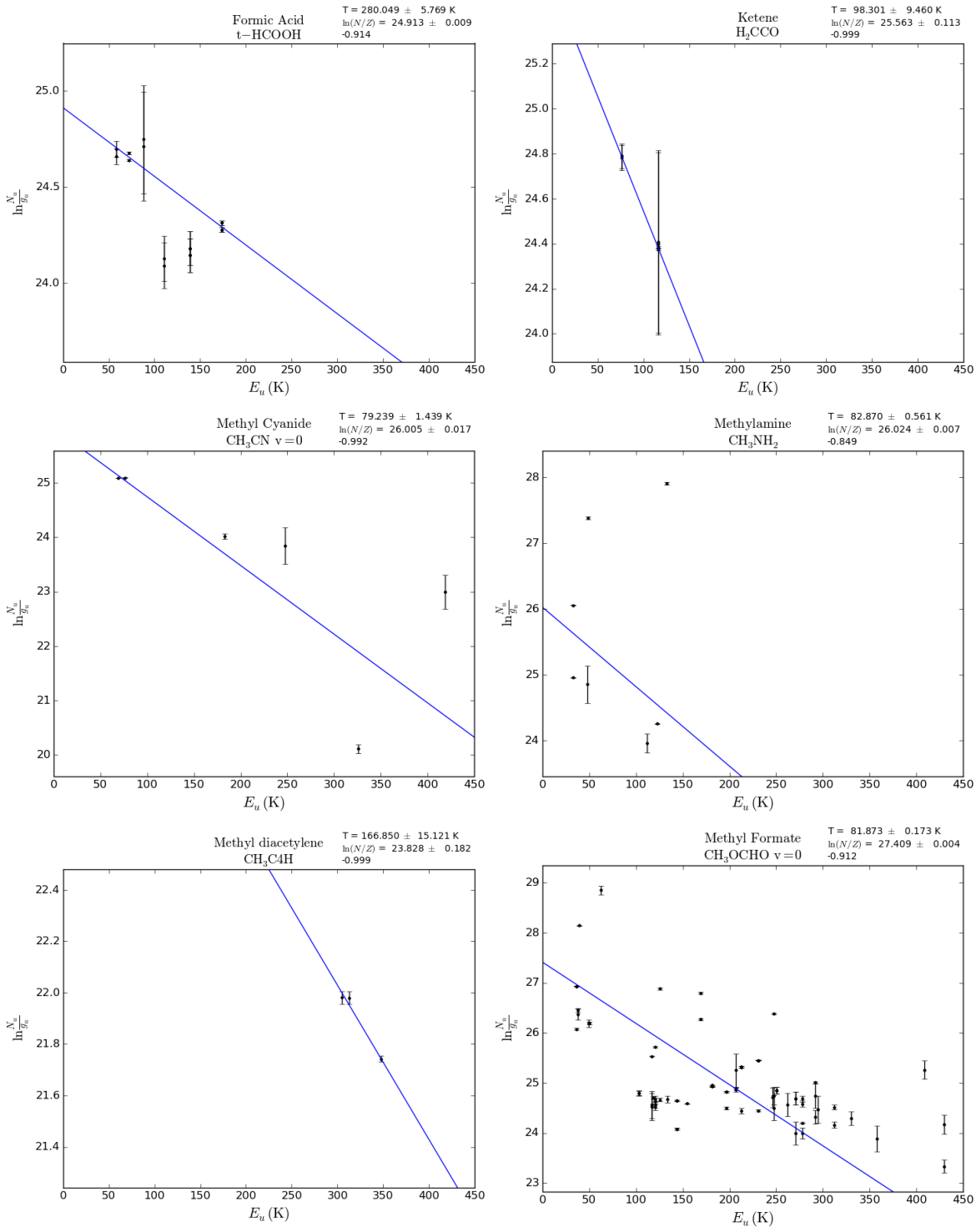

Figure D.2: (*Cont.*) Rotational diagrams for NGC 6334 I

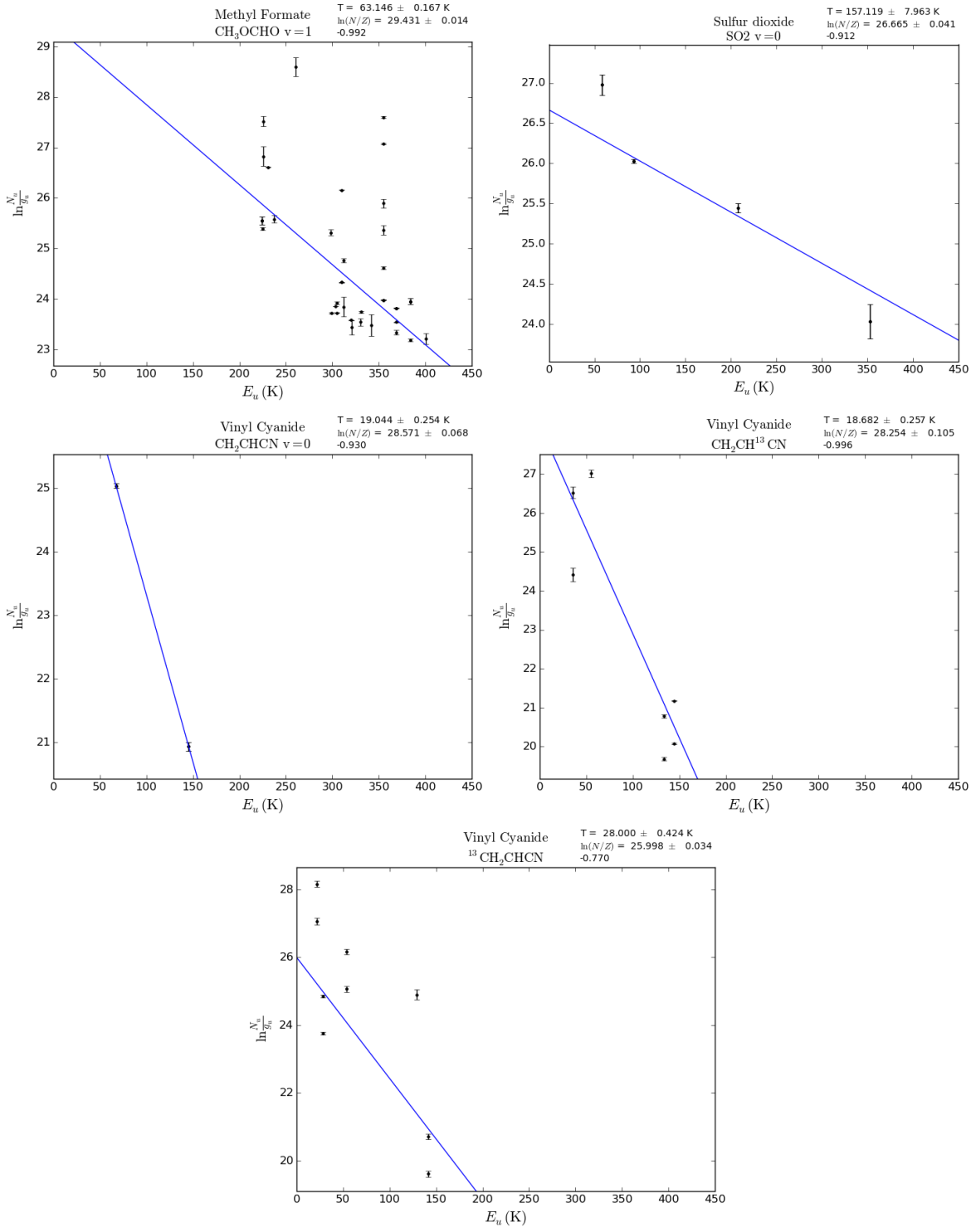

Figure D.2: (*Cont.*) Rotational diagrams for NGC 6334 I

Appendix E Population diagrams

E.1 Population diagrams for G327.3-0.6

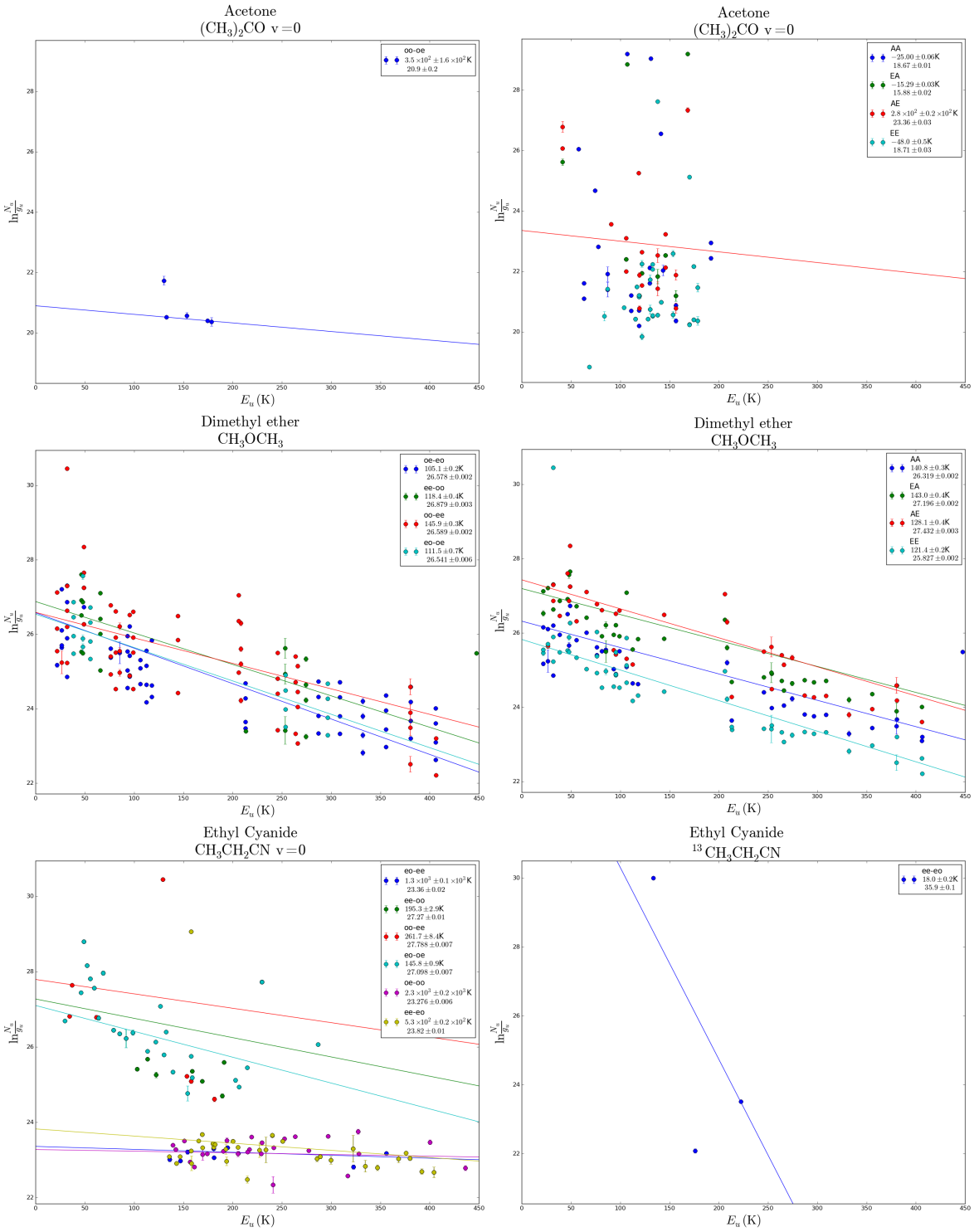

Figure E.1: Population diagrams for G327.3-0.6

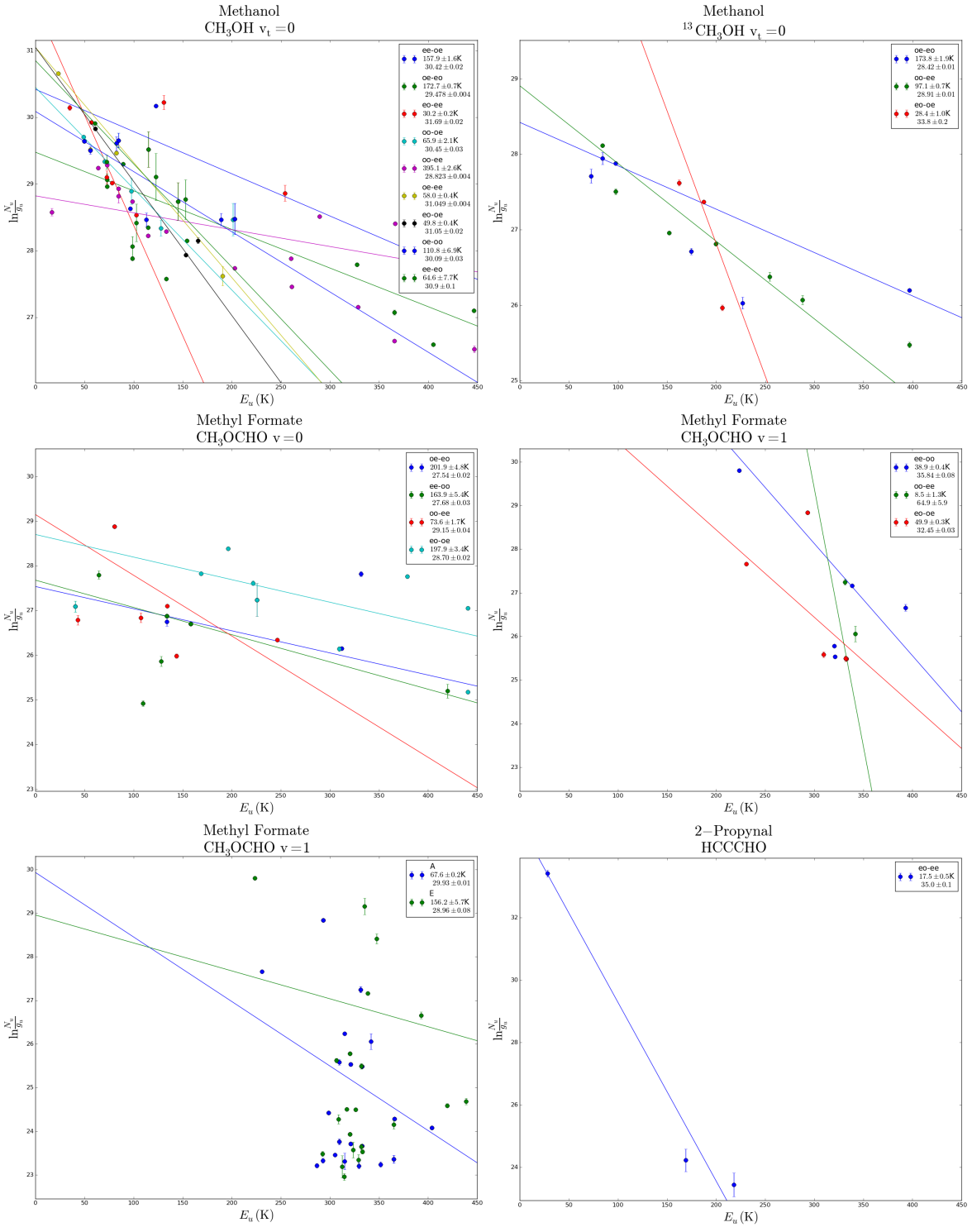

Figure E.1: (*Cont.*) population diagrams for G327.3-0.6

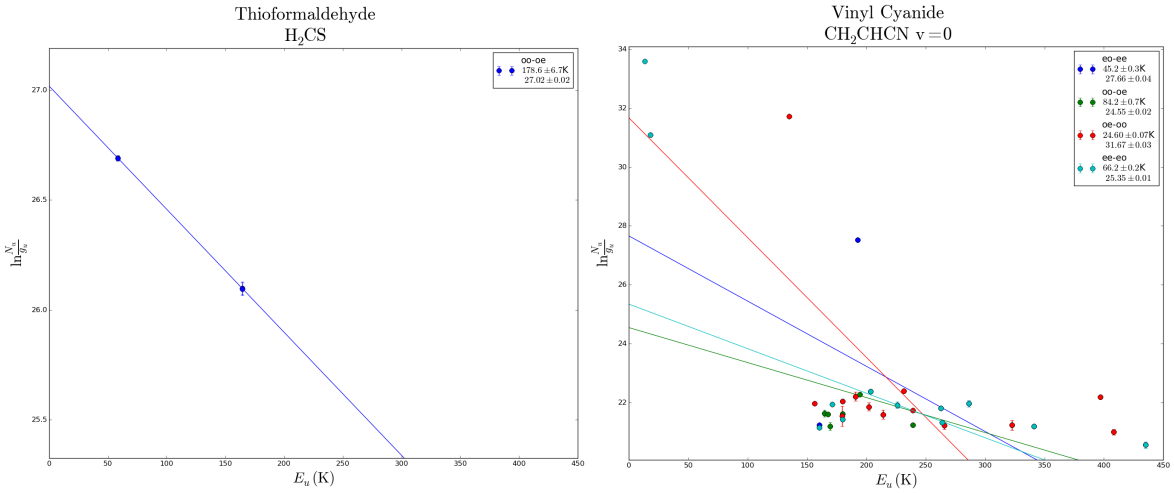

Figure E.1: (*Cont.*) population diagrams for G327.3-0.6

E.2 Population diagrams for NGC 6334 I

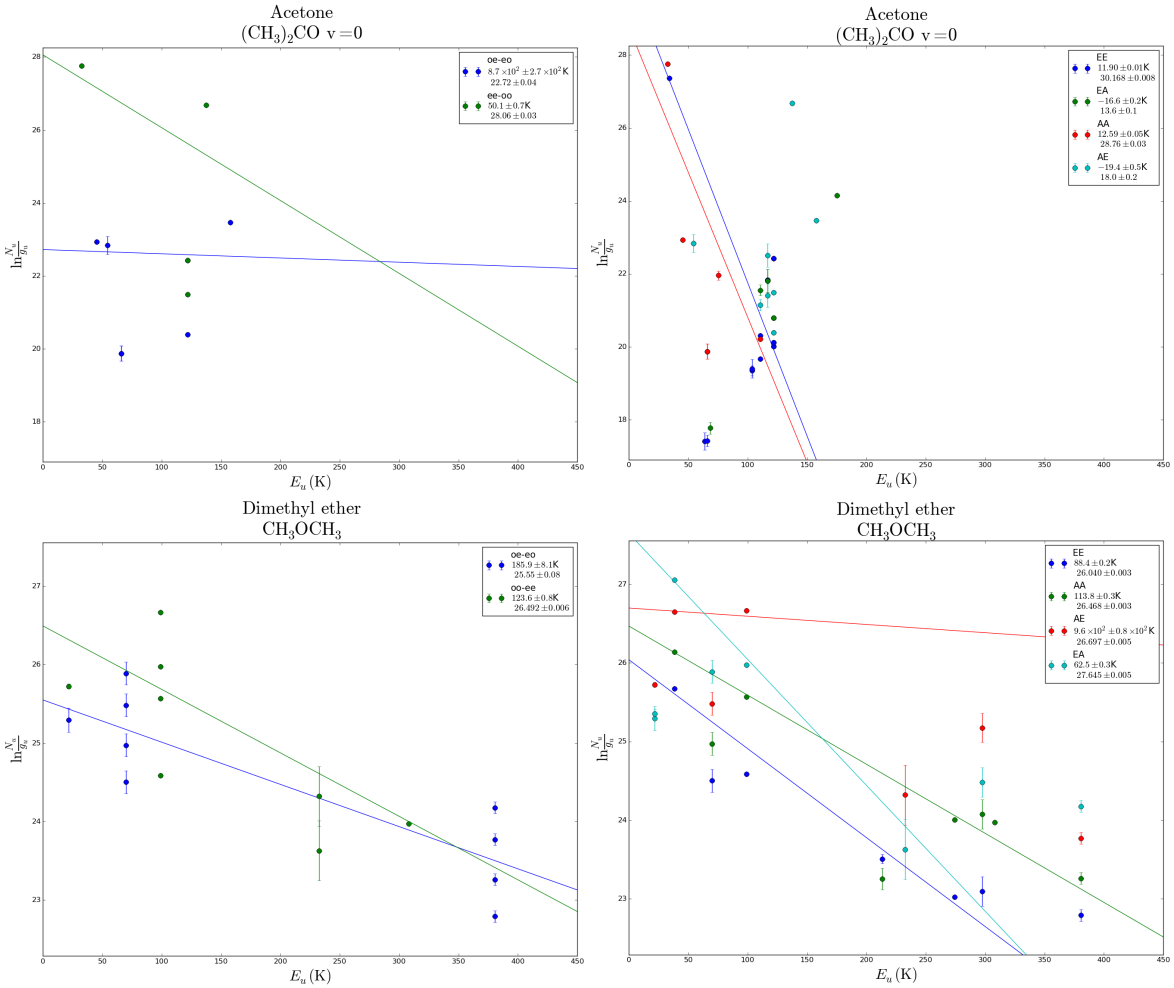

Figure E.2: Population diagrams for NGC 6334 I

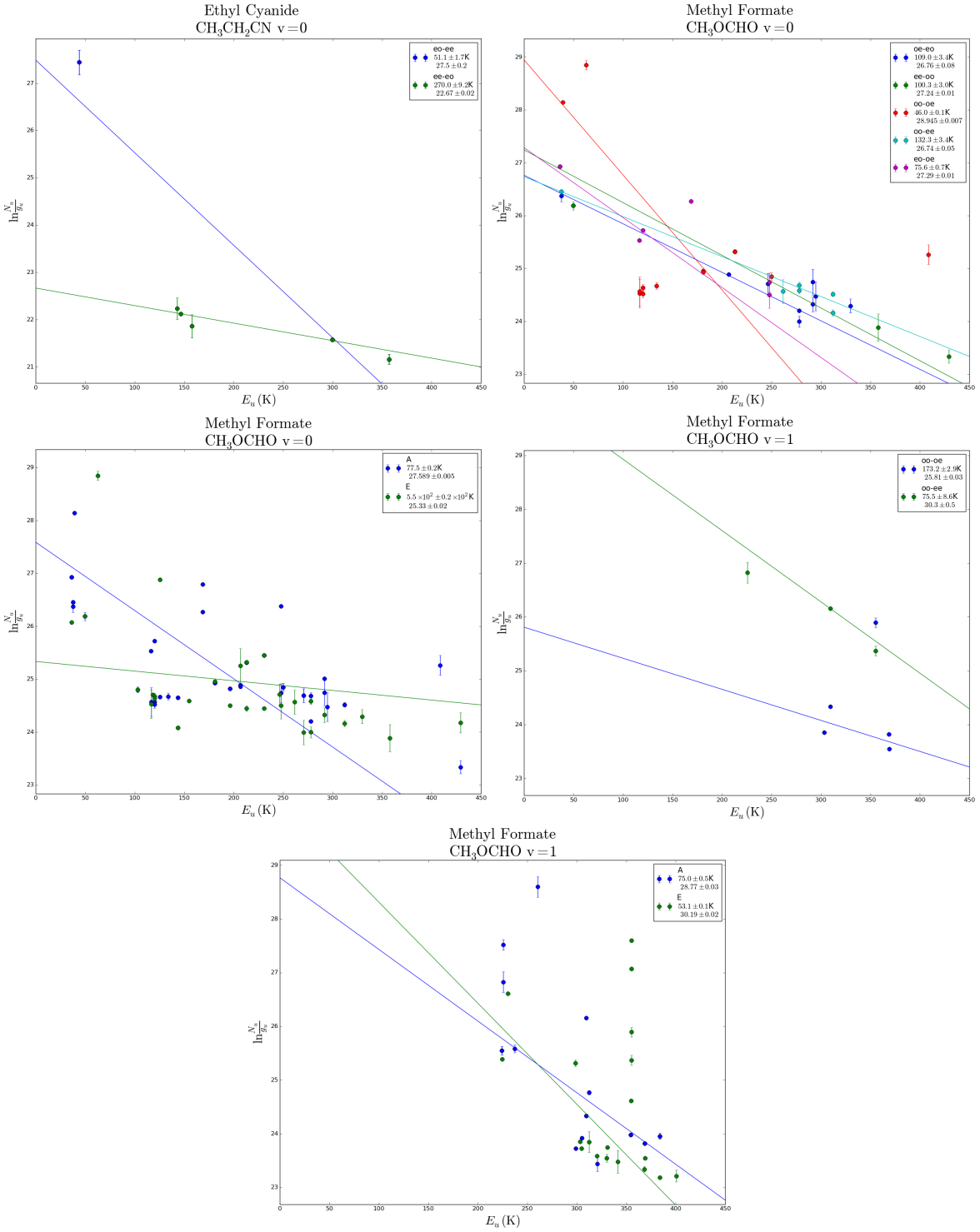

Figure E.2: (*Cont.*) Population diagrams for NGC 6334 I

Appendix F Comments on Python programs

F.1 splatsearch.py

This is a script for querying PHP from the Splatalogue[17] website[18]. It inputs a file containing following columns:

1. area of the line in $\mathrm{K\,MHz}$
2. area's error
3. line's peak position in MHz
4. line's peak error
5. linewidth in MHz
6. linewidth error
7. maximum of the fitted Gaussian in K
8. noise σ_{RMS} in K
9. frequency f_0 of the APEX file in MHz

The output is an ASCII file containing the following columns:

1. area of the line in $\mathrm{K\,MHz}$
2. area's error
3. line's peak position in MHz
4. line's peak error
5. linewidth in MHz
6. linewidth error
7. maximum of the fitted Gaussian in K
8. noise σ_{RMS} in K
9. frequency of the transition ij from Splatalogue in MHz
10. error of the transition frequency

[17] www.splatalogue.net

[18] Based on http://vilhelmp.blogspot.com/2011/10/querying-splataloguenet-with-python.html

11. $S_{ij}\mu^2$ in D^2, where μ is the permanent electric dipole moment of the molecule and S is the line strenght of the transition ij
12. line strenght S_{ij}
13. logarithm of the Einstein A coefficient, $\log A_{ij}$
14. energy of the upper state, E_u, in K
15. degeneracy of the upper state, g_u
16. molecule's name
17. molecule's chemical formula
18. f_0
19. unresolved quantum numbers
20. resolved quantum numbers

F.2 obrada12.py

This is the main analysis code. The preamble asks for following information:

- pearsonlimit - the cut in the Pearson ρ coefficient, default value is 0.5
- src - name of the source
- minfreq - minimum frequency of the dataset (in GHz)
- maxfreq - maximum frequency of the dataset (in GHz)
- removallist - a list of molecules to have a lower value of the temperature cut
- lowmaxt - the temperature cut (in K) for the removallist molecules
- v0 - the systemic velocity of the source
- H2a and H2b two hydrogen column densities (in cm^{-2})
- errors of the column densities H2a and H2b (in cm^{-2})

An example of the preamble for G327.3-0.6 is

```
pearsonlimit=0.5
tocke=80
errorcut=0.5
clight=300000
vrst=2
```

```
heightofplots=1.5
src='G327'
minfreq=213
maxfreq=352
removallist=['(CH3)2COv=0','CH3NH2']
lowmaxt=200
v0=-45
H2a=3.2*10**23
H2b=3*10**22
H2ae=0
H2be=0
```

The program needs the following files:

- izlaz.txt - a list of lines made with splatsearch.py
- izuzete.txt - a list of lines excluded from the analysis
- izbaciti.txt - a list of molecules excluded from the analysis
- Qs.txt - a list of partition functions
- molspec.txt - Splatalogue QN code
- freqplot.txt - spectra

Upon running the program, it asks for the following information:

- enter directory - a directory where the plots will be stored
- Remove multiples (y/n) - should lines with multiple candidates be excluded from the analysis
- Max Temperature - the upper limit in temperature
- Sigma - n in the $\sigma > n\sigma_{\mathrm{RMS}}$ cut, default value is $n = 3$

The program creates a set of folders. If the option to remove multiple candidates is selected, a folder named y is made, and if multiple candidates are not removed, a folder n is created.

References

Bachiller, R. & Cernicharo, J. 1990, A&A, 239, 276

Beuther, H., Churchwell, E. B., McKee, C. F., & Tan, J. C. 2007, Protostars and Planets V, 165

Bisschop, S. E., Schilke, P., Wyrowski, F., Belloche, A., Brinch, C., Endres, C. P., Güsten, R., Hafok, H., Heyminck, S., Jørgensen, J. K., Müller, H. S. P., Menten, K. M., Rolffs, R., & Schlemmer, S. 2013, A&A, 552, A122

Blake, G. A., Sutton, E. C., Masson, C. R., & Phillips, T. G. 1987, ApJ, 315, 621

Blake, G. A., Sutton, E. C., Masson, C. R., Phillips, T. G., Herbst, E., Plummer, G. M., & De Lucia, F. C. 1984, ApJ, 286, 586

Boch, T. & Fernique, P. in , Astronomical Society of the Pacific Conference Series, Vol. 485, Astronomical Data Analysis Software and Systems XXIII, ed. N. MansetP. Forshay, 277

Bonnarel, F., Fernique, P., Bienaymé, O., Egret, D., Genova, F., Louys, M., Ochsenbein, F., Wenger, M., & Bartlett, J. G. 2000, A&AS, 143, 33

Brown, P. D., Charnley, S. B., & Millar, T. J. 1988, MNRAS, 231, 409

Burton, M. G., Ashley, M. C. B., Marks, R. D., Schinckel, A. E., Storey, J. W. V., Fowler, A., Merrill, M., Sharp, N., Gatley, I., Harper, D. A., Loewenstein, R. F., Mrozek, F., Jackson, J. M., & Kraemer, K. E. 2000, ApJ, 542, 359

Carroll, B. W. & Ostlie, D. A. 2007, *An Introduction to Modern Astrophysics* (Addison Wesley)

Charnley, S. B. 1997, ApJ, 481, 396

Charnley, S. B., Ehrenfreund, P., Millar, T. J., Boogert, A. C. A., Markwick, A. J., Butner, H. M., Ruiterkamp, R., & Rodgers, S. D. 2004, MNRAS, 347, 157

Chibueze, J. O., Omodaka, T., Handa, T., Imai, H., Kurayama, T., Nagayama, T., Sunada, K., Nakano, M., Hirota, T., & Honma, M. 2014, ApJ, 784, 114

Clark, F. O., Lovas, F. J., & Johnson, D. R. 1979, ApJ, 229, 553

de Pree, C. G., Rodriguez, L. F., Dickel, H. R., & Goss, W. M. 1995, ApJ, 447, 220

Dunham, M. M., Stutz, A. M., Allen, L. E., Evans, II, N. J., Fischer, W. J., Megeath, S. T., Myers, P. C., Offner, S. S. R., Poteet, C. A., Tobin, J. J., & Vorobyov, E. I. 2014, Protostars and Planets VI, 195

Ehrenfreund, P., Dartois, E., Demyk, K., & D'Hendecourt, L. 1998, A&A, 339, L17

Ezoe, Y., Kokubun, M., Makishima, K., Sekimoto, Y., & Matsuzaki, K. 2006, ApJ, 638, 860

Friedel, D. N., Snyder, L. E., Remijan, A. J., & Turner, B. E. 2005, ApJL, 632, L95

Garay, G. & Lizano, S. 1999, PASP, 111, 1049

Gibb, E., Nummelin, A., Irvine, W. M., Whittet, D. C. B., & Bergman, P. 2000, ApJ, 545, 309

Goldsmith, P. F. & Langer, W. D. 1999, ApJ, 517, 209

Gordy, W. & Cook, R. L. 1984, *Microwave Molecular Spectra*

Irvine, W. M., Brown, R. D., Cragg, D. M., Friberg, P., Godfrey, P. D., Kaifu, N., Matthews, H. E., Ohishi, M., Suzuki, H., & Takeo, H. 1988, ApJL, 335, L89

Kraemer, K. E. & Jackson, J. M. 1999, ApJS, 124, 439

Kubo, R. 1965, *Statistical Mechanics: An Advanced Course with Problems and Solutions* (North-Holland Pub. Co.)

Kurtz, S., Cesaroni, R., Churchwell, E., Hofner, P., & Walmsley, C. M. 2000, Protostars and Planets IV, 299

Kutner, M. L. & Ulich, B. L. 1981, ApJ, 250, 341

Larson, R. B. 1981, MNRAS, 194, 809

Leurini, S., Wyrowski, F., Herpin, F., van der Tak, F., Güsten, R., & van Dishoeck, E. F. 2013, A&A, 550, A10

Loomis, R. A., McGuire, B. A., Shingledecker, C., Johnson, C. H., Blair, S., Robertson, A., & Remijan, A. J. 2015, ApJ, 799, 34

Loren, R. B., Wootten, A., & Mundy, L. G. 1984, ApJL, 286, L23

Lovas, F. J., Remijan, A. J., Hollis, J. M., Jewell, P. R., & Snyder, L. E. 2006, ApJL, 637, L37

Mangum, J. G. & Shirley, Y. L. 2015, PASP, 127, 266

Millar, T. J. & Nejad, L. A. M. 1985, MNRAS, 217, 507

Minier, V., André, P., Bergman, P., Motte, F., Wyrowski, F., Le Pennec, J., Rodriguez, L., Boulade, O., Doumayrou, E., Dubreuil, D., Gallais, P., Hamon, G., Lagage, P.-O., Lortholary, M., Martignac, J., Revéret, V., Roussel, H., Talvard, M., Willmann, G., & Olofsson, H. 2009, A&A, 501, L1

Morales Ortiz, J. L., Ceccarelli, C., Lis, D. C., Olmi, L., Plume, R., & Schilke, P. 2014, A&A, 563, A127

Müller, H. S. P., Schlöder, F., Stutzki, J., & Winnewisser, G. 2005, Journal of Molecular Structure, 742, 215

Myers, R. J. & Bright Wilson, Jr., E. 1960, J. Chem. Phys., 33, 186

Peng, T.-C., Despois, D., Brouillet, N., Baudry, A., Favre, C., Remijan, A., Wootten, A., Wilson, T. L., Combes, F., & Wlodarczak, G. 2013, A&A, 554, A78

Pickett, H. M., Poynter, R. L., Cohen, E. A., Delitsky, M. L., Pearson, J. C., & Müller, H. S. P. 1998, J. Quant. Spectrosc. Radiat. Transfer, 60, 883

Plume, R., Jaffe, D. T., Evans, II, N. J., Martín-Pintado, J., & Gómez-González, J. 1997, ApJ, 476, 730

Reid, M. J., Menten, K. M., Brunthaler, A., Zheng, X. W., Dame, T. M., Xu, Y., Wu, Y., Zhang, B., Sanna, A., Sato, M., Hachisuka, K., Choi, Y. K., Immer, K., Moscadelli, L., Rygl, K. L. J., & Bartkiewicz, A. 2014, ApJ, 783, 130

Remijan, A. J., Markwick-Kemper, A., & ALMA Working Group on Spectral Line Frequencies. 2007, in Bulletin of the American Astronomical Society, Vol. 39, American Astronomical Society Meeting Abstracts, 963, http://www.cv.nrao.edu/php/splat/

Sandell, G. 2000, A&A, 358, 242

Schilke, P., Comito, C., Thorwirth, S., Wyrowski, F., Menten, K. M., Güsten, R., Bergman, P., & Nyman, L.-Å. 2006, A&A, 454, L41

Simpson, J. P. & Rubin, R. H. 1990, ApJ, 354, 165

Turner, B. E. 1991, ApJS, 76, 617

Vassilev, V., Meledin, D., Lapkin, I., Belitsky, V., Nyström, O., Henke, D., Pavolotsky, A., Monje, R., Risacher, C., Olberg, M., Strandberg, M., Sundin, E., Fredrixon, M., Ferm, S.-E., Desmaris, V., Dochev, D., Pantaleev, M., Bergman, P., & Olofsson, H. 2008, A&A, 490, 1157

Wilson, T. L., Rohlfs, K., & Huttemeister, S. 2009, *Tools of Radio Astronomy* (Springer Verlag)

Wyrowski, F., Menten, K. M., Schilke, P., Thorwirth, S., Güsten, R., & Bergman, P. 2006, A&A, 454, L91

Xu, L.-H. & Lovas, F. J. 1997, Journal of Physical and Chemical Reference Data, 26, 17

Zhou, L., Kaiser, R. I., Gao, L. G., Chang, A. H. H., Liang, M.-C., & Yung, Y. L. 2008, ApJ, 686, 1493